July 2018

HYDROGEN STRESS AND SYNTROPHY OF HYPERTHERMOPHILIC HETEROTROPHS AND METHANOGENS

Begum Topcuoglu

HYDROGEN STRESS AND SYNTROPHY OF HYPERTHERMOPHILIC HETEROTROPHS AND METHANOGENS

A Dissertation Presented

by

BEGÜM D. TOPÇUOĞLU

Submitted to the Graduate School of the
University of Massachusetts Amherst in partial fulfillment
of the requirements for the degree of

DOCTOR OF PHILOSOPHY

May 2018

Microbiology

HYDROGEN STRESS AND SYNTROPHY OF HYPERTHERMOPHILIC HETEROTROPHS AND METHANOGENS

A Dissertation Presented

by

BEGÜM D. TOPÇUOĞLU

Approved as to style and content by:

_____
James F. Holden, Chair

_____
Kristen DeAngelis, Member

_____
Klaus Nüsslein, Member

_____
Steven Petsch, Member

_____
Steven Sandler
Microbiology Department Head

DEDICATION

This dissertation is dedicated to my parents Eser and Ersin for being the source of my perseverance. And to my best friend Başak who always has my back.

ACKNOWLEDGMENTS

I would like to thank my advisor Jim Holden for his unwavering support and invaluable mentorship throughout the years. His dedication to his work and to his students inspire me every day. I would like to acknowledge my dissertation committee – Klaus Nüsslein, Kristen DeAngelis and Steve Petsch for their support. I would also like to thank the Microbiology Deparment at UMass for being my home for the past six years.

Within our lab, I would like to thank my fellow graduate students – Lucy Stewart, Jenn Lin, Srishti Kashyap, Emily Moreira, Sarah Hensley, and James Llewellyn. I would also like to thank Roberto Orellana and Cem Meydan for their mentorship. I would like to thank our fieldwork collaborators for this research – Julie Huber, Caroline Fortunato, Joe Vallino, Chris Algar, Dave Butterfield, Ben Larson and the crews of the R/V Thomas G. Thompson, the R/V Ronald H. Brown, as well as the operating teams of ROV Jason II.

I am grateful for my chosen family, scattered around the world but always a phone call away, especially Duygu Ula who has been my rock. Your love and support made this possible. I am also grateful for the many friends I had in Amherst who made these six years a joyful time.

I would like to thank my family for their encouragement and support that made this transatlantic journey possible. Finally, I would like to thank my grandmother Aysel Deniz for being my first teacher. Thank you for giving me the love of reading.

ABSTRACT

HYDROGEN STRESS AND SYNTROPHY OF HYPERTHERMOPHILIC HETEROTROPHS AND METHANOGENS

MAY 2018

BEGÜM D. TOPÇUOĞLU

B.S., SABANCI UNIVERSITY

Ph.D., UNIVERSITY OF MASSACHUSETTS AMHERST

Directed by: Dr. James F. Holden

Approximately 1 giga ton (Gt, 10^{15} g) of CH_4 is formed globally per year from H_2, CO_2, and acetate through methanogenesis, largely by methanogens growing in syntrophic association with anaerobic microbes that hydrolyze and ferment biopolymers. However, our understanding of methanogenesis in hydrothermal regions of the subseafloor and potential syntrophic methanogenesis at thermophilic temperatures is nascent. This dissertation shows that thermophilic H_2 syntrophy can support methanogenesis within natural microbial assemblages at hydrothermal vents and that it can be an important alternative energy source for thermophilic autotrophs in marine geothermal environments. This dissertation also elucidates H_2 stress survival strategies of the H_2 producing heterotrophs and the H_2 consuming methanogens as well as their cooperation with one another for survival.

The growth of natural assemblages of thermophilic methanogens from Axial Seamount was primarily limited by H_2 availability. Heterotrophs supported thermophilic methanogenesis by H_2 syntrophy in microcosm incubations of hydrothermal fluids at 80°C supplemented with tryptone only. Based on 16S rRNA gene sequencing, H_2 producing

heterotrophs, *Thermococcus,* and H_2-consuming methanogens, *Methanocaldococcus* were abundant in 80°C tryptone microcosms from an Axial Seamount hydrothermal vent. In order to model the impact of H_2 syntrophy at hyperthemophilic temperatures, a coculture was established consisting of a H_2-producing hyperthermophilic heterotroph and a H_2-consuming hyperthermophilic methanogen.

The model organisms, hyperthermophilic heterotroph *Thermococcus paralvinellae* and the hydrogenotrophic methanogen *Methanocaldococcus jannaschii,* were examined in monocultures and cocultures for their H_2 stress and syntrophy strategies. In monocultures, H_2 inhibition changed the growth kinetics and the transcriptome of *T. paralvinellae*. A significant decrease in batch phase growth rates and steady state cell concentrations was observed with high H_2 background. Metabolite production measurements, RNA-seq analyses of differentially expressed genes, and *in silico* experiments performed with a constraint-based metabolic network model showed that *T. paralvinellae* produces formate by a formate hydrogenlyase to survive H_2 inhibition. H_2 limitation on *M. jannaschii* caused a significant decrease in batch phase growth rates and CH_4 production rates but also caused a significant increase in cell yields. In cocultures, H_2 syntrophy relieved H_2 stress for *T. paralvinellae* but not for *M. jannaschii. T. paralvinellae* only produced formate when grown in monoculture while no formate was detected during growth in coculture. While *M. jannaschii* was capable of growth and methanogenesis solely on the H_2 produced by *T. paralvinellae*, the growth and CH_4 production rates of *M. jannaschii* decreased in coculture compared to when *M. jannaschii* was grown in monoculture.

TABLE OF CONTENTS

Page

LIST OF TABLES

LIST OF FIGURES

CHAPTER 1

INTRODUCTION

1.1 Objectives

Hydrogen is one of the most common energy sources for chemolithoautotrophic microbial growth in anoxic environments. It is formed in the subsurface by high-temperature (>200°C) hydration of mafic and ultramafic rocks and by low-temperature (< 200°C) adsorption of water to spinel mineral phases such as magnetite (Sleep et al., 2004; Mayhew et al., 2013). In many deep terrestrial subsurface environments, such as coal and shale beds and anoxic aquifers, H_2 concentrations are too low to support the growth of hydrogenotrophic microorganisms without the assistance of H_2-producing microbes that catabolize organic compounds present in the environment (Lovley et al., 1994; Waldron et al., 2007; Ünal et al., 2012). However, our understanding of this process, called 'H_2 syntrophy', in deep hot subseafloor environments is very limited.

Each year, approximately 1 Gt of CH_4 is produced globally through methanogenesis, largely by methanogens growing syntrophically with fermentative microbes that hydrolyze biopolymers (Thauer et al., 2008), but it is not known how much methanogenesis is from thermophilic syntrophy. Deep-sea hydrothermal vents and hydrocarbon reservoirs are known habitats for thermophiles (Holden et al., 2009). Furthermore, it was estimated that 35% of all marine sediments are above 60°C (LaRowe et al., 2017) suggesting that these environments also provide a large global biosphere for thermophiles. Using growth-dependent and molecular analyses, H_2 producing heterotrophs that belong to genus *Thermococcus* and thermophilic methanogens have been shown to collocate in hydrothermal vents (Takai et al., 2004; Nakagawa et al., 2005;

Flores et al., 2011; Ver Eecke et al., 2012; Reveillaud et al., 2016; Fortunato et al., 2018), methane hydrate bearing sediments, ridge flanks (Inagaki et al., 2006; Ehrhardt et al., 2007) and produced waters from high-temperature petroleum reservoirs (Orphan et al., 2000; Bonch-Osmolovskaya et al., 2003; Nazina et al., 2006; Dahle et al., 2008; Kotlar et al., 2011; Lewin et al., 2014; Junzhang et al., 2014; Okpala et al., 2017). When these environments lack the sufficient environmental flux rates to provide abiotic H_2 to methanogens for growth and methanogenesis, H_2-producing microbes that catabolize organic compounds can provide energy to the methanogens they colocalize with. Therefore, studying the respiration and growth kinetics of thermophilic methanogens and H_2-producing heterotrophs when grown alone and in coculture is important to model the interspecies H_2 transfer in the hot subsurface.

The goal of this dissertation is to make fundamental advances in our understanding of interspecies microbe-microbe interactions in high-temperature subseafloor ecosystems by focusing on how hyperthermophilic heterotrophs and hyperthermophilic methanogens respond to H_2 stress and H_2 syntrophy. This study models the metabolic pathways, biomass and metabolite production, and energetics of subseafloor microbes, to better predict when, how and to what extent these types of organisms interact and depend on each other in various subseafloor environments.

This dissertation is divided into five chapters. The first chapter explains the microbiology, geology, and geochemistry of thermophilic subsurface ecosystems where thermophilic microbes impact biogeochemical cycles. It explains the metabolic potentials of model organisms used in the study. The second chapter describes the potential for thermophilic and hyperthermophilic H_2 syntrophy in hydrothermal vent fluids and

establishes a coculture with model organisms representative of *in-situ* H_2 syntrophy. The third chapter describes energetics of our model H_2-producing hyperthermophilic heterotroph, *Thermococcus paralvinellae*. It shows how the organism deals with H_2 stress. The fourth chapter describes energetics of our model H_2-consuming hyperthermophilic methanogen, *Methanocaldococcus jannaschii* and how it deals with H_2 stress. Then it discusses if H_2 stress (i.e., H_2 inhibition for the heterotroph, H_2 limitation for the methanogen) is ameliorated when *T. paralvinellae* and *M. jannaschii* are grown in coculture through H_2 syntrophy relative to when either organism is grown alone. The fifth chapter presents a brief conclusion and future directions.

1.2 Life in the Hot Subsurface Biosphere

Hot subsurface environments such as hydrothermal vents, hot springs, and hot sedimentary environments including petroleum reservoirs provide a large biosphere for many organisms and geochemical processes within them.

Thermophilic and hyperthermophilic microbes are found in hot environments (>70°C) and can grow up to 122°C. They belong to both the *Archaea* and the *Bacteria* and grow by chemolithoautotrophy and heterotrophy. Specifically, they are specialists such as methanogens; other autotrophs that reduce primarily sulfur compounds but also iron, nitrate, and oxygen; H_2-producing heterotrophs; and thermoacidophiles as well as facultative generalists that grow autotrophically and heterotrophically using a mix of terminal electron acceptors. These microbes sometimes dominate marine sedimentary environments and petroleum reservoirs and may contribute to natural gas formation through methanogenesis or cause oil and gas spoilage through sulfidogenesis. Some of

these organisms also provide useful biotechnological products such as DNA polymerases for the polymerase chain reaction (PCR). The study of hot environments also provides insight into early life on Earth and our search for life beyond Earth.

The first report of life in a hot environment, herein defined as being above 70°C, came from the observation of high concentrations of microbes (or 'chlorophylless filamentous Schizomycetes') in an 89°C hot spring in Yellowstone National Park sampled in 1898 (Brock, 1978). The hottest known microbes are 'hyperthermophiles', which are those organisms that grow optimally above 80°C (Stetter, 1999). In hot environments, they are commonly joined by the hottest thermophiles, which are those organisms that grow optimally above 55°C. After 1980, many microbes that grow above 70°C were cultured and characterized from terrestrial geothermal environments and shallow marine vents. At the same time, microbes from deep-sea hydrothermal vents were isolated from mid-ocean spreading centers and volcanic seamounts. The advent of metagenomics and microbial community analysis has shown that hyperthermophiles and hot thermophiles are also found in other hot environments such as in petroleum reservoirs and deep marine sediments.

The discovery and study of life that grows above 70°C have changed our perspective on life. We now have insight into how biological molecules such as proteins, DNA, and lipids can be thermostable at temperatures that normally denature these molecules. These organisms provide new enzymes and processes for industrial applications such as *in vitro* DNA replication using DNA polymerases from thermophiles and hyperthermophiles. They have also shown us unique adaptations to metabolic pathways such as the use of tungsten-containing enzymes and ADP-dependent kinases

for glycolysis. High-temperature environments have shown us that life can exist entirely without sunlight and use chemicals provided from hot water-rock reactions. This has provided new ideas about life on the early Earth and the possibility of life on other planets and moons that once had or currently have hydrothermal fluid circulation below their surfaces. Future research will continue to identify and characterize novel thermophiles and hyperthermophiles and will model and predict the impact of these organisms on the biogeochemistry of hot environments and their surroundings. These are becoming more relevant as we learn that hot environments are more widespread on the Earth than originally imagined.

1.2.1 Marine Hydrothermal Vents

Marine hydrothermal vents are sites where seawater percolates through cracks and pores in the Earth's crust and reacts with hot subsurface rocks. The seawater is transformed into hydrothermal fluid as the seawater exchanges ions with the rock. Fluid-mineral reactions result in the loss of some dissolved chemical and volatile components (e.g., O_2, SO_4^{2-}) and gain in others (e.g., H_2, CH_4, CO_2, S^{2-}, and reduced metals) at progressively higher temperatures as modified seawater migrates deeper into the crust. Hydrothermal venting is associated with mid-ocean spreading centers along tectonic plate boundaries, intra-plate volcanic hot spots, and back-arc basins and island-arc volcanoes in tectonic subduction zones. They are found in the deep-sea as well as in shallow coastal marine environments.

Deep-sea hydrothermal vents were first discovered in 1977 near the Galápagos Islands, and since then dozens of deep-sea hydrothermal vent fields in all the oceans have been discovered. The hydrothermal fluid emanating from these vents can reach

temperatures over 400°C, which are kept in a liquid state due to the high hydrostatic pressure exerted on the fluids. These temperatures are too hot to support life, but hydrothermal fluids mix with cool seawater inside the crust and within metal sulphide mineral deposits on the seafloor and create cooler habitats that support thermophilic and hyperthermophilic life. These organisms use chemicals from both the hydrothermal fluid and the seawater for growth. However, the chemical composition of the fluids varies depending on the kinds of rocks that the seawater reacts with. If seawater reacts with ultramafic rock as well as olivine from deep in the Earth's crust or with newly erupted magma in the shallow crust, then large concentrations of H_2 are produced in the fluids. The H_2 then supports the growth of thermophilic and hyperthermophilic autotrophs, particularly methanogens such as the *Methanococcales* (Huber et al., 2002; Takai et al., 2004; Flores et al., 2011). In contrast, along subduction zones where highly weathered seafloor that is millions of years old is melted and reacts with seawater, the hydrothermal fluids have low H_2 concentrations but are rich in metals and highly acidic. In these cases, as well as non-eruptive mid-ocean spreading centers, the thermophiles and hyperthermophiles found are other autotrophs such as iron reducers and microaerophiles (Holden et al., 2012). All deep-sea hydrothermal environments generally support the growth of heterotrophs such as the *Thermococcales* and marine generalists like the *Desulfurococcales* and the *Archaeoglobales* (Chaban et al., 2006; Orcutt et al., 2011).

The discovery of life in environments lacking sunlight and O_2 profoundly changed the way in which scientists view the history of life on Earth and the likelihood of life beyond Earth. It was suggested that deep-sea hydrothermal vents may be where life first began on Earth. Indeed, there is evidence of ancient microbial life in hydrothermal

vents from more than 3 billion years ago (Dodd et al., 2017). This life may have been thermophilic and hyperthermophilic living inside the crust and existing solely on geothermally derived gases, sulfur compounds, and minerals. Furthermore, there is evidence for past hydrothermal activity on Mars and for currently volcanic activity in ice-covered oceans on some of the moons of Jupiter and Saturn. If life can exist in hydrothermal vents on Earth, then it is possible that extraterrestrial hydrothermal vents could support life beyond Earth in the same manner. Therefore, extraterrestrial hydrothermal vent sites are targets for space exploration and the search for life beyond our own planet.

Shallow marine hydrothermal vents are found at water depths of less than 200 m. These include the summits of seamounts and the flanks of volcanic islands. Because of the lack of hydrostatic pressure, the hydrothermal fluid temperatures are much lower. The highest measured temperature at shallow marine vent is 135°C just 22 m below sea level. Shallow hydrothermal vents are in the photic zone and thus are influenced by photosynthetic processes that occur near the surface and are often iron or sulfur dominated. Hydrothermal processes create geochemically distinct features such as metal sulphide-poor mineral deposits and focused brines. Directly above hydrothermal discharges, there is an increase in richness of heterotrophs belonging to the *Thermococcales* and the *Thermoproteales* and autotrophs belonging to the *Aquificales* (Chaban et al., 2006; Price and Giovanelli, 2017).

1.2.1.1 Hydrothermal Vents at Axial Seamount on the Juan de Fuca Ridge

Axial Seamount is an active submarine volcano located 1400 m below sea level and approximately 500 km off the coast of the Pacific Northwestern United States on the

mid-ocean spreading center called the Juan de Fuca Ridge. Hydrothermal activity was first discovered at Axial Seamount in the early 1980's and due to the frequent volcanic eruptions since then, it has been the focus of many research expeditions and volcano observatories such as NeMO and Ocean Observatory Initiative (OOI). There is ~ 30 years of biological, geochemical, and geophysical time-series data from the hydrothermal vents at Axial Seamount. The fieldwork outlined in Chapter 2 of this thesis is performed at this field site.

1.2.2 Terrestrial Hot Springs

Hot springs are heated, low salinity (0.1-0.5% NaCl) ecosystems associated with active volcanoes. They have pH values ranging from pH 0.5 to pH 9. Steam vents (i.e., fumaroles) at hot springs are features where water boils away before reaching the surface and have steam temperatures that range 150-500°C. Solfataras are steam vents that are rich in H_2S gases and transport these gases to the surface. Hot springs provide many electron donors to the hyperthermophilic microbial communities such as H_2, H_2S, and Fe(II) and electron acceptors such as O_2 and elemental sulfur. Hot springs are found in places like Yellowstone National Park in the U.S.; Hokkaido Island in Japan; Krýsuvík, Hveragerthi, and Kerlingarfjöll in Iceland; the White Island in New Zealand; the Kamchatka Peninsula in Russia; and Pisciarelli Solfatara in Italy (Chaban et al., 2006; Purcell et al., 2007; Swingley et al., 2012).

Research on thermophilic life in Yellowstone National park resulted in characterization of many new *Crenarchaeota* in the 1990's. H_2 metabolism is the major energy source in these springs, especially at higher temperatures. The H_2 in the fluids is geothermally produced by the interaction of meteoric water with Fe(II). O_2 and oxidized

sulfur species are the major electron acceptors. Extensive studies at Yellowstone National Park have shown that hot springs have a range of geochemical gradients due to variations in pH, temperatures of diffusing fluids, and trace element and ammonia concentrations that provide a large biotope for different hyperthermophilic microbes as observed with the *Aquificales*-rich "filamentous-streamer" communities and *Sulfolobales*, *Desulfurococcales*, and *Thermoproteales*-rich "archaeal-dominated sediments". Like hydrothermal vents, some of the earliest signs of life have been found in ancient hot spring deposits that are more than 3 billion years old (Inskepp et al., 2013; Jay et al., 2016).

Hot springs have a range of geochemical characteristics. Some fluids are O_2-rich and have a pH $\leq$ 2 and some fluids are anoxic, metal sulphide-rich and have a pH 4-6. Transition zones between them are often rich in elemental sulfur. The thermoacidophiles *Sulfolobus*, *Metallosphaera, Stygiolobus*, and *Acidianus* are found in acidic, Fe(II)- and O_2-rich fluids whereas *Desulfurococcus, Thermoproteus*, *Pyrobaculum*, and *Thermofilum* are found in neutral pH fluids. In the Pisciarelli solfatara, arsenate was shown to be an electron acceptor for *Pyrobaculum arsenaticum* in presence of $S_2O_3^{2-}$ and organic compounds. The Japanese coastal solfataric vents in Kodakara-Jima Island is where one of the first aerobic hyperthermophiles, *Aeropyrum pernix*, was isolated (Chaban et al., 2006).

1.2.3 Marine Sediments and Hydrocarbon Reservoirs

It was estimated that 35% of all marine sediments are above 60°C, suggesting that they provide a large habitat for thermophiles and hyperthermophiles (LaRowe et al., 2017). In these environments, buried organic material from the surface is likely to be the

carbon and energy sources for the high-temperature microbes that are present. This environment represents a new and largely unexplored habitat that may have an impact on the production and quality of natural gas and petroleum. Hyperthermophilic heterotrophs such as *Thermococcus* and *Pyrococcus* were the predominant microorganisms found in sediment cores collected offshore of New Zealand and Newfoundland, Canada (Roussel et al., 2008; Ciobanu et al., 2014). *Thermococcus* were also found in an uncontaminated oil reservoir in the Norwegian Sea, in a 90°C water-flooded oil well in China, and in Marcellus and Utica shale bed produced waters in western Pennsylvania (Daly et al., 2014; Lewin et al., 2014; Lin et al., 2014). These organisms may be participating in the degradation of buried organics with concomitant H_2 production. The organics and H_2 present also support the growth of other thermophiles and hyperthermophiles such as hydrogenotrophic methanogens like *Methanothermococcus* and sulfate reducers like *Archaeoglobus* (Topçuoglu et al., 2016). The methanogens may enrich hydrocarbon reservoirs with biogenic CH_4 making them more economically profitable while sulfate reducers can spoil a petroleum reservoir if too much H_2S is generated in the fluids (Nilsen et al., 1996). Preventing microbial oil spoilage can be accomplished by preventing the introduction of SO_4^{2-} into the well or by the addition of inhibitory compounds such as NO_3^-. The upper temperature limit for life in hydrocarbon reservoirs was previously estimated near 85°C but new studies expand these limits (Jørgensen, 2017).

1.2.4 Microbiology of Hot Biosphere Habitats

This thesis focuses on those microbes that grow without sunlight and optimally above 70°C. These microbes can be described based on their metabolic function such as methanogens, other autotrophs, H_2-producing heterotrophs, and thermoacidophiles as well as metabolic generalists from freshwater and marine environments that grow either autotrophically or heterotrophically and use numerous inorganic compounds to support their growth (Table 1).

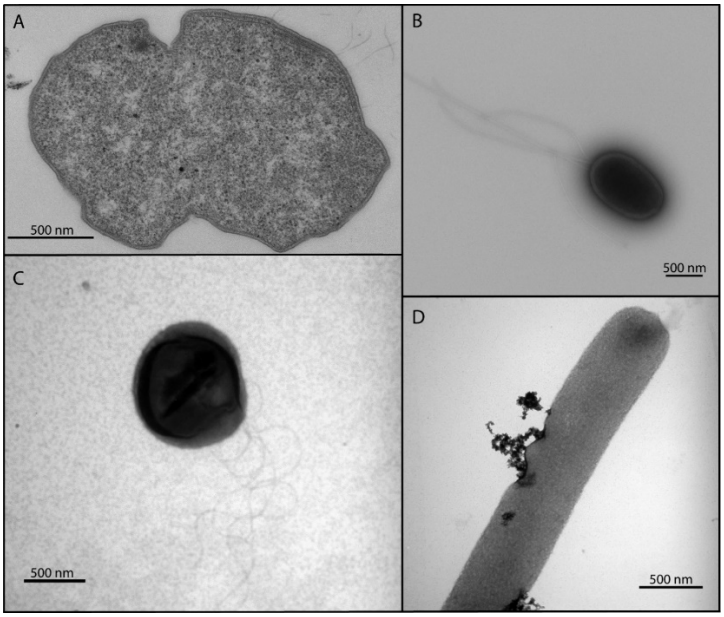

Figure 1 Electron micrographs of various thermophiles and hyperthermophiles. (A) Thin section of the hyperthermophilic methanogen *Methanocaldococcus bathoardescens* while undergoing cell replication. (B) The thermophilic, autotrophic sulfur reducer *Desulfurobacterium* sp strain HR11 with its flagella. (C) The hyperthermophilic marine generalist *Pyrodictium delaneyi* with its flagella. (D) The hyperthermophilic freshwater generalist *Pyrobaculum islandicum* shown with iron oxide mineral particles as part of its growth on iron.

1.2.3.1 Methanogens

Microbial methanogenesis is the largest source of methane globally with an annual production rate of one billion tons. All microbial methanogenesis is catalyzed by archaea and mediated by obligately anaerobic methanogens in the *Euryarchaeota*, although there is recent metagenomic evidence for possible methanogenesis in the *Bathyarchaeota* and *Verstraetearchaeota* (Evans et al., 2015; Vanwonterghem et al., 2016). Methanogens are most abundant in environments where alternative terminal electron acceptors such as SO_4^{2-}, NO_3^-, and metals are depleted. They generate CH_4 by using H_2 and CO_2, formate, methylated compounds, and acetate as carbon and energy sources (Borrel et al., 2016). The *Methanococcales*, *Methanobacteriales*, and *Methanopyrales* are the Orders that have representatives with optimal growth above 70°C (Table 1). Their growth is almost entirely hydrogenotrophic (*i.e.*, $4H_2 + CO_2 \rightarrow CH_4 + 2H_2O$), although a few species are capable of growth on formate. Like all methanogens, they couple methanogenesis to the Wood-Ljungdahl pathway for CO_2 fixation and energy conservation. The key enzyme in methanogenesis is methyl-CoM reductase, which serves as a genetic marker for methanogenesis in the environment (e.g., *mcrA*).

Methanocaldococcus (Fig. 1A) and *Methanotorris* are marine genera in the *Methanococcales* Order that grow best at temperatures of 80-88°C (Whitman and Jeanthon, 2006). *Methanocaldococcus jannaschii* is the most studied hyperthermophilic methanogen and was among the first microbes to have its complete genome sequenced. While N_2 fixation in high-temperature methanogens is unusual, *Methanocaldococcus* strain FS406-22 is the hottest known organism capable of this process (Mehta and Baross, 2006; Kim et al., 2015). The Order *Methanobacteriales* is divided into two

Families: the *Methanobacteriaceae* and the *Methanothermaceae*. The *Methanobacteriaceae* do not grow optimally above 70°C but include *Methanothermobacter* species that grow best around 65°C and are common in many mildly hot environments (Zeikus and Wolfe, 1972). In contrast, all *Methanothermaceae* grow optimally at 83-88°C (Bonin and Boone, 2006). Its sole genus is *Methanothermus*, whose species are the only hyperthermophilic methanogens found in terrestrial hot environments and grow up to 97°C (Stetter et al., 1981; Lauerer et al., 1986). The Order *Methanopyrales* has the highest optimal growth temperatures of any methanogen. *Methanopyrus kandleri* is marine and the only species in the Order. It is the hottest life form known anywhere with growth under hydrostatic pressure at temperatures up to 122°C (Takai et al., 2008).

1.2.3.2 Other Obligate Autotrophs

Other obligate autotrophs in hot environments include the *Aquificales* and the *Thermodesulfurobacteriales*, which are both bacteria (Table 1). They primarily use H_2 and sulfur compounds as their electron donor and acceptor, although there are a few facultative autotroph exceptions. The *Aquificales* grow optimally at 70-85°C and contains three Families: the *Aquificaceae*, the *Desulfurobacteriaceae*, and the *Hydrogenothermaceae*. With a few exceptions, the *Aquificaceae* are strict chemolithoautotrophs that fix CO_2 using the reductive tricarboxylic acid cycle and use H_2, $S_2O_3^{2-}$, and elemental sulfur as electron donors (Huber et al., 2001; Hügler et al., 2007). Most are microaerophiles that use low concentration of O_2 as a terminal electron acceptor, although sulfur compounds and NO_3^- can also be used as an electron acceptor (Huber et al., 2001; Eder and Huber, 2002). *Aquifex* uses O_2 as an electron acceptor at

very low concentrations, oxidizes H_2, and makes H_2O as the final product (i.e., Knallgas reaction) at temperatures up to 95°C (Huber et al., 2001). *Hydrogenivirga* and *Hydrogenobacter* use H_2, $S_2O_3^{2-}$, and elemental sulfur as electron donors and NO_3^- and O_2 as electron acceptors (Kawasumi et al., 1984; Shima and Suzuki, 1993; Nakagawa et al., 2004; Nunoura et al., 2008; Arai et al., 2010). *Thermocrinis* forms grey and pink filamentous masses in streams that are visible to the eye. *Thermocrinis albus* produces individual filaments up to 60 μm long, can also grow heterotrophically on formate and formamide under microaerophilic conditions (Huber et al., 2001; Eder and Huber, 2002).

The *Desulfurobacteriaceae* are strict anaerobes and chemolithoautotrophs that couple H_2 oxidation to the reduction of elemental sulfur, $S_2O_3^{2-}$, SO_3^{2-}, and NO_3^- (Holden, 2009). *Desulfurobacterium* (Fig. 1B) cells form filamentous masses that can be 8 cm in length (Alain et al., 2002). *Balnearium* only reduces elemental sulfur while *Thermovibrio* and *Phorcysia* reduce elemental sulfur as well as NO_3^- to NH_4^+ (Takai et al., 2003; Vetriani et al., 2004; Perez-Rodriguez et al., 2012).

The *Hydrogenothermaceae* are also strict chemolithoautotrophs, except for some *Sulfurihydrogenibium* that are facultative autotrophs (Nakagawa et al., 2005). *Persephonella* use H_2, $S_2O_3^{2-}$, and elemental sulfur as electron donors and elemental sulfur, NO_3^-, and O_2 as terminal electron acceptors (Reysenbach et al., 2002). *Sulfurihydrogenibium* are also metabolically versatile using these compounds plus Fe(II), arsenite, and selenite as electron donors and Fe(III), arsenate, and selenate as electron acceptors (Nakawaga et al., 2005). They are important in sulfur cycling and iron mineralization. In contrast, *Venenivibrio* species grow solely using H_2 and O_2 to make H_2O (Hetzer et al., 2008).

The *Thermodesulfurobacteriales* are mostly obligate autotrophs that grow best at 70-90°C, but a few are facultative autotrophs. *Caldimicrobium* use H_2 or ethanol as electron donors and $S_2O_3^{2-}$ or elemental sulfur as terminal electron acceptors (Miroshnichenko et al., 2009; Kojima et al., 2016). Freshwater *Caldimicrobium thiodismutans* and marine *Thermosulfurimonas dismutans* grow autotrophically by disproportionation of elemental sulfur, $S_2O_3^{2-}$, and SO_3^{2-} (Slobodkin et al., 2012; Kojima et al., 2016). *Thermosulfurimonas* fixes CO_2 using the Wood-Ljungdahl pathway (Mardanov et al., 2016). *Thermodesulfatator* are marine autotrophs that grow solely on SO_4^{2-} as an electron acceptor, while *Thermodesulfobacterium* are autotrophs that reduce SO_4^{2-}, SO_3^{2-}, $S_2O_3^{2-}$, or elemental sulfur (Alain et al., 2010; Hamilton-Brehm et al., 2013). Some *Thermodesulfobacterium* species can also use organic compounds as electron donors. *Geothermobacterium* are freshwater obligate iron reducers that couple H_2 oxidation with ferrihydrite reduction forming magnetite at temperatures up to 100°C, making them the hottest known bacteria (Kashefi et al., 2002).

1.2.3.3 Hydrogen Producers

High-temperature H_2 producers use a variety of organic substrates for growth, contain an unusually high number of glycosyl hydrolases and transferases, and in some cases use energetically favorable electron carriers such as ferredoxin that help the organisms overcome H_2 inhibition (Verhaart et al., 2010). Many of them also use sulfur compounds for growth and produce H_2 primarily in the absence of these electron acceptors. They can grow syntrophically with hydrogenotrophs through interspecies H_2 transfer (Bonch-Osmolovskaya and Stetter, 1991; Canganella and Jones, 1994; Muralidharan et al., 1997; Topçuoğlu et al., 2016).

Within the *Thermoanaerobacteriales*, *Caldicellulosiruptor* and *Thermoanaerobacter* are bacteria that grow optimally at 70-75°C with similar fermentation and H_2 generation pathways. *Caldicellulosiruptor* species degrade many organic compounds including lignocellulosic substrates and has high H_2 yields. They are studied extensively for potential biofuel production. *Thermoanaerobacter* is saccharolytic, but not cellulolytic, and reduces $S_2O_3^{2-}$ and elemental sulfur. Both genera use the Embden-Meyerhof pathway for sugar catabolism and generate H_2 using NADH-dependent hydrogenases. H_2 production is only possible at very low ambient H_2 concentrations. When H_2 concentrations increase, there is a shift to lactate production in *Caldicellulosiruptor* and ethanol in *Thermoanaerobacter*. In the *Thermotogales*, *Thermotoga* are bacteria that grow best at 70-80°C and catabolize sugars using the Embden-Meyerhof pathway to produce acetate, lactate, ethanol, CO_2, and H_2. They use a bifurcating enzyme, ferredoxin:NADH oxidoreductase, for H_2 generation and generate lactate when inhibited by H_2. *Thermotoga* will preferentially use elemental sulfur over protons as its terminal electron acceptor when it is available (Verhaart et al., 2010).

The *Thermococcales* are archaea in the *Euryarchaeota* that grow optimally at 80-100°C and either require or are stimulated by elemental sulfur. They are the most studied hyperthermophiles due to their industrial applications and ease of growth. They are often the source of DNA polymerases used for the polymerase chain reaction (PCR) and *in vitro* DNA replication. They all use a modified archaeal Embden-Meyerhof pathway for sugar catabolism that uses ADP-dependent rather than ATP-dependent hexokinases and phosphofructokinases as well as a ferredoxin-dependent glyceraldehyde-3-phosphate oxidoreductase in place of NADH-dependent glyceraldehyde-3-phosphate dehydrogenase

and ATP-producing 3-phosphoglycerate kinase (Verhees et al., 2003). This results in no net ATP production in this pathway. They also use ferredoxin-dependent oxidoreductases to catabolize peptides that are linked with NADH-producing glutamate dehydrogenase. *Pyrococcus furiosus* grows optimally at 100°C and is one of the most thoroughly studied hyperthermophiles. It preferentially reduces elemental sulfur to H_2S using a soluble disulfide reductase but also makes H_2 in the absence of sulfur. It uses a ferredoxin-dependent hydrogenase on its membrane to produce H_2 and generate a H^+/Na^+ gradient that is used for oxidative phosphorylation and ATP generation on the membrane. It also has a soluble NADH-dependent hydrogenase that is used for biosynthesis reactions (Adams et al., 2001). *Thermococcus* are widespread in hot marine environments with over 30 species in culture and more than 20 of their genomes sequenced (Hensley, 2015). They also preferentially reduce elemental sulfur to H_2S and in some cases protons to H_2 gas. In addition to the ferredoxin- and NADH-dependent hydrogenases found in *Pyrococcus*, some *Thermococcus* also have membrane-bound formate- and CO-dependent hydrogenases that expand the H_2 production and H^+/Na^+ translocation capabilities of these organisms (Kim et al., 2010, 2013; Bae et al., 2012; Schut et al., 2013; Topçuoğlu et al., 2018).

1.2.3.4 Marine Generalists

There are two Orders of marine generalist that are both archaea: the *Archaeoglobales* in the *Euryarchaeota* and the *Desulfurococcales* in the *Crenarchaeota*. They are obligate heterotrophs or facultative autotrophs that use a wide range of electron donors and acceptors. The *Archaeoglobales* reduce SO_4^{2-}, $S_2O_3^{2-}$, Fe(III), and NO_3^-; although elemental sulfur inhibits their growth. *Archaeoglobus* are facultative autotrophs

or heterotrophs that reduce SO_4^{2-} and $S_2O_3^{2-}$ to H_2S (Boone et al., 2001; Hartzell and Reed, 2006). In contrast, neither *Ferroglobus* nor *Geoglobus* can reduce SO_4^{2-} (Steinsbu et al., 2010). *Ferroglobus* species can oxidize Fe(II), H_2, H_2S, acetate, and aromatic compounds and reduce NO_3^-, $S_2O_3^{2-}$, Fe^{3+}-citrate, and ferrihydrite (Holden, 2009). *Geoglobus* species grow autotrophically by H_2 oxidation and are obligately dependent on either Fe^{3+}-citrate or ferrihydrite as terminal electron acceptors (Gaw Van Praagh et al., 2002; Kashefi et al., 2002; Slobodkina et al., 2009).

The *Desulfurococcales* are comprised of two families: the *Pyrodicteaceae* and the *Desulfurococcaceae*. The *Pyrodictiaceae* grow best at 90-106°C and often have unique cell structures that vary from coccoid to disk-shaped and the cells can form a network of cannulae that are tubular structures composed of glycoprotein subunits that connect the cells (Stetter et al., 1983). They are autotrophs, facultative autotrophs, and heterotrophs that sometimes require H_2 for growth and use a variety of terminal electron acceptors such as elemental sulfur, $S_2O_3^{2-}$, NO_3^-, O_2, and ferrihydrite (Lin et al., 2016). *Pyrolobus fumarii* is a strict H_2 oxidizing autotroph that reduces $S_2O_3^{2-}$, NO_3^-, and O_2 and can grow at temperatures up to 113°C (Blöchl et al., 1997). *Pyrodictium delaneyi* (Fig. 1C) reduces NO_3^- as well as ferrihydrite to the mineral magnetite (Lin et al., 2016). The *Desulfurococcaceae* have more genera than the *Pyrodicteaceae* and generally have cooler optimal growth temperatures of 85-95°C. They grow mixotrophically or heterotrophically (Caumette et al., 2015). *Desulfurococcus*, *Hyperthermus*, *Sulfophobococcus*, *Staphylothermus*, and *Thermosphaera* ferment sugars and peptides (Huber et al.; Fiala et al., 1986; Zillig et al., 1990; Hensel et al., 1997; Perevalova et al., 2005; Anderson et al., 2009). *Stetteria*, *Thermodiscus* and some *Desulfurococcus* species use organic

compounds to reduce elemental sulfur and generate H_2S, organic acids, and alcohols (Holden et al., 2009). They are obligate anaerobes except for *Aeropyrum pernix*, which is a microaerophile that respires O_2 (Sako et al., 1996). *Ignicoccus* species are strictly autotrophic elemental sulfur reducers that produce H_2S. *Ignicoccus hospitalis* forms a stable coculture with the archaeon *Nanoarchaeum equitans* that lives on the outer surface of *I. hospitalis* (Paper et al., 2007; Morris et al., 2013). *N. equitans*, in the *Nanoarchaeota*, has a genome size of 490 kb and a cell diameter of 350-500 nm. It lacks almost all known genes for lipid, cofactor, amino acid, and nucleotide biosynthesis and is completely dependent on *I. hospitalis* for survival (Waters et al., 2003; Das et al., 2006).

1.2.3.5 Freshwater Generalists

Like the marine generalists, freshwater generalists are all archaea that belong to the *Thermoproteales* in the *Crenarchaeota*. The *Thermoproteales* grow best at 75-100°C and consists of two families: the *Thermoproteaceae* and the *Thermofilaceae*. They can be distinguished from each other morphologically by the thickness of their cell size since *Thermofilum*, the only genus in the *Thermofilaceae*, form very thin (0.15-0.35 μm diameter) filaments. The *Thermoproteales* differ from other (hyper)thermophilic archaea in that they are rod-shaped instead of coccoids. They also form a unique 'golfclub' morphology where a spherical structure forms at the terminal end of the rod during certain growth conditions (Huber et al., 2006). *Pyrobaculum* (Fig. 1D) are the only members of the *Thermoproteaceae* that grow above 100°C. They are facultative autotrophs capable of growth on many terminal electron acceptors such as elemental sulfur, $S_2O_3^{2-}$, O_2, NO_3^-, NO_2^-, selenate, selenite, arsenate, glutathione, Fe^{3+}-citrate, and ferrihydrite (Völkl et al., 1993; Huber et al., 2000, 2006; Sako et al., 2001; Amo et al.,

2002; Feinberg et al., 2008). In contrast, *Thermoproteus* are facultative autotrophs that only respire elemental sulfur (Yim et al.; Bonch-Osmolovskaya et al., 1990; Huber et al., 2006; Siebers et al., 2011). *Vulcanisaeta*, *Caldivirga*, and *Thermocladium* are obligate heterotrophs that reduce elemental sulfur, SO_4^{2-}, and $S_2O_3^{2-}$ (Itoh et al., 1998, 1999; Nakase et al., 2002). *Caldivirga maquilingensis* and *Thermocladium modestius* are the only species in their genera, and both are also microaerophiles. Archaeal cell wall extract was shown to stimulate the growth of some *Thermofilum*, *T. modestius*, and *C. maquilingensis*, but the largest affect was observed on the growth of *Thermofilum pendens*. This latter organism is dependent upon the polar lipid extract of *Thermoproteus tenax* for growth (Zillig et al., 1983; Anderson et al., 2008).

1.2.3.6 Thermoacidophiles

Thermoacidophiles live in hot, acidic (pH <4) terrestrial environments. They are *Crenarchaeota* belonging to the *Acidilobales* and the *Sulfolobales*. The *Acidilobales* consist of the genera *Acidilobus* and *Caldisphaera*. Both are obligate anaerobes and heterotrophs that use sugars and peptides for growth and secrete short-chain fatty acids. Their growth is stimulated by elemental sulfur that they use to produce H_2S. *Acidilobus* live optimally at 80-85°C and pH 3.5-4.0, while *Caldisphaera* live optimally at 70-78°C and pH 3.5-4.5 (Prokofeva et al., 2000, 2009; Itoh et al., 2003; Huber and Stetter, 2006; Boyd et al., 2007). The *Sulfolobales* are more metabolically versatile than the *Acidilobales* and have an optimum pH near 2.0 (Huber and Prangishvili, 2006). They are facultative autotrophs that oxidize elemental sulfur, $S_2O_3^{2-}$, dithionite, Fe(II), metal sulphides, and H_2 while reducing O_2 or sulfur when growing autotrophically. Most *Sulfolobus* and all *Metallosphaera* species are aerobic, *Acidianus* and *Sulfurisphaera* are

facultative anaerobes, and *Stygiolobus* are anaerobic. *Stygiolobus* is the only obligate chemolithoatuotroph and grows by H_2 oxidation coupled with elemental sulfur reduction. *Acidianus* and *Sulfurisphaera* can both oxidize and reduce elemental sulfur. *Sulfolobus metallicus*, some *Acidianus* species, and *Metallosphaera sedula* can remove metals from metal sulphide minerals and have high resistance to metal toxicity (Segerer et al., 1986, 1991; Huber et al., 1989; Kurosawa et al., 1998; Jan et al., 1999; Huber and Prangishvili, 2006; Yoshida et al., 2006; Auernik et al., 2008).

Table 1 Hyperthemophilic Functional Groups by Order and their Characteristics

Functional groups by Order	Genera	T_{opt} (°C)	Carbon Sources	Electron Acceptors
Methanogens				
Methanobacteriales	*Methanothermus*	83-88	A	CO_2
Methanococcales	*Methanocaldococcus*, *Methanotorris*	80-88	A	CO_2
Methanopyrales	*Methanopyrus*	95-100	A	CO_2
Other obligate autotrophs				
Aquificales	*Aquifex*, *Balnearium*, *Caldimicrobium**, *Desulfurobacterium*, *Hydrogenivirga, Hydrogenobacter, Persephonella, Phorcysia, Sulfurihydrogenibium, Thermocrinis*, Thermosulfidibacter*, *Thermovibrio, Venenivibrio*	70-85	A	S°, $S_2O_3^{2-}$, O_2, NO_3^-, Fe(III), AsO_4^{3-}, SeO_4^{2-}
Thermodesulfobacteriales	*Geothermobacterium*, *Thermodesulfatator, Thermodesulfobacterium**, *Thermosulfurimonas*	70-90	A	S°, $S_2O_3^{2-}$, SO_4^{2-}, Fe(III)
H_2 producers				
Thermoanaerobacteriales	*Caldicellulosiruptor*, *Thermoanaerobacter*	70-75	H	H^+, S°, $S_2O_3^{2-}$
Thermococcales	*Pyrococcus*, *Thermococcus*	80-100	H	H^+, S°
Thermotogales	*Thermotoga*, *Fervidobacterium*	70-80	H	H^+, S°
Marine generalists				
Archaeoglobales	*Archaeoglobus*, *Ferroglobus*, *Geoglobus*	70-88	A, H, FA	SO_4^{2-}, $S_2O_3^{2-}$, NO_3^-, Fe(III)
Desulfurococcales	*Aeropyrum*, *Desulfurococcus*, *Hyperthermus*, *Ignicoccus*, *Ignisphaera*, *Pyrodictium*, *Pyrolobus*, *Staphylothermus*, *Stetteria*, *Sulfophobococcus*, *Thermodiscus*, *Thermogladius*, *Thermosphaera*	85-106	A, H, FA	H^+, S°, $S_2O_3^{2-}$, SO_3^{2-} Fe(III), NO_3^-, O_2

Freshwater generalists *Thermoproteales*	*Caldivirga*, *Pyrobaculum*, *Thermocladium*, *Thermofilum*, *Thermoproteus*, *Vulcanisaeta*	75-100	H, FA	O_2, S°, SO_4^{2-} $S_2O_3^{2-}$, NO_3^-, Fe(III), AsO_4^{3-}, SeO_4^{2-}
Thermoacidophiles *Acidilobales* *Sulfolobales*	 *Acidilobus*, *Caldisphaera* *Acidianus*, *Metallosphaera*, *Stygiolobus*, *Sulfolobus*, *Sulfurisphaera*	 70-85 70-85	 H A, FA	 S° S°, O_2, Fe(III)

1.3 Syntrophy Among Thermopiles

Microorganisms do not live in isolation but rather in complex communities and impact the environment around them through networks of interspecies interactions. Most laboratory-based studies on the physiology and biogeochemistry of high-temperature anaerobes have focused on pure cultures. It is likely that hyperthermophilic archaea, which are among the best extant representatives of early life on Earth (Nisbet and Sleep, 2001; Kelley et al., 2002; Stetter, 2006; Martin et al., 2008), diversified their cellular functions and became influenced by, and perhaps even dependent upon, each other under certain environmental conditions. However, our understanding of interspecies cell-cell interactions among extremophiles is very limited. We need to be able to model the physiological and biogeochemical behavior and cellular interactions of high-temperature microbial communities down to the molecular level.

H_2 syntrophy is a microbial interaction that is critical in carbon cycling at anoxic environments therefore it is crucial to understand the impact of H_2 syntrophy among thermophilic archaea and the energy production and carbon use of syntrophic microorganisms. In 1991, Bonch-Osmolovskaya and Stetter introduced the concept of interspecies H_2 transfer in cocultures of thermophilic archaea by establishing stable cocultures of marine heterotrophs *Thermococcus celer*, *Thermococcus stetteri*, *Staphylothermus marinus* and *Pyrococcus furiosus* with *Methanothermococcus thermolithotrophicus* or *Methancaldococcus jannaschii* (Bonch-Osmolovskaya and Stetter, 1991). Thermophilic heterotrophic archaeal isolates and hydrogenotrophic methanogenic archaeal isolates from the same hydrothermal vent fields have been shown to perform interspecies H_2 transfer in cocultures (Canganella and Jones, 1994; Ver Eecke

et al., 2012). Similarly, *Thermococcus* strains and hydrogenotrophic methanogen strains isolated from an oil pipeline that was > 70ºC also showed CH_4 production in cocultures through H_2 syntrophy (Davidova et al., 2012). This dissertation is the first report of H_2 syntrophy-driven methanogenesis within natural diffuse hydrothermal vent microbial communities at thermophilic or hyperthermophilic temperatures.

The physiology of the syntrophic partners and the mechanism and spatial organization of the syntrophic interactions are typically studied in cocultures of fatty acid oxidizing bacteria and hydrogenotrophic methanogens (Walker et al., 2012; Enoki et al., 2011; Luo et al., 2002; Ishii et al., 2005, 2006; Meyer et al., 2013). The proteomic and transcriptomic analyses in these studies highlight the metabolic flexibility of partners upon syntrophic growth but fall short on providing kinetic measurements to metabolic changes. This dissertation provides a comprehensive look on the adaptive physiology of syntrophic partners when they are grown alone and in coculture by providing kinetic measurements in tandem transcriptomic analyses.

1.4 Research Approach and Significance

This dissertation explores H_2 stress and syntrophy of hyperthermophilic heterotrophs and methanogens. First, it demonstrates that methanogenesis at hydrothermal vents is limited primarily by the availability of H_2 and that methanogenic H_2 syntrophy can occur in natural assemblages of thermophiles and hyperthermophiles. Then it shows the microbial taxa responsible for H_2 syntrophy in hydrothermal fluids and establishes a coculture among the dominant taxa. The syntrophs in the thermophilic coculture are H_2 producing heterotroph, *Thermococcus paralvinellae* and hydrogenotrophic methanogen *Methanocaldococcus jannaschii*. Furthermore, it

demonstrates how *T. paralvinellae* shifts its metabolism under H_2 stress; (1) kinetically in cells grown in a chemostat through enhanced growth yields and metabolite production rates, (2) transcriptionally through gene expression, and (3) through modeling the stoichiometric ratio of substrate, metabolites, and ATP generation in constraint-based metabolic network model. Then, it tests if H_2 syntrophy ameliorates H_2 stress (i.e., H_2 inhibition for the heterotroph, H_2 limitation for the methanogen) in the *M. jannaschii* and *T. paralvinellae* by exploring the shift in metabolism under H_2 stress and then comparing the kinetics and functional response during individual growth to *T. paralvinellae-M. jannaschii* cocultures.

The methodological approaches used in this thesis, namely differential gene expression of cocultures, constraint-based metabolic network modeling, and kinetic measurements in continuous growth cultures allow for a comprehensive analysis of microbial physiology that can be used by the subsurface geomicrobiology community. Through this and other similar studies, especially coculture experiments, we can better understand the growth, metabolite production, relationships, and competition between subseafloor microorganisms and provide context for the broad suite of metatranscriptomics data generated from field samples.

CHAPTER 2

HYDROGEN LIMITATION AND SYNTROPHIC GROWTH AMONG NATURAL ASSEMBLAGES OF THERMOPHILIC METHANOGENS AT DEEP-SEA HYDROTHERMAL VENTS

2.1 Abstract

Thermophilic methanogens are common autotrophs at hydrothermal vents, but their growth constraints and dependence on H_2 syntrophy *in situ* are poorly understood. Between 2012 and 2015, methanogens and H_2-producing heterotrophs were detected by growth at 80°C and 55°C at most diffuse (7-40°C) hydrothermal vent sites at Axial Seamount. Microcosm incubations of diffuse hydrothermal fluids at 80°C and 55°C demonstrated that growth of thermophilic and hyperthermophilic methanogens is primarily limited by H_2 availability. Amendment of microcosms with NH_4^+ generally had no effect on CH_4 production. However, annual variations in abundance and CH_4 production were observed in relation to the eruption cycle of the seamount. Microcosm incubations of hydrothermal fluids at 80°C and 55°C supplemented with tryptone and without H_2 showed CH_4 production indicating the capacity *in situ* for methanogenic H_2 syntrophy. 16S rRNA genes were found in 80°C microcosms from H_2-producing archaea and H_2-consuming methanogens, but not for any bacteria. In 55°C microcosms, sequences were found from the H_2-producing bacteria and H_2-consuming methanogens and sulfate-reducing bacteria. A coculture of representative organisms showed that *Thermococcus paralvinellae* supported the syntrophic growth of *Methanocaldococcus bathoardescens* at 82°C and *Methanothermococcus* sp. strain BW11 at 60°C. The results demonstrate that modeling of subseafloor methanogenesis should focus primarily on H_2

availability and temperature, and that thermophilic H_2 syntrophy can support methanogenesis within natural microbial assemblages and may be an important energy source for thermophilic autotrophs in marine geothermal environments.

2.2 Introduction

Approximately 1 Gt of CH_4 is formed globally per year from H_2, CO_2 and acetate through methanogenesis, largely by methanogens growing in syntrophic association with anaerobic microbes that hydrolyze and ferment biopolymers (Thauer et al., 2008). At deep-sea hydrothermal vents, methanogens are continuously flushed from the ocean crust where H_2 concentrations in hydrothermal fluids are high, but are scarce in low H_2 environments, as measured by culture-dependent techniques (Stewart et al., 2016), culture-independent techniques (Perner et al., 2007; Flores et al., 2011), and both techniques in tandem (Takai et al., 2004; Nakagawa et al., 2005; 2006; Takai et al., 2008; 2009; Ver Eecke et al., 2012; Lin et al., 2016). Thermophilic methanogens are consistently found in hydrothermal fluids at Axial Seamount, an active deep-sea volcano in the northeastern Pacific Ocean, and nearly all belong to the genera *Methanocaldococcus*, *Methanothermococcus*, and *Methanococcus* (Huber et al., 2002; Ver Eecke et al., 2012; Meyer et al., 2013; Fortunato and Huber, 2016). Axial Seamount erupted in 1998, 2011 and 2015 (Chadwick et al., 2012; 2013; Kelley et al., 2015), and basalt formed by these eruptions hosted hydrothermal niches that support methanogenesis (Huber et al., 2002; Meyer et al., 2013).

Hyperthermophilic heterotrophs capable of H_2 production, mostly *Thermococcales*, are generally co-localized with thermophilic and hyperthermophilic

methanogens in low-temperature hydrothermal vent fluids (Takai et al., 2004; Nakagawa et al., 2005; 2006; Takai et al., 2008; 2009; Flores et al., 2011; Ver Eecke et al., 2012; Lin et al., 2016). Some *Thermococcus* species produce H_2 and possess up to five different hydrogenases (Lee et al., 2008; Kim et al., 2010; 2013; Hensley et al., 2014; 2016) and may serve as an alternative source of H_2 for methanogens in low H_2 environments. Laboratory studies demonstrate that the lower H_2 threshold for the growth of *Methanocaldococcus* species at 70-82°C is 17-23 μM (Ver Eecke et al., 2012) and that H_2-producing hyperthermophilic heterotrophs can support the growth of pure *Methanocaldococcus* strains in the absence of added H_2 (Bonch-Osmolovskaya and Stetter, 1991; Canganella and Jones, 1994; Muralidharan et al., 1997; Johnson et al., 2006; Ver Eecke et al., 2012). However, there are no reports of H_2 syntrophy-driven methanogenesis within natural subseafloor microbial communities at thermophilic or hyperthermophilic temperatures. Other factors may also limit the growth of high-temperature methanogens *in situ*, e.g., nitrogen availability (Mehta and Baross, 2006; Ver Eecke et al., 2013), vitamins, or specific trace metal requirements as observed in terrestrial environments (Ünal et al., 2012). In some terrestrial anoxic environments, CH_4 formation is also inhibited when SO_4^{2-} concentrations are high (Lovley and Goodwin, 1988). Mesophilic sulfate-reducing bacteria have lower H_2 half-saturation constants for H_2 uptake and growth than mesophilic methanogens (Kristjansson et al., 1982; Lovley et al., 1982; Robinson and Tiedje, 1984; Karadagli and Rittman, 2005). This enables sulfate reducers to inhibit methanogen growth by lowering the partial pressure of H_2 to concentrations below levels that methanogens can use for growth.

The purpose of this study was to determine, among natural assemblages of thermophilic and hyperthermophilic methanogens, if methanogenesis at hydrothermal vents is limited primarily by the availability of H_2; if methanogenesis is stimulated by the addition of NH_4^+; and if H_2 syntrophy occurs when natural assemblages of thermophiles and hyperthermophiles are provided only with organic compounds as an energy source. Twenty low-temperature hydrothermal fluids and two nearby background seawater samples were collected from Axial Seamount. Time series samples were collected between and after the April 2011 and April 2015 volcanic eruptions at the site, and sampling included low-temperature vent sites formed by cooling lava flows from the eruptions. These field experiments and subsequent pure culture experiments demonstrate that thermophilic and hyperthermophilic methanogens are generally limited *in situ* by the availability of H_2, and that H_2 syntrophy can occur but is more likely at hyperthermophilic growth temperatures.

2.3 Methods

2.3.1 Field sampling

In August 2012, September and October 2013, August 2014, and August 2015, 7-40°C diffuse hydrothermal fluids were collected from 10 vent sites at 1515-1716 m depths from Axial Seamount on the Juan de Fuca Ridge (Figure 2). Descriptions of the fluid sample temperatures and the sample sites are provided in Table 2. The fluid samples were drawn into 650 ml Tedlar plastic bags with polyethylene valves within rigid housings using the NOAA Hydrothermal Fluid and Particle Sampler (Butterfield et al., 2004). The sampler pumped vent fluid through a titanium nozzle and recorded the

temperature of the fluid within the intake nozzle once every second during pumping. Samples were collected using the research submarines *Jason* II and *ROPOS*. Background seawater was collected by shipboard hydrocasts at 1500 m depth directly over the caldera (25 m above the bottom) and 3 km west of the summit with 10 L Niskin bottles (Figure 2). The hydrothermal fluid and background seawater samples were divided for cultivation-dependent Most Probable Number (MPN) concentration estimates of thermophiles and hyperthermophiles (100 ml), microcosm incubations (400 ml), and total cell counts (40 ml). All operations at sea occurred on the research vessels *Marcus G. Langseth*, *Thomas G. Thompson*, *Falkor*, and *Ronald H. Brown*.

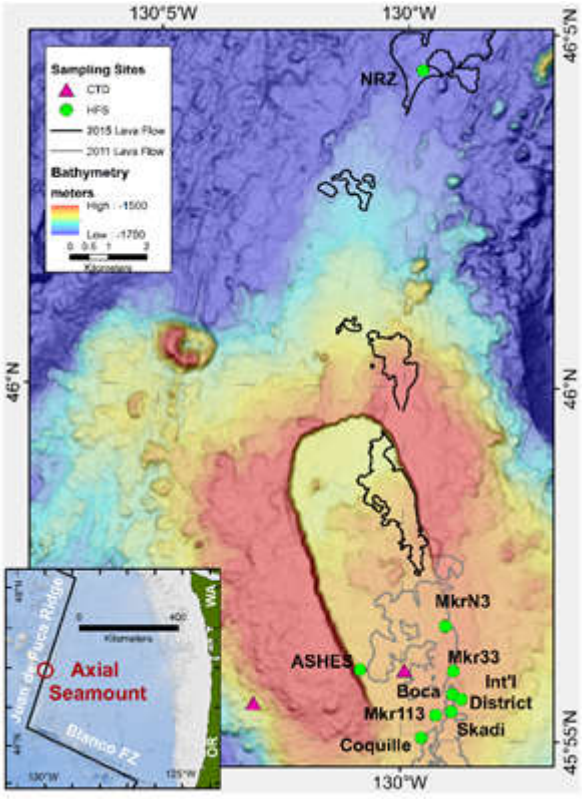

Figure 2 Map of Axial Seamount and the sample locations. The hydrothermal sampling sites were along the southeastern rim of the caldera, the western rim of the caldera (ASHES), and 10 km north of the caldera along the North Rift Zone (NRZ). Background seawater was collected 3 km west of the caldera at 1500 m depth and 25 m above the center of the caldera. The outlines of the 2011 and 2015 lava flows are from Caress et al. (2012) and Kelley et al. (2015). The inset shows the location of Axial Seamount in the NE Pacific Ocean.

Table 2 Description of Axial Seamount hydrothermal sampling sites.

Site	Description
Marker 113	Basalt-hosted diffuse hydrothermal vent field on the edge of a lava flow collapse zone (1521 m depth). The temperatures of the diffuse fluids were 28°C in 2012, 24°C in 2013, 25°C in 2014, and 25°C in 2015.
Marker 33	Basalt-hosted diffuse hydrothermal vent field flowing from the cooled 2011 eruptive lava flow (1516 m depth). The temperatures of the diffuse fluids were 27°C in 2013, 20°C in 2014, and 34°C and 40°C in 2015.
Anemone (ASHES)	Diffuse hydrothermal venting emanating from the top of a 0.5 m tall sulfide mound (1543 m depth) within 10 m of the Hell metal sulfide hydrothermal edifice emitting 286-297°C fluid. The temperatures of the diffuse fluids were 29°C in 2012 and 2013, 35°C in 2014, and 20°C in 2015.
Boca	Basalt-hosted diffuse hydrothermal vent field flowing from the cooled 2011 eruptive lava flow (1517 m depth). The temperatures of the diffuse fluids were 10°C in 2012 and 7°C in 2013.
Fuzzy Tubeworm Bush (ASHES)	Basalt-hosted diffuse hydrothermal venting (1544 m depth) within 10 m of the Inferno metal sulfide edifice emitting 319°C fluid. The temperature of the diffuse fluid was 28°C in 2012.
Skadi	Basalt-hosted diffuse hydrothermal vent field on the edge of a lava flow collapse zone within 10 m of a metal sulfide hydrothermal edifice emitting 218°C hydrothermal fluid (1521 m depth). The temperature of the diffuse fluid was 35°C in 2013.
International District	Diffuse hydrothermal venting emanating from the base and side of the El Guapo metal sulfide hydrothermal edifice emitting 342°C hydrothermal fluid (1515 m depth). The temperature of the diffuse fluid was 24°C in 2013.
Marker N3	Basalt-hosted diffuse hydrothermal vent field flowing from the cooled 2011 eruptive lava flow (1522 m depth). The temperature of the diffuse fluid was 19°C in 2013.
Coquille	Basalt-hosted diffuse hydrothermal venting (1533 m depth) within 10 m of the Vixen anhydrite-forming hydrothermal venting emitting 344°C hydrothermal fluid. The temperature of the diffuse fluid was 34°C in 2013.
North Rift Zone	Basalt-hosted diffuse hydrothermal vent field flowing from the cooled 2015 eruptive lava flow 15 km north of the axial summit caldera (1716 m depth). The temperature of the diffuse fluid was 19°C in 2015.

2.3.2 Microcosm incubations

For each sample site, 25 ml of hydrothermal fluid or background seawater was added without exposure to air to each of 16 sealed 60 ml serum bottles that had been pre-flushed with either H_2:CO_2 (80%:20%) or N_2:CO_2 (80%:20%), depending on the headspace composition used for incubation (Table 3).

Table 3 Description of microcosms. Each 60 ml serum bottle contained 25 ml of low-temperature diffuse hydrothermal fluid that was incubated in pairs at 55°C and 80°C.

Group	Years	Description
Set A (high H_2)	All	200 kPa H_2:CO_2 (80%:20%)
Set B (low H_2)	All	200 kPa N_2:CO_2 (80%:20%), 1 ml of headspace replaced with 1 ml of H_2:CO_2
Set C (no H_2)	All	200 kPa N_2:CO_2
Set D (high H_2 + NH_4^+)	2012-2013	200 kPa H_2:CO_2 plus 4.7 mM NH_4Cl (2012) or 47 μM NH_4Cl (2013)
Set E (no H_2, tryptone added)	2014-2015	200 kPa N_2:CO_2 plus 0.5% tryptone and 0.01% yeast extract

The bottles were divided into four sets of four bottles with a pair of bottles from each set incubated at 55°C and 80°C for up to a week or until visibly turbid. Three of the four sets of microcosms (sets A-C) were incubated each of the four study years. Set A was flushed and filled with 200 kPa of H_2:CO_2 yielding an estimated aqueous H_2 concentration of 1.2 mM at their incubation temperatures based on calculations using the geochemical prediction software Geochemist's Workbench. Sets B and C were flushed and filled with 200 kPa of N_2:CO_2, and half of these bottles (set B) were given 1 ml of H_2:CO_2 in exchange for 1 ml of N_2:CO_2 to produce an estimated aqueous H_2 concentration of 20 μM at their incubation temperatures. In 2012 and 2013, the remaining four serum bottles (set D) were amended with 4.7 mM NH_4Cl (2012 only) or 47 μM

NH_4Cl (2013 only) and flushed and filled with 200 kPa of H_2:CO_2 to test for growth stimulation by ammonium. The NH_4Cl concentration was based on that added to our defined methanogen growth medium (see below). In 2014 and 2015, the remaining four serum bottles (set E) were amended with 0.5% (wt vol^{-1}) tryptone plus 0.01% (wt vol^{-1}) yeast extract and flushed and filled with 200 kPa of N_2:CO_2 to test for H_2 syntrophy. All samples were reduced with 0.025% (wt vol^{-1}) each of cysteine-HCl and $Na_2S•9H_2O$. Growth of methanogens was determined by analyzing for CH_4 in the headspace using gas chromatography once the cells in the bottle had reached stationary growth phase. In 2015, an aliquot of the 80°C and 55°C tryptone/no H_2 samples (set E) that showed CH_4 production were filtered onto 0.2-µm pore size nucleopore filters prestained with Irgalan black (Sterlitech, Kent, WA), stained with acridine orange (Francisco et al., 1973), and examined using epifluorescence microscopy. In 2015, the 80°C and 55°C tryptone/no H_2 samples from the Marker 113 vent site were also separately filtered through Sterivex GP 0.22 µm sterile filter units (Millipore, Billerica, MA) and frozen at -80°C until analyzed. In 2015, 10 ml of hydrothermal fluid was added to sealed Balch tubes without exposure to air, amended separately with 0.1% (wt vol^{-1}) sodium formate and 0.5% (wt vol^{-1}) sodium acetate, flushed and filled with 200 kPa N_2:CO_2, and incubated in duplicate at 80°C and 55°C for up to seven days to determine if these substrates can support methanogenesis at high temperatures.

Total cell counts in the original hydrothermal fluids were done by preserving in duplicate 18 ml of hydrothermal fluid with 1.8 ml of 37% formaldehyde. Samples were stored at 4°C for less than a month prior to counting by epifluorescence microscopy as described above.

2.3.3 DNA extraction and 16S rRNA amplicon sequencing

In this study and elsewhere (Butterfield et al., 2004; Mehta and Baross, 2006; Ver Eecke et al., 2012; 2013; Fortunato and Huber, 2016), Marker 113 vent showed the highest concentrations of methanogens and methanogenesis at Axial Seamount. Therefore, DNA from each 2015 Marker 113 microcosm that had been amended with tryptone (i.e., set E) and concentrated with a Sterivex filter was extracted and eluted using the MoBio PowerWater DNA extraction kit (MoBio, Carlsbad, CA) as described by the manufacturer to determine which methanogens and other microorganisms were present following the microcosm incubations. The DNA was quantified using a Nanodrop 2000 spectrophotometer (Thermo Scientific, Wilmington, DE) and stored at -20°C. The v4v5 regions of the 16S rRNA gene were amplified separately for bacteria and archaea and prepared for Illumina sequencing from the DNA extractions. Bacterial amplification was carried out as previously described (Huse et al., 2014). The archaeal v4v5 16S rRNA gene was targeted by a combination of five forward primer variants (517F; GCCTAAAGCATCCGTAGC, GCCTAAARCGTYCGTAGC, GTCTAAAGGGTCYGTAGC, GCTTAAAGNGTYCGTAGC, GTCTAAARCGYYCGTAGC) and a single reverse primer (958R; CCGGCGTTGANTCCAATT). Amplification primers were designed based on information from probeBase (Alm et al., 1996; Loy et al., 2003; Huber et al., 2007) and the SILVA database (Ludwig et al., 2004). 16S rRNA amplicon sequencing was performed using an Illumina MiSeq Benchtop sequencer (Illumina, San Diego, CA) at the Marine Biological Laboratory in Woods Hole, MA as described on the Visualization and Analysis of Microbial Population Structures (VAMPS) website

(https://vamps.mbl.edu/resources/primers.php). Paired-end sequences were assessed for quality and merged using the code base previously described (Eren et al., 2013). The sequences were binned into operational taxonomic units (OTUs) using subsampled open reference OTU picking method at 97% sequence identity based on the Greengenes database and taxonomies assigned using the RDP Classifier (Wang et al., 2007) with minimum confidence score 0.8 in QIIME (Caporaso et al., 2010). Sequences are available at the NCBI Sequence Read Archive under accession number SRP071807.

2.3.4 Growth Media

The defined methanogen growth medium for laboratory experimentation and MPN analyses was a modification of DSM 282 medium (Jones et al., 1983; Ver Eecke et al., 2012), which contained (per liter in ddH_2O): 0.14 g of K_2HPO_4, 0.14 g of $CaCl_2•7H_2O$, 0.25 g of NH_4Cl, 3.4 g of $MgSO_4•7H_2O$, 5.1 g of $MgCl_2•6H_2O$, 0.34 g of KCl, 0.05 mg of $NiCl_2•6H_2O$, 0.05 mg of $Na_2SeO_3•5H_2O$, 30 g of NaCl, 1 g of $NaHCO_3$, 1 g of NaS_2O_3, 0.24 g of $Na_2MoO_4•2H_2O$, 10 ml of Wolfe's minerals, 10 ml of Wolfe's vitamins, and 0.25 mg of resazurin. For the 2012 MPNs, 0.24 g of $Na_2MoO_4•2H_2O$ was also added to suppress sulfate reduction but was omitted in subsequent years. The medium was pH balanced to 6.0, reduced with 0.025% each of cysteine-HCl and $Na_2S•9H_2O$, and pressurized with 200 kPa of H_2:CO_2 headspace. The autotrophic sulfur-reducer medium was the same as the methanogen medium except that 10 g l^{-1} of elemental sulfur were added and the medium was reduced with 3.2 mM dithiothreitol (DTT). The heterotroph medium for MPN estimates was based on the Adams medium (Adams et al., 2001) and contained 0.5% tryptone plus 0.01% yeast extract. It was pH balanced at 6.8, reduced with 0.025% each of cysteine-HCl and $Na_2S•9H_2O$, and

pressurized with 100 kPa of N_2:CO_2 headspace. The heterotroph-methanogen coculture medium was the modified DSM 282 medium with 0.1 ml of 10 mM Na_2WO_4•$2H_2O$, 1 ml of 0.2% $(NH_4)_2Fe(SO_4)_2$-$(NH_4)_2Ni(SO_4)_2$, and 0.5% tryptone plus 0.01% yeast extract added with 200 kPa of N_2:CO_2 headspace. The medium was pH balanced to 6.8.

2.3.5 Most Probable Number (MPN) cell estimates

Three-tube MPN analyses were used by adding 3.3 ml, 0.33 ml, and 0.03 ml of the hydrothermal fluid samples in triplicate to 10 ml of the methanogen, autotrophic sulfur reducer, and heterotroph media as previously described (Ver Eecke et al., 2009). After inoculation, the tubes were incubated at 80°C and 55°C for up to 7 days. Growth in the tubes was confirmed using phase-contrast light microscopy. Growth of methanogens and H_2-producing heterotrophs was verified by analyzing all the tubes for CH_4 and H_2, respectively, in the headspace using gas chromatography. Total and H_2-producing heterotroph cell concentration estimates were scored and reported separately based on tubes that had cells versus those with H_2. To estimate the concentration of non-methanogenic autotrophs in the autotrophic sulfur medium, the estimated number of methanogens in the autotrophic sulfur medium MPN tubes was subtracted from the estimated concentration of total cells.

2.3.6 Pure and coculture growth conditions

Methanocaldococcus bathoardescens JH146 (DSM 27223) (Ver Eecke et al., 2013; Stewart et al., 2015), *Methanothermococcus* sp. strain BW11 (DSM 100453) (Stewart et al., 2016), and *Thermococcus paralvinellae* ES1 (DSM 27261) (Pledger and Baross, 1989; Hensley et al., 2014; 2016) were used for pure and coculture experiments

from our hyperthermophile culture collection. *Methanocaldococcus jannaschii* JAL-1 (DSM 2661) (Jones et al., 1983) and *Methanothermococcus thermolithotrophicum* (DSM 2095) (Huber et al., 1982) were purchased from the Deutsche Sammlung von Mikrooganismen und Zellkulturen GmbH (DSMZ, Braunschweig, Germany).

M. jannaschii and *M. bathoardescens* were grown at 80°C and *M. thermolithotrophicum* and *Methanothermococcus* sp. strain BW11 were grown at 55°C in 25 ml of modified DSM 282 methanogen medium in 60 ml serum bottles with 200 kPa of H_2:CO_2 for up to 5 days to compare their maximum CH_4 production amounts with those of the field microcosms. *M. jannaschii* and *M. thermolithotrophicum* were grown at 82°C and 65°C, respectively, in the methanogen medium described above minus cysteine and all other sources of nitrogen with varying concentrations of NH_4Cl to determine the effect of nitrogen availability. *M. jannaschii* and *M. bathoardescens* were also grown at 82°C in Balch tubes in modified DSM 282 medium without added vitamins following five transfers on vitamin-free medium to determine the effect of vitamins on their growth.

For each growth kinetic experiment, 18 Balch tubes containing growth medium were inoculated simultaneously with a logarithmic growth phase culture that had been transferred three times on that medium and incubated in a forced-air incubator. Three tubes were permanently removed from the incubator at various time points. The cell concentration in each tube was determined using a Petroff-Hausser counting chamber and phase contrast light microscopy. The growth rate (μ) of the culture was determined by fitting an exponential curve to the growth data. The total amount of CH_4 in each tube that had been cooled to room temperature was determined by measuring the volume of gas in each tube and the amount of CH_4 in 100 μl of headspace using gas chromatography. The

CH_4 production yield ($Y_{p/x}$) was determined from the slope of the amount of CH_4 per tube plotted against the total number of cells per tube. The rate of CH_4 production per cell is calculated from $Y_{p/x} \times \mu/0.693$ as previously described (Ver Eecke et al., 2013). The 95% confidence intervals for growth and CH_4 production rates were calculated as previously described (Zar, 1996).

T. paralvinellae was grown separately on the coculture base medium described above with either 0.5% tryptone plus 0.01% yeast extract; 0.5% maltose plus 0.01% yeast extract; or 0.5% each of tryptone and maltose plus 0.01% yeast extract media, each with 200 kPa of N_2:CO_2 headspace, at 82°C and 60°C to determine how temperature affects its rate of H_2 production on various substrates. The rate of H_2 production was measured as described above for the rate of CH_4 production by the methanogens. For the coculture experiments, *T. paralvinellae* was grown alone at 82°C and 60°C, in coculture with *M. bathoardescens* at 82°C, and in coculture with *Methanothermococcus* sp. strain BW11 at 60°C in 160 ml serum bottles containing 50 ml of modified DSM 282 medium supplemented with 0.5% each of maltose and tryptone plus 0.01% yeast extract with 200 kPa of N_2:CO_2 headspace. The heterotrophs and methanogens were combined during inoculation in a 10:1 cell ratio. The coculture was established immediately and did not require prior coculture transfers. At various time points during growth, the amount of H_2 and CH_4 was measured from triplicate incubation bottles using gas chromatography.

2.4 Results

2.4.1 MPN cell estimates in hydrothermal fluids

In 2012, the concentrations of all thermophiles and hyperthermophiles in all samples were very low compared to the concentrations in subsequent years (Table 4). In 2013, methanogens that grew at 80°C were detected in low-temperature hydrothermal fluids at Marker 113, Marker 33, ASHES, Boca and Skadi. They were not detected in vent fluids from Coquille, Marker N3 or the International District (Table 4). Methanogens that grew at 55°C were found at lower concentrations at Marker 113, Marker 33, ASHES, Boca, Skadi, Marker N3, and Coquille, but were not detected at the International District (Table 4). Heterotrophs that grew at 80°C and 55°C were present in relatively high concentrations at each vent site in 2013 (Table 4). The concentrations of heterotrophs that produced H_2 were lower at 330-7,200 cells L^{-1} at 80°C, and only Marker 113 and Boca showed any H_2 producing heterotrophs at 55°C, which were at low concentrations (120-270 cells L^{-1}). The heterotrophs that grew at 80°C were all coccoids, while those that grew at 55°C were predominantly rods. Non-methanogenic autotrophs that grew at 80°C and 55°C were also present at most of the vent sites in 2013 (Table 4).

The Marker 113, Marker 33 and ASHES vent sites were selected for time series measurements in 2014 and 2015 (Table 4). During those years, methanogens that grew at 80°C were found at each site. From 2012 to 2015, methanogens that grew at 55°C increased in abundance from not detectable to 33,000 cells L^{-1} at Marker 113, were not detectable at Marker 33 in 2015, and were consistently present at relatively low concentrations at ASHES. Heterotrophs that grew at 80°C and 55°C were often present in high concentrations, but in 2015 decreased significantly in concentration at 80°C at

Marker 113 and at 55°C at Marker 113 and Marker 33. The concentrations of H_2-producing heterotrophs that grew at 80°C was relatively high at all three vents in 2014 but decreased significantly in 2015. Similarly, H_2-producing heterotrophs that grew at 55°C were higher in concentration at the three vents in 2014 than in 2015. As in 2013, the heterotrophs that grew at 80°C were all coccoids, while those that grew at 55°C were predominantly rods. From 2013 to 2015, non-methanogenic autotrophs decreased in concentration at 80°C and 55°C at Marker 113 until they were no longer detectable, increased in concentration at 80°C at Marker 33, and remained relatively constant at ASHES. At the North Rift Zone eruption site in 2015, there were 2,790 methanogens L^{-1} that grew at 80°C and 33,000 methanogens L^{-1} that grew at 55°C (Table 4). No non-methanogenic autotrophs grew at either 80°C or 55°C from North Rift Zone fluids. No methanogens, heterotrophs or non-methanogenic autotrophs grew at either 80°C or 55°C from background seawater collected at 1,500 m depth 3 km away from the seamount summit or 25 m above the summit caldera, except for 90 heterotrophs L^{-1} that grew at 55°C from over the caldera (Table 4).

Table 4 Most-probable number (MPN, L^{-1}) estimates of heterotrophs, H_2-producing heterotrophs, methanogens, and non-methanogenic hydrogenotrophs that grow at 55°C and 80°C. [a]ND, not detected. [b]Total cell concentration for the hydrothermal fluid sample prior to incubation.

	80°C				55°C			
	2012	2013	2014	2015	2012	2013	2014	2015
Marker 113								
Heterotrophs	2,790	>33,000	>33,000	1,140	ND[a]	>33,000	>33,000	1,140
H_2-prod. heterotrophs	220	330	33,000	ND	ND	120	2,250	276
Methanogens	120	1,050	6,300	1,140	ND	330	13,800	33,000
Other autotrophs	102	5,220	ND	ND	270	5,610	1,350	ND
Initial total cells ($\times 10^8$, L^{-1})[b]	3.4	5.4	8.5	15.0				
Marker 33								
Heterotrophs	-	>33,000	>33,000	33,000	-	>33,000	>33,000	1,290
H_2-prod. heterotrophs	-	7,200	4,500	ND	-	ND	840	108
Methanogens	-	13,800	13,800	1,290	-	330	2,790	ND
Other autotrophs	-	ND	ND	33,000	-	32,310	4,224	13,800
Initial total cells ($\times 10^8$, L^{-1})	-	2.8	9.6	8.1				
Anemone (ASHES)								
Heterotrophs	7,200	13,800	>33,000	>33,000	690	7,200	>33,000	13,800
H_2-prod. heterotrophs	2,790	1,290	1,290	120	ND	ND	13,800	450
Methanogens	ND	276	1,290	1,290	ND	690	120	450
Other autotrophs	276	1,170	2,340	13,680	270	2,670	4,500	4,380
Initial total cells ($\times 10^8$, L^{-1})	0.8	4.1	9.4	10.0				
Boca								
Heterotrophs	690	>33,000	-	-	270	>33,000	-	-
H_2-prod. heterotrophs	ND[a]	ND	-	-	ND	270	-	-
Methanogens	ND	276	-	-	120	276	-	-
Other autotrophs	270	120	-	-	330	630	-	-
Initial total cells ($\times 10^8$, L^{-1})[b]	2.3	5.0	-	-				
Fuzzy Tubeworm Bush (ASHES)								
Heterotrophs	2,790	-	-	-	270	-	-	-
H_2-prod. heterotrophs	2,790	-	-	-	270	-	-	-
Methanogens	ND	-	-	-	ND	-	-	-
Other autotrophs	1,290	-	-	-	6,300	-	-	-
Initial total cells ($\times 10^8$, L^{-1})		-	-	-				
Skadi								
Heterotrophs	-	3,600	-	-	-	>33,000	-	-

H_2-prod. heterotrophs	-	330	-	-	-	ND	-	-
Methanogens	-	13,800	-	-	-	450	-	-
Other autotrophs	-	1,080	-	-	-	690	-	-
Initial total cells ($\times 10^8$, L^{-1})	-	5.6	-	-				
International District								
Heterotrophs	-	>33,000	-	-	-	>33,000	-	-
H_2-prod. heterotrophs	-	120	-	-	-	ND	-	-
Methanogens	-	ND	-	-	-	ND	-	-
Other autotrophs	-	210	-	-	-	4,500	-	-
Initial total cells ($\times 10^8$, L^{-1})	-	0.68	-	-				
Marker N3								
Heterotrophs	-	>33,000	-	-	-	>33,000	-	-
H_2-prod. heterotrophs	-	ND	-	-	-	ND	-	-
Methanogens	-	ND	-	-	-	120	-	-
Other autotrophs	-	120	-	-	-	720	-	-
Initial total cells ($\times 10^8$, L^{-1})	-	4.1	-	-				
Coquille								
Heterotrophs	-	6,300	-	-	-	6,300	-	-
H_2-prod. heterotrophs	-	ND	-	-	-	ND	-	-
Methanogens	-	ND	-	-	-	690	-	-
Other autotrophs	-	840	-	-	-	6,300	-	-
Initial total cells ($\times 10^8$, L^{-1})	-	1.4	-	-				
North Rift Zone								
Heterotrophs	-	-	-	-	-	-	-	-
H_2-prod. heterotrophs	-	-	-	-	-	-	-	-
Methanogens	-	-	-	2,790	-	-	-	33,000
Other autotrophs	-	-	-	ND	-	-	-	ND
Initial total cells ($\times 10^8$, L^{-1})	-	-	-	3.7				
CTD cast 25 m over caldera								
Heterotrophs	-	-	ND	-	-	-	90	-
H_2-prod. heterotrophs	-	-	ND	-	-	-	ND	-
Methanogens	-	-	ND	-	-	-	ND	-
Other autotrophs	-	-	ND	-	-	-	ND	-
Initial total cells ($\times 10^8$, L^{-1})	-	-	0.76	-				
CTD cast off-summit (1,500 m)*								
Heterotrophs	ND	-	-	-	ND	-	-	-

H_2-prod. heterotrophs	ND	-	-	-	ND	-	-	-
Methanogens	ND	-	-	-	ND	-	-	-
Other autotrophs	ND	-	-	-	ND	-	-	-
Initial total cells ($\times 10^8$, L^{-1})	0.25	-	-	-				

2.4.2 Growth in microcosms on H_2, CO_2 and NH_4^+

In 2012, consistent with the MPN concentration estimates, no CH_4 was detected in any of the microcosms at either 80° or 55°C, except for one high H_2 microcosm and one low H_2 microcosm incubated at 80°C from Marker 113. In 2013, CH_4 production occurred in microcosms amended with H_2, CO_2 and NH_4Cl at 80°C in hydrothermal fluids from Marker 113, ASHES, Marker 33 and Skadi with up to 31.6 mmol CH_4 produced L^{-1} of vent fluid (Figure 3A). Methanogenesis also occurred in microcosms at 55°C in fluids from the same sites plus Boca vent with up to 31.0 mmol CH_4 produced L^{-1} (Figure 3B). The amount of CH_4 produced when only 1 ml of H_2:CO_2 (20 µM H_2) was added to each bottle was 1-3% the amount of CH_4 produced when 200 kPa of H_2:CO_2 were added (Figure 3). The amount of CH_4 produced when the microcosms were amended with 47 µM NH_4Cl in addition to 200 kPa of H_2:CO_2 was generally the same as the amount of CH_4 produced when only 200 kPa of H_2:CO_2 were added, with the exceptions of the microcosms from ASHES at both incubation temperatures and from Marker 33 incubated at 55°C (Figure 3). Consistent with the MPNs, there was no methanogenesis at 80°C and 55°C in hydrothermal fluids from Marker N3 and the International District, nor in either background seawater sample. There was no CH_4 in any 80°C or 55°C microcosms amended only with N_2:CO_2. For comparison, the total amounts of CH_4 produced by *M. bathoardescens* and *M. jannaschii* grown to stationary growth phase at 82°C in modified DSM 282 methanogen medium were the same as the 80°C microcosms (Figure 3A). Similarly, the total amounts of CH_4 produced by *M. thermolithotrophicum* and *Methanothermococcus* sp. strain BW11 at 55°C were the same as the 55°C microcosms (Figure 3B).

M. jannaschii grown at 82°C and *M. thermolithoautotrophicum* grown at 65°C at varying NH_4Cl concentrations in otherwise nitrogen-free medium did not show any change in cell specific CH_4 production rate in medium with 47 µM to 9.4 mM NH_4Cl added (Figure 4, Table 5). Furthermore, the growth rates of *M. jannaschii* and *M. bathoardescens* grown at 82°C without vitamins were 1.19 h^{-1} ± 0.32 h^{-1} (± 95% confidence interval) and 2.74 h^{-1} ± 1.01 h^{-1}, respectively, and were not significantly different than the rates for each organism with added vitamins.

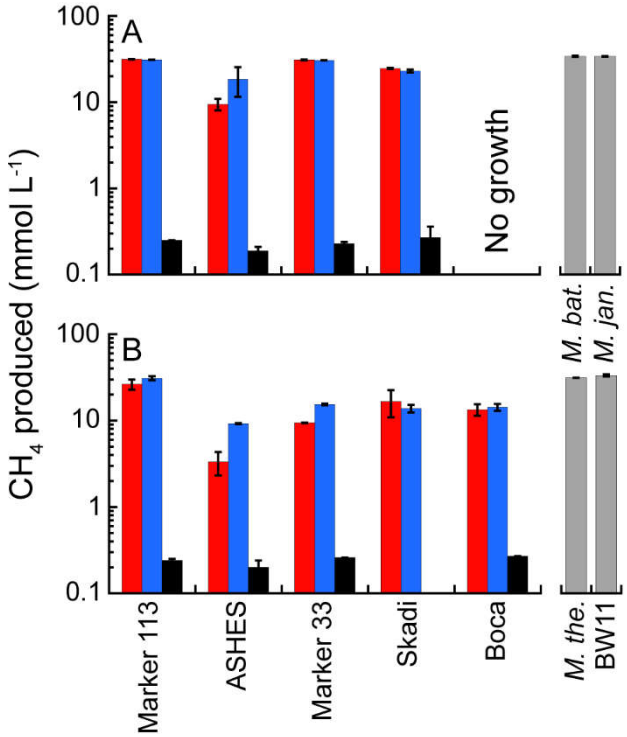

Figure 3 Average total CH_4 production in 2013 microcosms. The microcosms were incubated at 80°C (A) and 55°C (B) and amended with 200 kPa of H_2:CO_2 (red); 200 kPa of H_2:CO_2 plus 47 µM NH_4Cl (blue); and 2 kPa of H_2 and 198 kPa of N_2:CO_2 (black). The grey columns show the total CH_4 production for the four pure cultures in modified DSM 282 medium for comparison. The sample bars represent the range of the duplicate incubations.

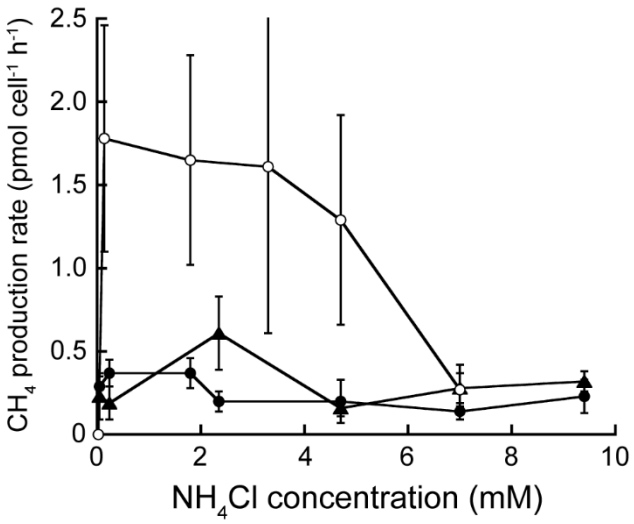

Figure 4 Cell-specific rate of CH_4 production at varying NH_4Cl concentrations. *M. jannaschii* (●) and *M. bathoardescens* (○) were grown at 82°C, and *M. thermolithotrophicum* (▲) was grown at 65°C. The data for *M. bathoardescens* are from Ver Eecke et al. (2013) and are provided for comparison. The error bars represent the 95% confidence intervals.

Table 5 Growth rate, cell yield based on methane production and cell specific CH_4 production rate for *Methanocaldococcus jannaschii*, *Methanothermococcus thermolithotrophicus*, *Methanocaldococcus bathoardescens* (from Ver Eecke *et al.*, 2013) grown with varying concentrations of NH_4Cl in otherwise nitrogen-free medium. The error represents the 95% confidence interval ($\alpha = 0.05$).

NH_4Cl Concentration	Growth rate (k) (h^{-1})	Yield (Y) (10^{12} cells mol^{-1} CH_4)	CH_4 Prod. Rate (v) (pmol CH_4 $cell^{-1}$ h^{-1})
M. jannaschii:			
47 μM	0.84 ± 0.08	4.14 ± 0.81	0.29 ± 0.06
235 μM	0.79 ± 0.14	3.10 ± 0.44	0.37 ± 0.08
1.8 mM	1.12 ± 0.24	4.04 ± 0.53	0.37 ± 0.09
2.4 mM	0.94 ± 0.16	6.63 ± 1.68	0.20 ± 0.06
4.7 mM	0.64 ± 0.28	4.71 ± 2.15	0.20 ± 0.13
7.0 mM	0.87 ± 0.30	9.21 ± 1.35	0.14 ± 0.05
9.4 mM	0.96 ± 0.34	6.13 ± 1.61	0.23 ± 0.10
M. thermolithotrophicus:			
47 μM	0.75 ± 0.28	4.61 ± 2.10	0.23 ± 0.14
235 μM	0.73 ± 0.18	5.57 ± 2.66	0.19 ± 0.10
2.4 mM	0.64 ± 0.14	1.51 ± 0.43	0.61 ± 0.22
4.7 mM	0.99 ± 0.27	8.79 ± 1.51	0.16 ± 0.05
7.0 mM	0.97 ± 0.24	5.03 ± 2.16	0.28 ± 0.14
9.4 mM	0.78 ± 0.13	3.57 ± 0.36	0.32 ± 0.06
M. bathoardescens:			
24 μM	0	0	0
140 μM	1.53 ± 0.35	1.24 ± 0.38	1.78 ± 0.68
1.8 mM	1.78 ± 0.49	1.56 ± 0.41	1.65 ± 0.63
3.3 mM	1.93 ± 0.86	1.73 ± 0.75	1.61 ± 1.00
4.7 mM	1.72 ± 0.52	1.92 ± 0.74	1.29 ± 0.63
7.0 mM	1.73 ± 0.39	9.26 ± 2.78	0.27 ± 0.10

2.4.3 H_2 syntrophy in microcosms

In 2014, methanogenesis occurred in microcosms amended with 200 kPa of H_2:CO_2 or separately with tryptone plus N_2:CO_2 at 80°C and 55°C in hydrothermal fluids from Marker 113, ASHES and Marker 33 with up to 9.5 mmol CH_4 produced L^{-1} (Figure 5). The amount of CH_4 produced was lower and less consistent than observed in 2013 and 2015.

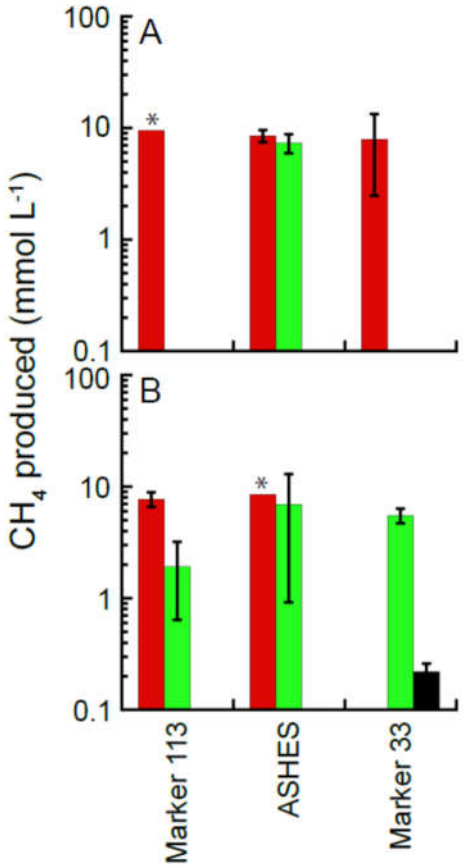

Figure 5 Average total CH_4 production in 2014 microcosms. The microcosms were incubated at 80°C (A) and 55°C (B) and amended with 1.6 atm of H_2 and 0.4 atm of CO_2 (red); 1.6 atm of N_2, 0.4 atm of CO_2, 0.5% tryptone and 0.01% yeast extract (green); and 0.02 atm H_2, 1.58 atm of N_2, and 0.4 atm of CO_2 (black). The sample bars represent the range of the duplicate incubations. The asterisks show where there was growth in only one microcosm bottle.

In contrast, in 2015 methanogenesis occurred at 80°C in hydrothermal fluids from Marker 113, ASHES, Marker 33 and the North Rift Zone eruption site with up to 49.3

mmol CH_4 produced L^{-1} (Figure 6A). Methanogenesis occurred at 55°C in hydrothermal fluids from Marker 113, ASHES, and the North Rift Zone with up to 38.2 mmol CH_4 produced L^{-1} (Figure 6B). Similar to MPN observations, there was no methanogenesis at 55°C in two separate sets of microcosms containing fluid from Marker 33 that were amended only with 200 kPa of H_2:CO_2 (Figure 6B). As seen in 2013, the amount of CH_4 produced in 2015 when only 1 ml of H_2:CO_2 was added to each bottle was 1-3% the amount of CH_4 produced when 200 kPa of H_2:CO_2 were added (Figure 6). The amount of CH_4 produced when microcosms were amended with tryptone plus N_2:CO_2 was 4.7-11.4 mmol L^{-1} at 80°C and was less (1.1-2.0 mmol L^{-1}) at 55°C (Figure 6).

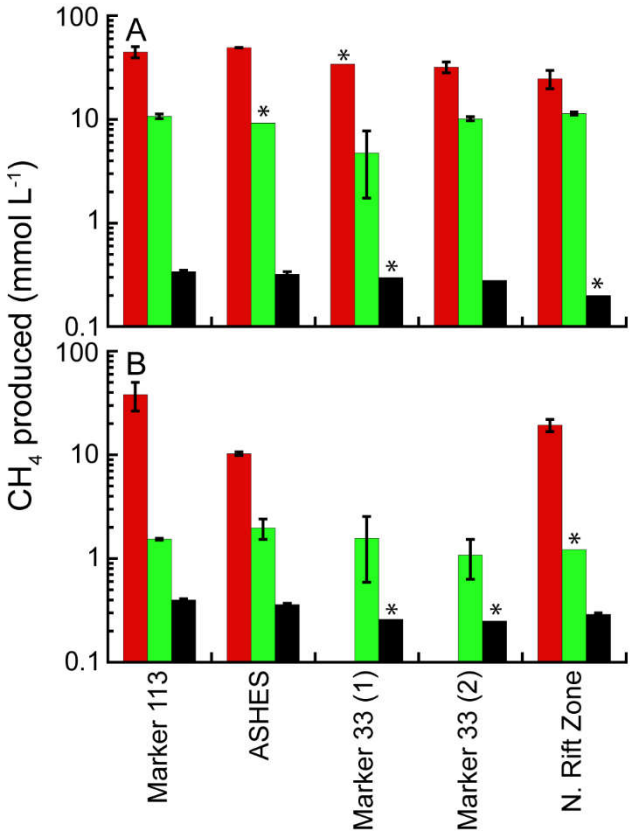

Figure 6 Average total CH4 production in 2015 microcosms. The microcosms were incubated at 80°C (A) and 55°C (B) and amended with 200 kPa of H_2:CO_2 (red); 200 kPa of N_2:CO_2, 0.5% tryptone and 0.01% yeast extract (green); and 2 kPa of H_2 and 198 kPa of N_2:CO_2 (black). The sample bars represent the range of the duplicate incubations. The asterisks show where there was growth in only one microcosm bottle.

Microscopic observations of the 2015 tryptone plus N_2:CO_2 microcosms following incubation show that the 80°C microcosms contain almost all coccoid-shaped cells (Figure 7A) while the 55°C microcosms contain mostly rod-shaped cells with some coccoids (Figure 7B). There was no CH_4 in any 80°C or 55°C microcosms amended only with N_2:CO_2 or in 80°C and 55°C microcosms amended with tryptone plus N_2:CO_2 containing background seawater collected 25 m above the caldera. There also was no CH_4 in any 80°C and 55°C microcosms amended with either acetate or formate with 200 kPa of N_2:CO_2 in the headspace.

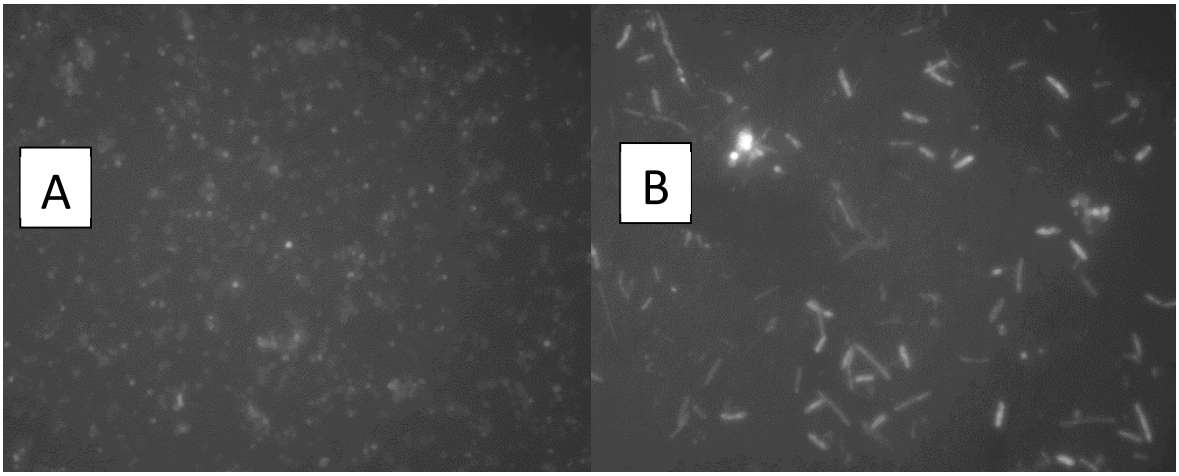

Figure 7 Epifluorescence micrographs of Marker 113 cells grown in the microcosms on 0.5% tryptone and 0.01% yeast extract at 55°C (A) and 80°C (B). All of the 55°C microcosm incubations containing organic supplements contained mostly rods, while all of the 80°C microcosm incubations containing organic supplements contained nearly exclusively coccoids. The scale bars are 10 μm.

Phylogenetic analysis showed that DNA from microcosms incubated at 80°C only amplified with archaeal primers. Microcosms incubated at 55°C amplified with bacterial primers but only one of the replicates amplified with archaeal primers. Sequencing depths ranged from 78,143 to 163,507 sequences, with a mean of 114,736 reads per sample. Rarefaction analysis showed that sequencing efforts were sufficient to represent the

diversity of the samples examined. Archaeal sequence reads were binned into 161 operational taxonomic units (OTUs) based on 97% sequence identity after singletons were removed. Archaeal sequences in the 80°C microcosms belonged to genera *Thermococcus* (46-73% of sequences), *Methanocaldococcus* (17-37% of sequences), and *Archaeoglobus* (9-14% of sequences) with some sequences that belong to *Methanothermococcus*, *Palaeococcus*, and *Nitrosopomilus* (Figure 8A). Archaeal sequences observed in 55°C microcosms were dominated by the genera *Methanothermococcus* (96% of sequences) and *Methanocaldococcus* (3% of sequences) (Figure 8A). Bacterial sequence reads were binned into 188 operational taxonomic units (OTUs) based on 97% sequence identity after singletons were removed. The sequences were dominated by the genera *Tepidibacter* (34-42% of sequences), *Caloranaerobacter* (26-36% of sequences), *Caminicella* (17-23% of sequences), and *Desulfotomaculum* (6-10% of sequences) (Figure 8B), which all belong to the order *Clostridiales* (98% of sequences in both replicates).

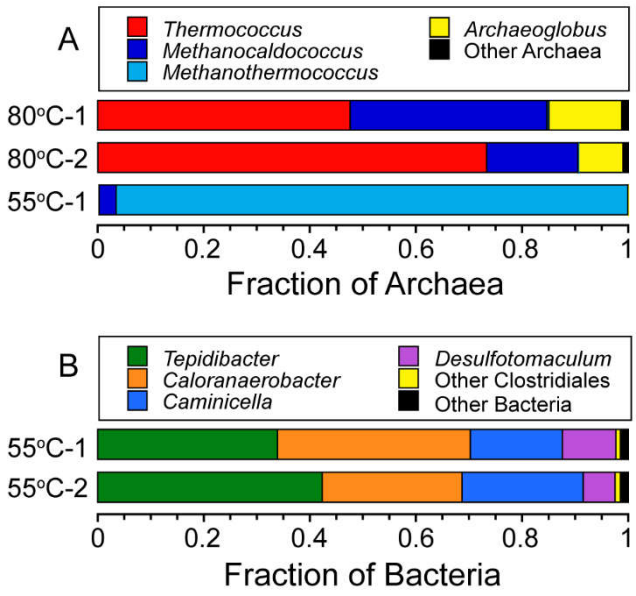

Figure 8 Phylogenetic diversity of Archaea and Bacteria in the 80°C and 55°C microcosms. Taxonomic breakdown and relative abundance at the genus level for archaeal (A) and bacterial (B) 97% 16S rRNA gene OTUs from microcosms following incubation at 80°C and 55°C using diffuse hydrothermal fluids collected from the Marker 113 vent site.

The cell specific rates of H_2 production by *T. paralvinellae* grown on maltose, tryptone, and combination of maltose and tryptone were not significantly different from each other at either temperature examined (Figure 9A). The rates decreased from 3.4-6.2 fmol H_2 cell^{-1} h^{-1} at 82°C to 1.2-1.9 fmol H_2 cell^{-1} h^{-1} at 60°C. *T. paralvinellae* grown alone at 82°C and 60°C produced up to 6.7 mmol H_2 L^{-1} at specific production rates of 0.22 h^{-1} and 0.04 h^{-1}, respectively (Figure 9B). When grown in coculture with *M. bathoardescens* at 82°C and with *Methanothermococcus* strain BW11 at 60°C, the amount of H_2 produced remained below 0.3 mmol L^{-1} and 0.1 mmol L^{-1}, respectively. The amount of CH_4 produced in coculture at 82°C and 60°C was 3.9 mmol L^{-1} and 2.8 mmol L^{-1} and the specific rates of CH_4 production were 0.16 h^{-1} and 0.06 h^{-1}, respectively (Figure 9B).

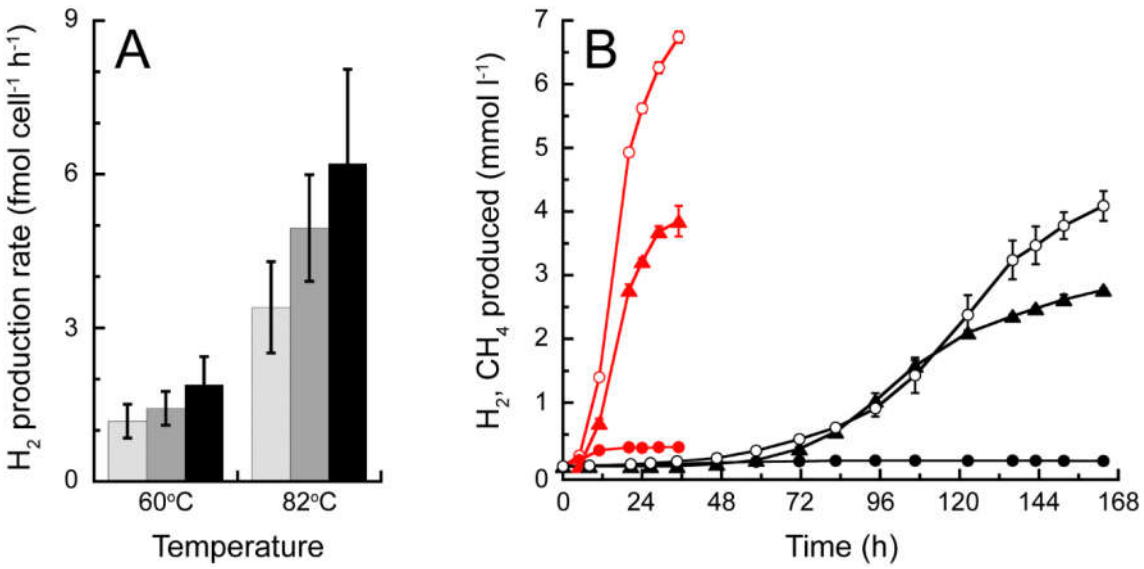

Figure 9 H_2 production by *T. paralvinellae* and CH_4 production by *M. bathoardescens* and *Methanothermococcus* sp. BW11 grown alone and in coculture. (A) Cell-specific H_2 production rate of *T. paralvinellae* at 82°C and 60°C when grown on 0.5% maltose and 0.01% yeast extract (light grey), 0.5% tryptone and 0.01% yeast extract (grey), and 0.05% each of maltose and tryptone and 0.01% yeast extract (black). (B) H_2 (circles) and CH_4 (triangles) produced when *T. paralvinellae* was grown alone (open circles) and in coculture (filled symbols) with *M. bathoardescens* at 82°C (red) and with *Methanothermococcus* sp. BW11 at 60°C (black).

2.5 Discussion

This study demonstrated that naturally occurring methanogens at Axial Seamount are primarily limited by H_2 availability and not by the availability of other compounds such as nitrogen sources, trace metals or vitamins. It also showed that methane production can occur among natural assemblages of methanogens by H_2 syntrophy but appears to be more prevalent at hyperthermophilic temperatures rather than thermophilic temperatures due to the growth of competitors at the lower temperatures.

The eruption cycle at Axial Seamount provided the opportunity to examine the impact of eruption events on methanogenic and heterotrophic microbial communities in hydrothermal fluids there. Previous work at Axial Seamount after eruptive events showed that microbial diversity appears to increase in the year following the eruption, with some

vents, including snowblowers, quickly dying out, while other pre-existing vents continue to vent post-eruption (Huber et al. 2002, 2003, 2006a; Ver Eecke et al., 2012; Meyer et al. 2013). In 2012, 16 months after the 2011 eruption, the concentrations of thermophiles, hyperthermophiles and total cells at Marker 113, ASHES, and Boca were lower than at any other time during the sampling time series suggesting there is a period of microbial quiescence between eruptions that is widespread throughout the caldera. In 2014, as the magma chamber inflated leading up to the 2015 eruption (Kelley et al., 2015), the concentrations of cultivable hyperthermophilic and thermophilic methanogens and heterotrophs reached their highest points at Marker 113 and Marker 33 on the eastern flank of the caldera, close to the eruptive fissures and the underlying magma chamber, but remained relatively constant at ASHES on the western flank of the caldera. Methanogen and heterotroph concentrations decreased at Marker 113 and Marker 33 in 2015 four months after the eruption. This suggests that the eastern flank of Axial Seamount may be heading towards another period of microbial quiescence within the anoxic subseafloor. The exception was at Marker 113 where methanogens that grew at 55°C increased in concentration through 2015 while other autotrophs that grew at 55°C decreased in concentration until they were undetectable. In contrast, CH_4 production in microcosms was lower in 2014 than in 2013 and 2015 suggesting that the elevated concentrations of cultivable methanogens may have partially depleted some growth factor in the system other than H_2 that year which led to poorer growth in the microcosms. As previously observed at Boca following the 2011 eruption (Meyer et al., 2013), methanogens were relatively abundant in hydrothermal fluids emanating from new basalt

flows on the North Rift Zone (NRZ) caused by the 2015 eruption. No other thermophilic or hyperthermophilic hydrogenotrophs were found at the site.

Low-temperature hydrothermal fluids at Axial Seamount (e.g., < 40°C) are typically depleted or nearly depleted in H_2 (e.g., <3 μmol kg^{-1}) due to microbial H_2 consumption or low-H_2 source fluids (Ver Eecke et al., 2012). In these environments, H_2 syntrophy may serve as an alternative source of H_2 to help sustain methanogens and other hydrogenotrophs. Mesophilic sulfide-oxidizing bacteria, abundant macrofauna, and seawater ingress into hotter hydrothermal environments may provide the labile organic compounds necessary to support H_2-producing heterotrophs. The predominant heterotrophs at hyperthermophilic temperatures in low-temperature fluids at Axial Seamount are *Thermococcus* species (Huber et al., 2002; 2006a). All *Thermococcus* species possess at least one hydrogenase (Schut et al., 2012), and some have as many as seven hydrogenases (Lee et al., 2008; Jung et al., 2014). In this study, *T. paralvinellae*, which possesses the genes for seven hydrogenases (Jung et al., 2014), produced H_2 from protein and carbohydrate substrates at equal rates that both increased with increasing temperature. Microcosm incubations at both 80°C and 55°C demonstrated that it is H_2 and not formate or acetate that is used by the methanogens at high temperatures. This is likely due to the lower energy yield for methanogenesis using formate and acetate as carbon and energy sources (Deppenmeier, 2002). *Thermococcus* is widely representative of H_2 producers in many diverse subseafloor ecosystems. They were the only archaeal 16S rRNA gene sequences found 99 and 194 meters below the seafloor (mbsf) in Nankai Trough sediments (Kormas et al., 2003). They dominated the archaeal 16S rRNA gene diversity of a sediment horizon collected 634 mbsf in the Canterbury Basin (Ciobanu et

al., 2014) and in 80-90°C water-flooded oil reservoirs in the Sinopec Shengli oil field (Junzhang et al., 2014). They are commonly found in ridge flanks basement outcrops (Huber et al., 2006b; Ehrhardt et al., 2007) and petroleum reservoirs (Stetter et al., 1993; L'Haridon et al., 1995; Miroshnichenko et al., 2001; Dahle et al., 2008). Therefore, *Thermococcus* may have the potential to degrade local organic compounds and provide H_2 to collocated hydrogenotrophic microbes in non-hydrothermal vent subseafloor anoxic environments as well.

The taxonomic analysis of microcosm incubations demonstrates a transition from hyperthermophilic archaeal H_2 syntrophy to thermophilic bacterial H_2 syntrophy with decreasing incubation temperature. In 55°C microcosms, the amount of CH_4 produced through syntrophy decreased relative to the 80°C microcosms, suggesting that H_2 syntrophy-driven methanogenesis may be more pronounced at hyperthermophilic temperatures. The 80°C microcosms produced the most CH_4 and only archaeal DNA was amplified from these incubations, including the H_2-producing heterotroph *Thermococcus* and the H_2-consuming methanogens *Methanocaldococcus* and *Methanothermococcus* species. These were the predominant organisms found in previous Marker 113 fluids incubated at 80°C with H_2 and bicarbonate for stable-isotope probing analysis (Fortunato and Huber, 2016) and other hyperthermophile culture- and molecular-based analyses (Ver Eecke et al., 2012). In contrast, the 55°C microcosms produced significantly less CH_4, bacterial DNA was amplified in both samples, and archaeal DNA was amplified in only one sample. The predominant bacteria found in these samples were most closely related to the genera *Tepidibacter*, *Caloranaerobacter*, and *Caminicella*. Each of these genera is a thermophilic member of the *Clostridia* and has representatives that were

isolated from hydrothermal vents that ferment peptides and carbohydrates and produce H_2, CO_2, carboxylic acids, alcohols, and alanine (Wery et al., 2001; Alain et al., 2002; Slobodkin et al., 2003; Jiang et al., 2014). Among hydrogenotrophs, *Methanothermococcus* was the predominant archaeon sequence found in one 55°C microcosm, and sequences most closely related to *Desulfotomaculum* were also found among the bacteria. *Desulfotomaculum thermosubterraneum* is a thermophilic sulfur reducer that can consume H_2, CO_2, carboxylic acids, alcohols, and alanine (Kaksonen et al., 2006). These results indicate the capacity of hydrothermal vent microbial communities to perform various forms of H_2 syntrophy depending on growth temperature.

In order to quantify how H_2 limitation and syntrophy impact CH_4 production, primary production, and total biomass within subseafloor environments at hydrothermal vents and elsewhere, it will be necessary to develop models of growth and cell-cell interactions that can be applied to these environments. All models make certain *a priori* assumptions, and this study demonstrated that in most circumstances, the growth of thermophilic and hyperthermophilic methanogens *in situ* is primarily limited by the availability of H_2 and heat. The ability of some *Methanocaldococcus* and *Methanothermococcus* species to fix N_2 suggests that they are adapted to low-nitrogen environments (Belay et al., 1984; Mehta and Baross, 2006; Nishizawa et al., 2014). Depleted NO_3^- concentrations in diffuse vent fluids at Axial (Butterfield et al., 2004; Bourbonnais et al., 2012) suggest that NO_3^- may be limited in the subseafloor, although metatranscriptomic analysis of Marker 113 hydrothermal fluids shows that the genes for denitrification are expressed (Fortunato and Huber, 2016). However, ΣNH_3 in high-

temperature source fluids at Axial is variable and reaches 16 μmol kg^{-1} (approximately 1/3 of the ambient deep seawater NO_3^-), providing a modest nitrogen source for primary producers. In most of the microcosm incubations in this study, the addition of 47 μM NH_4Cl did not enhance the production of CH_4, the amount of CH_4 produced by natural methanogen assemblages in hydrothermal fluid was the same as those by pure cultures in nutrient-replete medium, and the omission of vitamins to pure cultures had no effect on their growth. Therefore, natural assemblages of thermophilic methanogens do not appear to be limited by nitrogen or trace nutrient requirements in most cases. Methane production was low in the 2014 microcosms relative to 2013 and 2015, even though the number of cultivable methanogens was relatively high, suggesting that there are periods where methanogens might be at least partially limited in their growth by factors other than H_2 and heat.

2.6 Conclusion

In conclusion, the microcosm results validate the modeling assumption made in the lab that the artificial conditions generated are generally representative of the growth of natural assemblages of methanogens in a mixture of hydrothermal fluid and seawater. They also define the constraints on methanogenesis at hydrothermal vents and tie together metagenomics and metatranscriptomic data with ecosystem functioning. These will help reveal the physiological state of methanogens *in situ* and assist in the effort to model the rates of methane formation in hydrothermal systems on varying substrates.

CHAPTER 3

FORMATE HYDROGENLYASE AND FORMATE SECRETION AMELIORATE H2 INHIBITION IN THE HYPERTHERMOPHILIC ARCHAEON *THERMOCOCCUS PARALVINELLAE*

3.1 Abstract

Some hyperthermophilic heterotrophs in the genus *Thermococcus* produce H_2 in the absence of elemental sulfur (S°) and have up to seven hydrogenases, but their combined physiological roles are unclear. Here, we show which hydrogenases in *Thermococcus paralvinellae* are affected by added H_2 during growth without S°. Growth rates and steady-state cell concentrations decreased while formate production rates increased when *T. paralvinallae* was grown in a chemostat with 65 μM of added $H_{2(aq)}$. Differential gene expression analysis using RNA-Seq showed consistent expression of six hydrogenase operons with and without added H_2. In contrast, expression of the formate hydrogenlyase 1 (*fhl*1) operon increased with added H_2. Flux balance analysis showed H_2 oxidation and formate production using FHL became an alternate route for electron disposal during H_2 inhibition with a concomitant increase in growth rate relative to cells without FHL. *T. paralvinellae* also grew on formate with an increase in H_2 production rate relative to growth on maltose or tryptone. Growth on formate increased *fhl*1 expression but decreased expression of all other hydrogenases. Therefore, *Thermococcus* that possess *fhl*1 have a competitive advantage over other *Thermococcus* species in hot subsurface environments where organic substrates are present, S° is absent, and slow H_2 efflux causes growth inhibition.

3.2 Introduction

Thermococcus species are hyperthermophilic heterotrophs that reduce elemental sulfur (S°) to H_2S (Bertoldo and Antranikian, 2006), or in some cases H^+ to H_2 (Kanai et al., 2005; Nohara et al., 2014; Hensley et al., 2016), during anaerobic respiration. They are commonly associated with shallow marine hot springs and hydrothermal vents (Bertoldo and Antranikian, 2006), but they are increasingly reported in many other hot environments that are anoxic, organic rich, and saline. It was estimated that 35% of all marine sediments are above 60°C suggesting that they may provide a large global biotope for thermophiles (LaRowe et al., 2017). *Thermococcus* and its close relative *Pyrococcus* were the predominant archaea detected 634 and 1,626 meters below the seafloor (mbsf) in sediment cores collected offshore of New Zealand and Newfoundland, Canada, respectively (Roussel et al., 2008; Ciobanu et al., 2014). *Thermococcus* were also the predominant archaea found in an uncontaminated oil reservoir 2,500 mbsf in the Norwegian Sea and in a 90°C water-flooded oil well in China (Lewin et al., 2014; Lin et al., 2014). Furthermore, *Thermococcus* bloomed in Marcellus and Utica shale bed produced waters in western Pennsylvania, USA seven days after hydraulic fracturing (Daly et al., 2016). If these latter environments lack both S° and sufficient environmental flux rates to remove excess metabolic products, then H_2 buildup in these closed environments can inhibit the growth and metabolism of the *Thermococcus* present. Therefore, it is important to study the H_2 production mechanisms and H_2 inhibition survival strategies in *Thermococcus* to better understand their biogeochemical impact in these hot subsurface environments.

H_2 is produced or consumed by hydrogenases using the following reversible reaction.

$$2\ H^+ + 2\ e^- \leftrightarrow H_2$$

All *Thermococcus* species have a membrane-bound, ferredoxin (Fd)-oxidizing hydrogenase (Mbh) for H_2 production that during the reaction translocates a H^+ across the cytoplasmic membrane that is exchanged for a Na^+ by a H^+/Na^+ antiporter (Sapra et al., 2003; Schut *et al.*, 2013; Mayer and Müller, 2014). The Na^+ then drives a membrane-bound ATP synthase for ATP production by oxidative phosphorylation (Sapra et al., 2003; Schut et al., 2013; Mayer and Müller, 2014). Only a few *Thermococcus* species can also grow on formate or CO with concomitant H_2 production and H^+/Na^+ translocation using membrane-bound, formate- or CO-oxidizing (Codh) hydrogenases (Sokolova et al., 2004; Kim et al., 2010; Bae et al., 2012; Lim et al., 2014). The formate-dependent hydrogenase in *Thermococcus onnurineus* is structurally and functionally like the formate hydrogenlyase (FHL) found in mesophilic bacteria with formate dehydrogenase and hydrogenase complexes both associated in the cytoplasm with a H^+/Na^+ antiporter in the membrane (Kim et al., 2010; Lim et al., 2014; McDowall et al., 2014). Additionally, all *Thermococcus* have a cytoplasmic $NAD(P)^+$-reducing hydrogenase (SH) (van Haaster et al., 2008; Schut et al., 2013; Mayer and Müller, 2014). Other *Thermococcus* have a second cytoplasmic hydrogenase that is phylogenetically like F_{420}-reducing hydrogenases (Frh) in methanogens, but the physiological function of the enzyme in *Thermococcus* is unknown (Jeon et al., 2015). The combined roles of these multiple hydrogenases and the nature of H_2 metabolism in *Thermococcus* are largely unknown, especially as it relates to their growth *in situ*.

Thermococcus paralvinellae was isolated from a hydrothermal vent (Pledger and Baross, 1989) and produced H_2 and formate when grown without S° (Hensley et al., 2016). *T. paralvinellae* and the hyperthermophilic heterotroph *Pyrococcus furiosus* produced H_2 at comparable rates when grown on the same media without S° at their optimal growth temperatures (Hensley et al., 2016). However, methyl viologen-dependent hydrogenase activity, which represents the Fd-oxidizing hydrogenase, was up to 30-fold higher in *P. furiosus* than in *T. paralvinellae*, especially during periods of cell stress (Hensley et al., 2016). This suggests that other hydrogenases were active in *T. paralvinellae* under the same growth conditions. *P. furiosus* has one Mbh and two SH (Schut et al., 2013) while the *T. paralvinellae* genome contains seven hydrogenase operons: two *fhl*s, two *mbh*s, a *codh*, a *sh*, and a *frh* (Table 7) (Jung et al., 2014).

Shifts in varying hydrogenase activities could be related to the similar midpoint potentials of Fd, H_2, and formate. The midpoint potential of hyperthermophilic Fd (-398 mV) is like that of H_2/H^+ (-414 mV), suggesting that Fd-dependent H_2 production by Mbh is easily inhibited by H_2 buildup in the environment (Verhaart et al., 2010). Similarly, formate oxidation to H_2 and CO_2 is modestly exergonic ($\Delta G°$ = -2.6 kJ mol^{-1}) at 80°C under otherwise standard conditions (Lim et al., 2014) indicating that the thermodynamic favorability of the FHL reaction depends on relative H_2 and formate concentrations. Therefore, the purpose of this study is two-fold, the first being to determine which of the seven hydrogenase genes are expressed by *T. paralvinellae* when it is grown on maltose, tryptone, or formate without S°. The second aim is to examine the effects of added H_2 on *T. paralvinellae* growth and expression of its hydrogenases, particularly *mbh* and *fhl*. Growth and metabolite production kinetics were determined in a chemostat during

continuous growth. Genome-wide differential gene expression analysis using RNA-Seq was performed on cells harvested at the end of each chemostat growth experiment. These data were used to constrain a genome-scale metabolic network model. The flux balance analyses of the metabolic model were then used to predict varying hydrogenase roles and how varying putative formate production schemes might impact growth rates during H_2 inhibition.

3.3 Methods

3.3.1 Growth media and chemostat conditions

T. paralvinellae DSM 27261 (Hensley et al., 2014) was provided by Deutsche Sammlung von Mikroorganismen und Zellkulturen (DSMZ). The growth media are based DSM medium 282 (Jones et al., 1983) and is composed of the following per liter: 30 g of NaCl, 3.40 g of $MgSO_4 \cdot 7H_2O$, 4.1 g of $MgCl_2 \cdot 6H_2O$, 0.33 g of KCl, 0.25 g of NH_4Cl, 0.14 g of K_2HPO_4, 0.14 g of $CaCl_2 \cdot 2H_2O$, 0.5 mg of $NiCl_2 \cdot 6H_2O$, 0.5 mg of $Na_2SeO_3 \cdot 5H_2O$, 1 g of $NaHCO_3$, 0.63 g of $Na_2S_2O_3$, 0.1 g of yeast extract (vitamin B_{12}-fortified; Difco), 10 mL of DSM medium 141 trace elements solution, 10 mL of DSM medium 141 vitamins solution, 1 mL of 0.01% (wt vol^{-1}) each of $(NH_4)_2Fe(SO_4)_2 \cdot 6H_2O$ and $(NH_4)_2Ni(SO_4)_2$, 1 μM of $Na_2WO_4 \cdot 2H_2O$, and 50 μL of 0.5% (wt vol^{-1}) resazurin. The primary carbon and energy source added (per liter) was 5 g of maltose (Sigma), 5 g of tryptone (Oxoid), or 1 g of sodium formate (Fluka). The medium was pH-balanced to 6.80 ± 0.05. The medium was reduced with 0.025% (wt vol^{-1}) each of cysteine-HCl and $Na_2S \cdot 9H_2O$ before inoculation. No elemental sulfur was added.

For the chemostat runs, a 2-L bioreactor with gas flow control, an incubation temperature of 82°C (± 0.1°C), and a pH of 6.8 (± 0.1 unit) was prepared with 1.5 L of growth medium. The reactor was gas flushed through a submerged fritted bubbler with a mixture of CO_2 (7 ml of gas min^{-1}) and either N_2 or H_2 (65 ml of gas min^{-1}). Pure gases were blended using a mass flow controller (Matheson Tri-Gas). Maltose- and tryptone-containing media were flushed in separate runs with either N_2 or H_2 while the formate-containing medium was only flushed with N_2. The aqueous H_2 concentration in the reactor was measured by drawing 25 mL of fluid from the bottom of the reactor directly into an anoxic 60-mL serum bottle and measuring the head-space gas with a gas chromatograph. The aqueous H_2 concentration in the reactor flushed with H_2 was ~ 65 μM prior to inoculation. The reactor was inoculated with 50-100 mL of a logarithmic growth-phase culture of *T. paralvinellae* that had been transferred at least three times on the carbon source used. During growth, samples were drawn from the reactor and cell concentrations were determined using phase-contrast light microscopy and a Petroff-Hausser counting chamber.

The cells were grown in batch reactor mode until they reached late logarithmic growth phase, then the reactor was switched to a chemostat by pumping sterile growth medium into the bioreactor from a sealed 12-L reservoir that was degassed through a submerged glass tube with N_2 and heated to 75°C. Simultaneously and at the same rate, spent growth medium was pumped out of the bioreactor using a dual-channel peristaltic pump. The growth rate of the cells was determined by cell counts during batch phase growth, then the dilution rate of the chemostat was set to match this growth rate. The aqueous and headspace H_2 concentrations in the bioreactor were measured with a gas

chromatograph. Soluble metabolites (formate, acetate, butyrate, isovalerate, 2-methylbutyrate) were measured from the media using an ultra-high pressure liquid chromatography (UHPLC) system as previously described (Hensley et al., 2016). The microbial population in the chemostat was stable after three volume replacements of the medium within the reactor and was monitored for an additional ~0.5 volume replacements to obtain kinetic data. Following this, the complete contents of the bioreactor were drained into ice-cooled centrifuge bottles, spun in a centrifuge at 4°C and 10,000 × g for 60 min, resuspended in 1 mL of TRIzol (Invitrogen), and frozen at -80°C until processed. Chemostats were run in triplicate sequentially for each growth condition.

3.3.2 RNA-Seq analysis

Total RNA was extracted from 15 cell pellets (three from each growth condition) using a Direct-zol RNA extraction kit (Zymo). RNA quantity was determined using Qubit fluorometry. RNA integrity was checked using an Agilent 2100 bioanalyzer, a Nanodrop 2000 spectrophotometer, and gel electrophoresis of the RNA followed by staining with ethidium bromide. Removal of rRNA, library construction, multiplexing, and sequencing of the mRNA using an Illumina HiSeq2500 sequencer with 2×100 paired-ends was performed commercially by GENEWIZ, LLC (South Plainfield, NJ, USA) as described by the company. Sequencing depths ranged from 29,974,378 to 45,240,342 sequence reads per sample, with a mean of 38,990,002 and a median of 38,951,352 reads per sample. The RNA-Seq reads were aligned to the *T. paralvinellae* genome using the STAR aligner version 2.5.1b (Dobin et al., 2013) and aligned sequence reads were assigned to genomic features and quantified using featureCounts read summarization tool (Liao et al., 2014). The output of the analyses generated BAM files

containing the sequence of every mapped read, its mapped location, and a gene count file in which each gene expression levels are reported as transcripts per million (TPM). An unsupervised t-distributed stochastic neighbor embedding (t-SNE) algorithm (Van Der Maaten and Hinton, 2008) was used to predict outliers among the total RNA sample replicates.

Genes that were differentially expressed were identified using 'limma' and 'DESeq2' in the Bioconductor software framework (www.bioconductor.org) in R (version 3.3 [http://www.r-project.org]) and on a Galaxy platform, respectively (Anders et al., 2010; Goecks et al., 2010; Phipson et al., 2016). TMM (trimmed mean of M-values)-normalization was performed by using the R package 'edgeR' and the 'calcNormFactors' command. These normalized values were then used for library size calculations in the 'voom' command in the R package 'limma'. The limma package allows for transformation of count data to $\log_2$-counts per million (logCPM), estimation of the mean-variance relationship, and uses these to compute appropriate observation-level weights. A linear model is then fit to our data and empirical Bayesian statistics are used to compute moderated t-statistics, moderated F-statistics, and log-odds of differential expression. The genes were reported as differentially regulated if $\log_2 FC > 1$ and false discovery rate (FDR) adjusted p-value < 0.05. Heatmaps were plotted in R (version 3.3 [http://www.r-project.org]) using the 'pheatmap' package. The heatmap color scale represents the z-score, which is the number of standard deviations the mean score of the treatment is from the mean score of the entire population. The count files and raw sequences are available in the NCBI Gene Expression Omnibus (GEO) database under GSE 101078.

3.3.3 Flux balance analysis

A genome-scale metabolic network model for *T. paralvinellae* was developed using the automated ModelSEED program (Aziz et al., 2008; Henry et al., 2010). The draft metabolic network model contained 672 reactions. It was manually curated using available biochemical, physiological, and genomic information from the KEGG database (www.genome.jp/kegg/), the ModelSEED database, and primary literature as well as the kinetic information from chemostat runs performed as described above. 180 reactions were added manually because they were reported in prior literature and genome annotations or were required to fill a gap in the reconstructed network. The Biomass Objective Function was developed using previous templates (Feist et al., 2006, 2007; Ahsanul Islam et al., 2010). Flux balance simulations were performed utilizing the COBRA toolbox (Ebrahim et al., 2013). The model assumed maltose as the growth substrate and yeast extract as the source of essential amino acids and was constrained by measured acetate production rates. Initially, the rate of the H_2 exchange reaction was not constrained to measure the rate of the exchange at optimal conditions. Then for the FBA analysis, the H_2 exchange flux value was fixed to percentage decreases (% inhibition) of the optimal rate to simulate increasing H_2 inhibitory conditions. In response to decreasing H_2 exchange and thus, increasing extracellular H_2 concentrations that prohibit H_2 diffusion out of the cell, individual and combined options of formate metabolism were added to the model. A reversible FHL reaction was added, as well as an irreversible PFL reaction and the PPK pathway (Fig. 3). This model was deposited in EMBL-EBI BioModels (Chelliah et al., 2015) and assigned the identifier MODEL1707280000.

3.4 Results and Discussion

3.4.1 Growth kinetics with and without added H_2

When grown on maltose, there was a significant decrease in the batch-phase growth rate of *T. paralvinellae* leading up to chemostatic growth (Fig. 10A) and in the steady-state cell concentration during chemostatic growth (Fig. 10B) when H_2 was added to the reactor relative to growth without added H_2 (Table 6). A similar trend was observed for growth on tryptone where the batch-phase growth rate decreased (Fig. 10A) and steady-state growth in a chemostat could not be maintained (Fig. 10B) with added H_2 relative to growth without added H_2 (Table 6). *T. paralvinellae* also grew on formate without added H_2 (Fig. 10, Table 6). The cell-specific H_2 production rate was 71- and 81-fold higher when cells were grown on formate relative to growth on tryptone or maltose, respectively (Fig. 10C). Growth on formate in this study and elsewhere (Kim et al., 2010; Kozhevnikova et al., 2016) required the addition of at least 0.01% yeast extract suggesting that formate is used primarily for energy generation on the membrane by FHL rather than for biosynthesis.

Table 6 Growth kinetic values for *T. paralvinellae* (± 95% confidence intervals). [a]Maximum cell concentration attained in batch-phase growth. [b]n.d., not determined due to high background concentrations

Condition	Batch-phase growth rate (h^{-1})	Steady-state cell concentration (10^{10} l^{-1})	Cell-specific H_2 prod. rate (fmol $cell^{-1}$ h^{-1})	Cell-specific formate prod. rate (fmol $cell^{-1}$ h^{-1})	Cell-specific acetate prod. rate (fmol $cell^{-1}$ h^{-1})
Maltose	0.52 ± 0.10	4.8 ± 1.0	2.7 ± 0.6	10.5 ± 8.5	1.7 ± 1.3
Maltose + H_2	0.30 ± 0.04	1.9 ± 0.4	n.d.[b]	20.8 ± 10.0	3.3 ± 0.7
Tryptone	0.36 ± 0.08	3.0 ± 0.6	3.2 ± 0.3	below detection	1.3 ± 0.8
Tryptone + H_2	0.23 ± 0.20	0.9 ± 0.5[a]	n.d.	30.0 ± 10.3	2.9 ± 2.3
Formate	0.27 ± 0.15	4.5 ± 0.5	218.8 ± 33.0	n.d.	n.d.

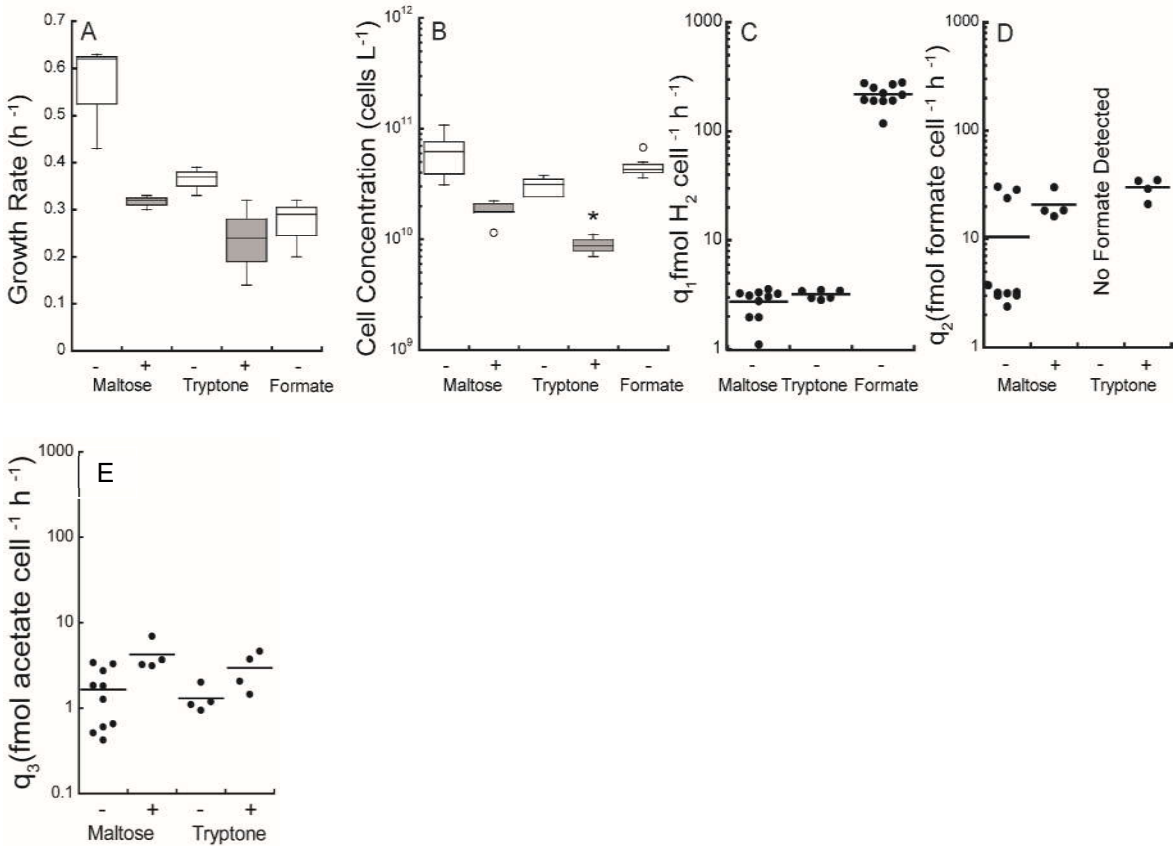

Figure 10 *T. paralvinellae* growth and metabolite production kinetics. Growth rate during batch growth phase (A) and steady-state cell concentration in the chemostat (B) for each condition. The asterisk (*) indicates the data are for the maximum cell concentration achieved during batch-phase growth because chemostat growth was unattainable. The cell-specific H_2 (C) and formate (D) production rates for cells grown in the chemostat following three volume changes in the reactor. The cell-specific acetate production rates (E) for cells grown in the chemostat following three volume changes in the reactor. The horizontal bar represents the mean value. -, no added H_2; +, 65 μM H_2 added to the growth medium.

Without added H_2, the cells produced formate when grown on maltose but not on tryptone (Fig. 10D). However, when cells were grown with added H_2, formate production occurred in cells grown on tryptone (Table 6). The cell-specific acetate production rates remained unchanged when cells were grown on maltose or tryptone with and without added H_2 (Fig. 10E). *T. paralvinellae* produced H_2 and acetate at near a 2:1 ratio when grown on maltose, as expected for use of the archaeal Embden-Meyerhof pathway (Table

6). 2-methylbutyric acid was also detected when cells were grown on tryptone. No ethanol or other alcohols were detected in any growth condition.

3.4.2 Transcriptomic analyses

Of the 2,138 genes in the *T. paralvinellae* genome, 2,084 gene transcripts were detected by RNA-Seq. Of the fifteen samples that span the five growth conditions run in triplicate, one sample of tryptone growth without added H_2 was excluded from further analyses based on the t-Distributed Stochastic Neighbor Embedding (t-SNE) results (Fig. 11) (Van Der Maaten and Hinton, 2008).

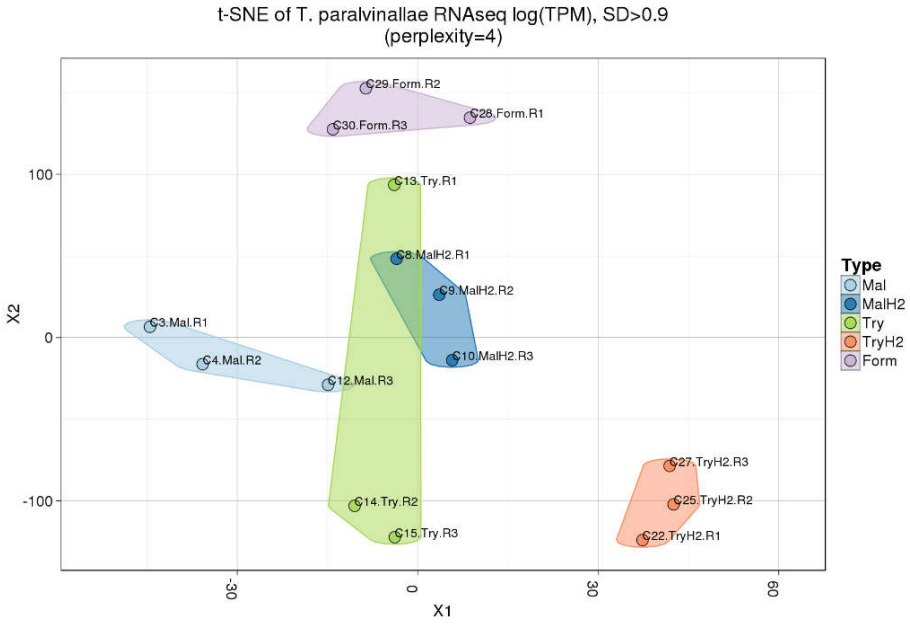

Figure 11 t-SNE analysis. Unsupervised non-linear embedding method where similar samples are embedded closely. Most variable genes (top 10th percentile by expression) were used and tryptone replicate 1 was excluded from differential expression analyses.

Pairwise comparisons of maltose- and tryptone-grown cells with and without added H_2 showed up to 48 genes to be differentially expressed (Tables 8-10). Eighteen of the genes up-regulated in cells grown with added H_2 comprise a putative *fhl* operon (*fhl*1, TES1_RS07740-TES1_RS07825) (Fig. 12A). The operon contains genes for a formate

transporter, a formate dehydrogenase, a [NiFe] hydrogenase, and a membrane-bound H^+/Na^+ antiporter. Expression of the hydrogenase catalytic subunit of *fhl1* (TES1_RS07795) was also significantly higher in maltose- and tryptone-grown cells with added H_2 (Fig. 12B). In contrast, expression of the CODH catalytic subunit of *codh* (TES1_RS06365, Fig. 12C) and the membrane hydrogenase catalytic subunits of *mbh1* (TES1_RS07610, Fig. 12D) and *mbh2* (TES1_RS07680, Fig. 12E) remained consistent for the same growth conditions. Similarly, expression of the hydrogenase catalytic subunits of *fhl2* (TES1_RS00505), sh (TES1_RS00850), and *frh* (TES1_RS07845) were not different with added H_2 (Fig. 13). The *fhl2* operon (TES1_RS07740-TES1_RS07830), which lacks genes for a formate transporter and an *fdh* subunit, was not differentially expressed.

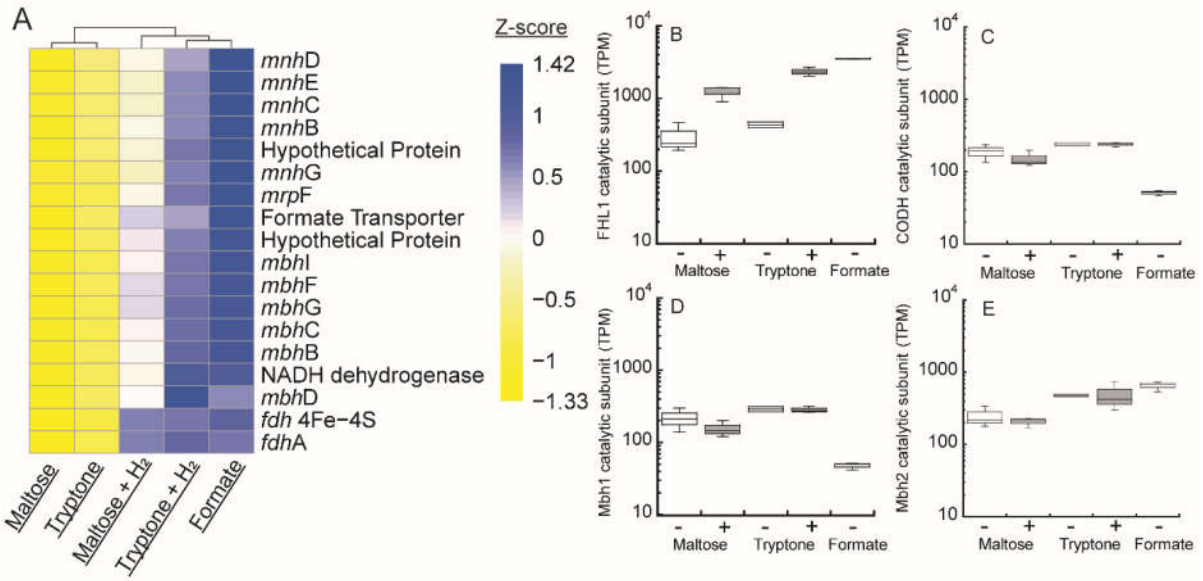

Figure 12 Differential gene expression analysis of *T. paralvinellae*. (A) RNA-Seq heat map for the formate hydrogenlyase 1 (*fhl1*) operon with mnh-mrp genes that encode H+/Na+ antiporter (TES1_RS07740-TES1_RS07770), formate transporter (TES1_RS07775), *mbh* genes that encode [NiFe] hydrogenase (TES1_RS07780-TES1_RS077815), and *fdh* genes that encode formate dehydrogenase (TES1_RS07820-TES1_RS07825). Transcript levels (transcripts-per-million, [TPM]) for the hydrogenase catalytic subunits of *fhl1* (TES1_RS07795) (B), CO-dependent hydrogenase (*codh*) (TES1_RS06370) (C), Fd-oxidizing hydrogenase 1 (*mbh1*) (TES1_RS07610) (D), and Fd-oxidizing hydrogenase 2 (*mbh2*) (TES1_RS07680) (E) for each growth condition.

When cells were grown on formate, expression of the *fhl1* was significantly upregulated compared to when cells were grown on maltose or tryptone (Fig. 12A, Table 11). Specifically, the expression of the hydrogenase catalytic subunit of *fhl1* was up-regulated 10-fold (Fig. 12B). In contrast, expression of the catalytic subunits of *codh* (Fig. 12C), *mbh1* (Fig. 12D) and *fhl2* (Fig. 13) were down-regulated. Together with the elevated cell-specific H_2 production rate, transcript analysis for growth on formate demonstrated that *T. paralvinellae* imported and oxidized formate to CO_2 and H_2 by relying on FHL1 for this reaction.

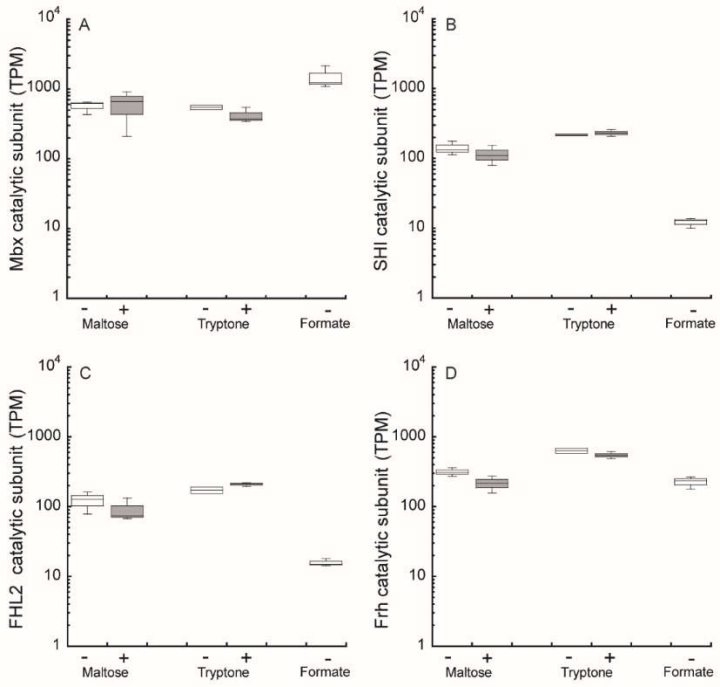

Figure 13 Transcript levels (transcripts-per-million, [TPM]) for the main catalytic subunit of *mbx* (TES1_RS04530) (A) and for the hydrogenase catalytic subunits of *sh* (TES1_RS00850) (B), *fhl2* (TES1_RS00505) (C), and *frh* (TES1_RS07845) (D) for each growth condition.

Twenty-six genes were down-regulated with added H_2 for cells grown on tryptone that were primarily related to biosynthesis reactions for cobalamin (vitamin B_{12}), phospholipids, and guanine and for DNA replication (Table 10). Growth on maltose

relative to tryptone led to up-regulation of 43 genes, including those for sugar processing proteins such as PEP synthetase, maltotriose binding protein, and amylopullulanase. It also led to down-regulation of 51 genes, including those for amino acid metabolism such as CAAX protease, peptidase, aminotransferase, and glutamate synthase (Table 12).

Table 7 List of hydrogenase operons and genes

Gene	Description
Formate hydrogenlyase 1 (*fhl*1)	
TES1_RS007740	Na^+/H^+ antiporter MnhD
TES1_RS007745	Na^+/H^+ antiporter MnhE
TES1_RS007750	Na^+/H^+ antiporter MnhC
TES1_RS007755	Na^+/H^+ antiporter MnhB
TES1_RS007760	hypothetical protein
TES1_RS007765	Na^+/H^+ antiporter MnhG
TES1_RS007770	Na^+/H^+ antiporter MnhF
TES1_RS007775	formate transporter
TES1_RS007780	hypothetical protein
TES1_RS007785	hydrogenase 4 subunit I
TES1_RS007790	formate hydrogen lyase subunit 6
TES1_RS007795	hydrogenase 4 subunit G
TES1_RS007800	hydrogenase 4 subunit C
TES1_RS007805	hydrogenase 4 subunit B
TES1_RS007810	NADH dehydrogenase
TES1_RS007815	hydrogenase 4 subunit D
TES1_RS007820	FDH 4Fe-4S subunit
TES1_RS007825	FDH alpha subunit
TES1_RS007830	FDH subunit D
Ferredoxin-dependent hydrogenase 1 (*mbh*1)	
TES1_RS07600	hydrogenase EchF (MbhN)
TES1_RS07605	hydrogenase EchB (MbhM)
TES1_RS07610	hydrogenase EchE (MbhL)
TES1_RS07615	hydrogenase EchD (MbhK)
TES1_RS07620	hydrogenase EchC (MbhJ)
TES1_RS07625	hydrogenase subunit (MbhI)
TES1_RS07630	hydrogenase EchA (MbhH)
TES1_RS07635	Na^+/H^+ antiporter MrpC (MbhG)
TES1_RS07640	Na^+/H^+ antiporter MrpB (MbhF)
TES1_RS07645	Na^+/H^+ antiporter MrpB (MbhE)
TES1_RS07650	Na^+/H^+ antiporter MrpB (MbhD)
TES1_RS07655	Na^+/H^+ antiporter MrpG (MbhC)
TES1_RS07660	Na^+/H^+ antiporter MrpF (MbhB)
TES1_RS07665	Na^+/H^+ antiporter MrpE (MbhA)

Gene	Description
Formate hydrogenlyase 2 (*fhl*2)	
TES1_RS00480	FDH alpha subunit
TES1_RS00485	FDH 4Fe-4S subunit
TES1_RS00490	hydrogenase 4 subunit D
TES1_RS00495	hydrogenase 4 subunit B
TES1_RS00500	hydrogenase 4 subunit C
TES1_RS00505	hydrogenase 4 subunit G
TES1_RS00510	formate hydrogen lyase subunit 6
TES1_RS00515	hydrogenase 4 subunit I
TES1_RS00520	hypothetical protein
TES1_RS00525	Na^+/H^+ antiporter MnhF
TES1_RS00530	Na^+/H^+ antiporter MnhG
TES1_RS00535	hypothetical protein
TES1_RS00540	Na^+/H^+ antiporter MnhB
TES1_RS00545	Na^+/H^+ antiporter MnhC
TES1_RS00550	Na^+/H^+ antiporter MnhE
TES1_RS00555	Na^+/H^+ antiporter MnhD
Ferredoxin-dependent hydrogenase 2 (*mbh*2)	
TES1_RS07670	hydrogenase EchF (MbhN)
TES1_RS07675	hydrogenase EchB (MbhM)
TES1_RS07680	hydrogenase EchE (MbhL)
TES1_RS07685	hydrogenase EchD (MbhK)
TES1_RS07690	hydrogenase EchC (MbhJ)
TES1_RS07695	hydrogenase subunit (MbhI)
TES1_RS07700	hydrogenase EchA (MbhH)
TES1_RS07705	Na^+/H^+ antiporter MrpC (MbhG)
TES1_RS07710	Na^+/H^+ antiporter MrpB (MbhF)
TES1_RS07715	Na^+/H^+ antiporter MrpB (MbhE)
TES1_RS07720	Na^+/H^+ antiporter MrpB (MbhD)
TES1_RS07725	Na^+/H^+ antiporter MrpG (MbhC)
TES1_RS07730	Na^+/H^+ antiporter MrpF (MbhB)
TES1_RS07735	Na^+/H^+ antiporter MrpE (MbhA)

Gene	Description
CO-dependent hydrogenase (*codh*)	
TES1_RS06295	Na^+/H^+ antiporter MnhA
TES1_RS06300	Na^+/H^+ antiporter MnhE
TES1_RS06305	Na^+/H^+ antiporter MnhC
TES1_RS06310	Na^+/H^+ antiporter MnhB
TES1_RS06315	Na^+/H^+ antiporter MnhD
TES1_RS06320	Na^+/H^+ antiporter MnhG
TES1_RS06325	Na^+/H^+ antiporter MnhF
TES1_RS06330	NADH dehydrogenase
TES1_RS06335	MbhN
TES1_RS06340	NADH dehydrogenase
TES1_RS06345	hypothetical protein
TES1_RS06350	MbhH
TES1_RS06355	RNA binding protein
TES1_RS06360	CODH accessory protein (CooC)
TES1_RS06365	CODH catalytic subunit
TES1_RS06370	CODH 4Fe-4S subunit (RS06370)

Gene	Description
Sulfhydrogenase (*sh*)	
TES1_RS00840	Sulf2 subunit b
TES1_RS00845	Sulf2 subunit g
TES1_RS00850	Sulf2 subunit d
TES1_RS00855	Sulf2 subunit a
F_{420}-dependent-like hydrogenase (*frh*)	
TES1_RS07835	F_{420} hydrogenase subunit alpha
TES1_RS07840	F_{420} hydrogenase subunit beta
TES1_RS07845	F_{420} hydrogenase subunit gamma
TES1_RS07850	F_{420} hydrogenase subunit alpha

Table 8 Coding sequences that showed more than two-fold differences in gene expression for grouped maltose and tryptone growth versus grouped maltose plus H_2 and tryptone plus H_2 growth. Expression counts are in transcripts-per-million.

	Coding sequence	Name	0.5% maltose			0.5% tryptone		0.5% malt. + 70 µM H_2			0.5% tryp. + 70 µM H_2			Log_2FC
			M1	M2	M3	T2	T3	MH1	MH2	MH3	TH1	TH2	TH3	
	Upregulated with H_2													
Formate hydrogenlyase 1	TES1_RS05180	alcohol dehydrogenase	538	694	878	1506	1343	2609	3149	2535	8654	10478	3239	2.237
	TES1_RS07770	H^+/Na^+ antiporter F	475	445	738	429	433	2161	7475	4771	1123	1608	1231	1.501
	TES1_RS07775	formate transporter	475	445	737	1387	870	2162	7474	4770	4603	7256	7640	2.858
	TES1_RS07780	hypothetical protein	324	404	617	888	711	1339	3177	2520	3173	5032	4775	2.468
	TES1_RS07785	hydrogenase subunit I	261	377	573	677	585	1041	1777	1750	2285	3675	3218	2.168
	TES1_RS07790	FHL subunit 6	244	274	530	666	507	1333	2187	2060	2740	3966	3392	2.576
	TES1_RS07795	hydrogenase subunit G	194	240	465	474	398	900	1408	1411	2047	2692	2321	2.343
	TES1_RS07800	hydrogenase subunit C	134	153	368	316	279	614	917	989	1539	2168	1772	2.388
	TES1_RS07805	hydrogenase subunit B	150	188	452	455	341	683	1106	1229	2400	2766	2309	2.415
	TES1_RS07810	NADH dehydrogenase	163	226	489	446	357	694	695	1014	2061	2339	2141	2.046
	TES1_RS07815	hydrogenase subunit D	156	181	410	436	316	670	489	925	2095	2133	1967	2.059
	TES1_RS07820	FDH 4Fe-4S subunit	502	442	965	1140	684	7063	4758	5439	5763	6450	6427	3.059
	TES1_RS07825	Fdh α subunit	417	372	838	1107	617	5818	3588	4679	5585	5242	5911	3.044

Table 9 Coding sequences that showed more than two-fold differences in gene expression for maltose growth versus maltose plus H_2 growth. Expression counts are in transcripts-per-million.

	Coding sequence	Name	0.5% maltose			0.5% malt. + 70 µM H_2			Log_2FC
			M1	M2	M3	MH1	MH2	MH3	
	Down-regulated with H_2:								
	TES1_RS08035	riboflavin transport	1639	1047	1239	287	396	448	1.65
	Up-regulated with H_2:								
FHL 1	TES1_RS05180	alcohol dehydrogenase	538	694	878	2609	3149	2535	2.142
	TES1_RS07775	formate transporter	475	445	737	2161	7474	4771	3.094
	TES1_RS07780	hypothetical protein	324	404	617	1339	3178	2520	2.489
	TES1_RS07790	FHL subunit 6	244	274	530	1332	2187	2060	2.616
	TES1_RS07820	FDH 4Fe-4S subunit	502	442	965	7060	4758	5439	3.360
	TES1_RS07825	Fdh α subunit	417	372	838	5817	3588	4679	3.315

Table 10 Coding sequences that showed more than two-fold differences in gene expression for tryptone growth versus tryptone plus H_2 growth. Expression counts are in transcripts-per-million.

Coding sequence	Name	0.5% tryptone		0.5% tryp. + 70 μM H_2			Log_2FC
		T2	T3	TH1	TH2	TH3	
Down-regulated with H_2:							
TES1_RS04455	hypothetical protein	1249	1033	522	557	739	1.089
TES1_RS04620	hypothetical protein	822	718	363	327	335	1.298
TES1_RS05065	adenosylcobinamide amidohydrolase	696	640	335	366	387	1.025
TES1_RS05100	cobalamin (B_{12}) biosynthesis protein	757	703	242	339	319	1.438
TES1_RS05105	adenosylcobinamide-GDP ribazoletransferase	657	629	269	331	329	1.199
TES1_RS05110	phosphatidylglycero-phosphatase A	971	926	433	471	495	1.163
TES1_RS05115	ATP pyrophosphatase	796	756	276	306	333	1.488
TES1_RS05120	Asp. aminotransferase	922	872	304	363	379	1.491
TES1_RS05125	radical SAM protein	558	499	199	264	288	1.243
TES1_RS05130	uracil-DNA glycosylase	502	438	192	262	255	1.147
TES1_RS05135	ATPase	624	589	252	321	316	1.180
TES1_RS05140	hypothetical protein	1060	892	246	381	390	1.666
TES1_RS05145	B_{12} biosynthesis	468	411	130	216	221	1.405
TES1_RS05160	aminotransferase	818	738	196	316	344	1.639
TES1_RS05200	ATPase	707	793	265	408	348	1.282
TES1_RS05245	xanthine phosphoribosyltransferase	1593	1632	684	932	643	1.405
TES1_RS05280	ABC transporter	6843	7703	2163	2856	3394	1.521
TES1_RS05885	chromatin protein	929	926	414	438	402	1.273
TES1_RS05890	chromosome segregation protein	714	679	339	364	379	1.074
TES1_RS07310	cystathionine gamma-synthase	678	580	330	296	338	1.106
TES1_RS07370	Fe-S assembly	2206	1874	633	877	1028	1.437
TES1_RS07375	ABC transporter	1656	1360	561	759	785	1.265
TES1_RS08085	transcription factor	1198	996	610	662	530	1.004
TES1_RS08480	permease	503	500	267	282	264	1.012
TES1_RS08770	ATPase	770	728	414	381	431	1.005
TES1_RS08850	ABC transporter	2947	2305	1096	968	1016	1.473
Up-regulated with H_2:							
TES1_RS07740	H^+/Na^+ antiporter D	314	261	615	999	813	1.310
TES1_RS07745	H^+/Na^+ antiporter E	530	475	1207	1864	1543	1.459
TES1_RS07750	H^+/Na^+ antiporter C	509	465	1262	2016	1550	1.575
TES1_RS07755	H^+/Na^+ antiporter B	424	344	1082	1639	1249	1.633
TES1_RS07760	Hypothetical protein	551	508	1373	1935	1640	1.514
TES1_RS07765	H^+/Na^+ antiporter G	576	600	1268	1875	1475	1.253
TES1_RS07770	H^+/Na^+ antiporter F	429	433	1123	1608	1231	1.494
TES1_RS07775	formate transporter	1388	870	4604	7256	7641	2.363
TES1_RS07780	hypothetical protein	888	711	3173	5032	4775	2.272
TES1_RS07785	hydrogenase subunit I	677	585	2285	3675	3219	2.103
TES1_RS07790	FHL subunit 6	666	507	2740	3966	3393	2.373
TES1_RS07795	hydrogenase subunit G	474	398	2047	2692	2321	3.017
TES1_RS07800	hydrogenase subunit C	316	279	1540	2169	1773	2.475
TES1_RS07805	hydrogenase subunit B	455	341	2400	2767	2309	2.510
TES1_RS07810	NADH dehydrogenase	446	357	2061	2340	2141	2.294
TES1_RS07815	hydrogenase subunit D	436	316	2095	2133	1967	2.316
TES1_RS07820	FDH 4Fe-4S subunit	1140	684	5763	6450	6427	2.613
TES1_RS07825	Fdh α subunit	1107	617	5585	5242	5911	2.600
TES1_RS09550	ABC transporter	210	244	421	681	856	1.327
TES1_RS09555	Gfo-Idh oxioreductase	210	244	421	681	856	1.327

Formate hydrogenlyase 1

Table 11 Coding sequences that showed more than 10-fold differences in gene expression for grouped maltose and tryptone growth versus formate growth. Expression counts are in transcripts-per-million.

	Coding sequence	Name	0.5% maltose			0.5% tryptone		0.1% formate			Log2FC
			M1	M2	M3	T2	T3	F1	F2	F3	
	Down-regulated with formate:										
	TES1_RS00835	Fd-NADP$^+$ reductase α subunit	171	273	294	227	278	8	7	10	3.640
	TES1_RS02780	hypothetical protein	177	303	478	348	429	13	9	13	3.572
	TES1_RS03660	hypothetical protein	206	472	601	414	527	19	11	22	3.387
	TES1_RS04195	hypothetical protein	198	402	445	420	531	14	9	9	3.945
	TES1_RS04200	hypothetical protein	119	226	267	238	295	60	68	59	3.544
	Up-regulated with formate:										
	TES1_RS05180	alcohol dehydrogenase	538	694	878	1505	1342	6086	5681	6924	3.961
Formate hydrogenlyase 1	TES1_RS07740	H^+/Na^+ antiporter D	106	132	214	314	261	2086	2236	2153	4.721
	TES1_RS07745	H^+/Na^+ antiporter E	180	303	429	530	475	3430	3799	3484	4.545
	TES1_RS07750	H^+/Na^+ antiporter C	176	276	445	509	464	3567	4150	3587	4.665
	TES1_RS07755	H^+/Na^+ antiporter B	129	195	307	424	343	2675	2929	2815	4.665
	TES1_RS07760	hypothetical protein	189	298	419	550	507	2643	2637	2936	4.129
	TES1_RS07765	H^+/Na^+ antiporter G	211	398	627	575	599	2689	2885	2913	3.890
	TES1_RS07770	H^+/Na^+ antiporter F	164	279	465	429	433	2128	2192	2298	3.976
	TES1_RS07775	formate transporter	475	445	738	1387	870	18065	23026	16021	5.928
	TES1_RS07780	hypothetical protein	324	404	617	888	711	8909	10019	8387	5.262
	TES1_RS07785	hydrogenase subunit I	261	377	573	677	585	5691	5788	5135	4.773
	TES1_RS07790	FHL subunit 6	244	274	530	666	507	6101	6040	5784	5.056
	TES1_RS07795	hydrogenase subunit G	194	240	465	423	474	3596	3553	3466	3.321
	TES1_RS07800	hydrogenase subunit C	134	153	368	316	279	2340	3539	2375	4.758
	TES1_RS07805	hydrogenase subunit B	150	188	451	455	341	6263	4967	3259	4.914
	TES1_RS07810	NADH dehydrogenase	163	226	489	446	357	1625	2800	1829	3.933
	TES1_RS07815	hydrogenase subunit D	156	181	410	436	316	670	489	925	4.576
	TES1_RS07820	FDH 4Fe-4S subunit	502	442	965	1140	684	6447	9868	5950	4.259
	TES1_RS07825	Fdh α subunit	417	372	838	1107	617	4477	6451	4573	4.101
	TES1_RS08850	ABC transporter	3203	2755	4113	2946	2304	23541	25036	19223	3.990
	TES1_RS10065	ABC transporter	604	447	636	610	570	3807	5011	3056	4.298
	TES1_RS10070	ABC transporter	3009	1542	2119	2853	2210	19055	23518	16213	4.758

Table 12 Coding sequences that showed more than two-fold differences in gene expression for maltose growth versus tryptone growth. Expression counts are in transcripts-per-million.

Coding sequence	Name	0.5% maltose			0.5% tryptone		Log_2FC
		M1	M2	M3	T2	T3	
Up-regulated with maltose:							
TES1_RS00080	ribonucleotide reductase	562	410	390	209	236	1.149
TES1_RS00315	PEP synthetase	3545	3738	1835	704	673	2.191
TES1_RS00345	paraslipin	502	338	354	197	234	1.010
TES1_RS00640	glucose-6-phosphate isomerase	913	896	767	324	338	1.499
TES1_RS00760	carbamoyltransferase	836	837	764	403	424	1.102
TES1_RS01535	phosphorylase	813	796	758	297	338	1.448
TES1_RS01920	fructose-bisphosphate aldolase	1018	997	759	303	320	1.682
TES1_RS02135	hydroxymethyltransferase	766	716	577	347	356	1.078
TES1_RS04730	ribosomal protein	2625	3097	1662	901	1050	1.409
TES1_RS04735	DNA endonuclease	735	922	598	284	344	1.367
TES1_RS04740	ribosomal protein	1019	1289	784	425	511	1.226
TES1_RS04745	transcription factor	1144	1382	830	501	571	1.149
TES1_RS04960	coenzyme F390 synthetase	719	642	490	295	315	1.123
TES1_RS05485	UMP kinase	859	865	700	421	438	1.026
TES1_RS05610	GTPase	547	511	455	206	220	1.367
TES1_RS06220	sugar-related operon	2401	848	1313	193	204	2.950
TES1_RS06400	ADP-specific phosphofructokinase	420	398	418	211	238	1.014
TES1_RS06535	ABC transporter	639	615	529	298	304	1.101
TES1_RS06545	ABC transporter	1373	1334	1149	669	682	1.051
TES1_RS06570	helicase	383	488	387	156	198	1.365
TES1_RS07520	hypothetical protein	457	423	546	201	221	1.304
TES1_RS07855	RNA binding protein	4149	3819	2435	953	1084	1.855
TES1_RS07860	hypothetical protein	1230	1107	796	395	432	1.437
TES1_RS08030	aminotransferase	2638	2229	2032	631	616	2.003
TES1_RS08035	membrane protein	1639	1047	1239	274	320	1.159
TES1_RS08695	maltotriose binding protein	6899	4992	5082	783	702	3.043
TES1_RS08700	sugar transporter	768	628	1126	311	324	1.513
TES1_RS08705	sugar transporter	832	644	1335	343	342	1.536
TES1_RS08710	amylopullulanase	1617	1257	2414	522	527	1.839
TES1_RS08715	ABC transporter	1205	915	1690	395	394	1.788
TES1_RS08910	ATP synthase	768	628	1126	311	324	1.013
TES1_RS09250	transcriptional regulator	1801	1581	1430	915	820	1.014
TES1_RS09310	peptidase	539	383	415	214	260	1.045
TES1_RS09480	Fe-S oxidoreductase	907	520	460	193	221	1.676
TES1_RS09520	GAPOR	763	701	666	330	347	1.196
TES1_RS09525	triose-phosphate isomerase	1114	1074	950	432	475	1.333
TES1_RS09925	carbohydrate related	886	782	859	184	211	2.233
TES1_RS10260	ribosomal protein	1920	2485	1129	616	702	1.520
TES1_RS10295	ribosomal protein	1665	1656	1052	611	671	1.274
TES1_RS10300	ribosomal protein	1617	1693	1219	750	844	1.034
TES1_RS10430	elongation factor	1295	1359	851	554	574	1.141
TES1_RS10660	glycosyl hydrolase	556	424	522	254	252	1.114
TES1_RS10685	hypothetical protein	1814	1282	982	354	378	1.974
Up-regulated with tryptone:							
TES1_RS01870	hypothetical protein	559	410	658	1649	1317	1.328
TES1_RS02575	argininosuccinate synthase	106	141	191	460	356	1.396
TES1_RS02590	carbamoyl-phosphate synthase	90	119	160	319	273	1.182
TES1_RS03680	HSP70-related protein	214	202	235	2627	2010	3.290
TES1_RS03685	HSP70-related protein	305	271	313	8483	6963	4.572
TES1_RS03690	HSP70-related protein	303	214	308	5894	4867	4.185
TES1_RS03695	GTP binding protein	137	148	181	1096	909	2.577
TES1_RS04235	transcriptional regulator	121	127	164	321	313	1.083
TES1_RS04915	YbjQ family protein	147	168	235	576	471	1.400

TES1_RS05015	hypothetical protein	135	111	197	407	387	1.339
TES1_RS05055	Transporter	106	159	175	358	325	1.122
TES1_RS05065	adenosylcobinamide amidohydrolase	195	239	273	696	640	1.388
TES1_RS05095	hypothetical protein	192	233	324	687	646	1.313
TES1_RS05100	cobalamin biosyn.	170	151	245	757	702	1.862
TES1_RS05105	adenosylcobinamide-GDP ribazoletransferase	162	188	288	657	629	1.515
TES1_RS05110	Phosphatidylglycerophosphatase	293	321	422	971	926	1.349
TES1_RS05115	ATP pyrophosphatase	235	231	323	796	756	1.453
TES1_RS05120	hypothetical protein	273	234	335	922	872	1.566
TES1_RS05125	radical SAM protein	111	117	173	558	499	1.888
TES1_RS05130	uracil-DNA glycosylase	125	140	187	502	438	1.536
TES1_RS05135	ATP-binding protein	166	202	272	624	589	1.402
TES1_RS05140	hypothetical protein	167	169	269	1060	892	2.173
TES1_RS05145	cobalamin biosyn.	127	92	143	468	411	1.767
TES1_RS05150	DNA polymerase	376	242	334	865	755	1.255
TES1_RS05155	hypothetical protein	294	226	284	655	596	1.103
TES1_RS05160	Aminotransferase	246	248	342	818	738	1.365
TES1_RS05165	formate dehydrogenase	645	801	1129	2624	2303	1.425
TES1_RS05170	glutamate synthase	448	532	802	1837	1598	1.435
TES1_RS05175	4Fe-4S ferredoxin	247	268	364	940	834	1.493
TES1_RS05195	hypothetical protein	222	216	260	654	719	1.426
TES1_RS05200	ATP-binding protein	170	217	273	707	793	1.653
TES1_RS05205	Peptidase	202	287	314	733	846	1.448
TES1_RS05215	hypothetical protein	285	279	333	2227	1982	2.690
TES1_RS05220	CAAX protease	378	474	507	1704	1625	1.762
TES1_RS05285	hypothetical protein	247	219	227	968	1009	1.009
TES1_RS05235	hypothetical protein	746	952	887	2002	2523	1.253
TES1_RS05240	Peptidase	294	353	334	766	923	1.235
TES1_RS05255	hypothetical protein	353	422	379	1170	1330	1.572
TES1_RS05260	ABC transporter	507	611	528	1332	1501	1.245
TES1_RS05265	ABC transporter	1190	1787	1335	3843	4433	1.421
TES1_RS05270	ABC transporter	887	1294	983	2892	3277	1.441
TES1_RS05275	ABC transporter	636	807	629	1893	2133	1.426
TES1_RS05285	hypothetical protein	247	219	227	968	1009	1.967
TES1_RS05575	hypothetical protein	268	313	385	942	806	1.331
TES1_RS06470	CoA-binding protein	166	178	216	462	413	1.107
TES1_RS06640	hypothetical protein	233	174	301	825	639	1.538
TES1_RS08075	ABC transporter	185	192	223	462	442	1.052
TES1_RS08480	nitroreductase	192	216	216	504	501	1.145
TES1_RS09040	potassium transporter	133	136	141	497	327	1.451
TES1_RS10405	GTP cyclohydrolase	133	93	152	240	317	1.019
TES1_RS10720	hypothetical protein	283	327	447	1128	968	1.475

3.4.3 Flux balance analysis

Some *Thermococcus*, such as *T. zilligii*, *T. kodakarensis*, and *T. paralvinellae*, secrete formate by an unknown mechanism when grown on glucose or tryptone (Xavier et al., 2000; Nohara et al., 2014; Hensley et al., 2016). When H_2 concentrations become inhibitory and reduced Fd cannot be oxidized, *Thermococcus* could be oxidizing the excess H_2 to form formate using FHL1 at the expense of ATP formation due to translocation of a H^+ back into the cell (Fig. 14). Alternatively, *T. paralvinellae* has gene homologs for a soluble, Fd-dependent formate dehydrogenase (Jung et al., 2014), but there was no increase in expression of these genes with added H_2, and previous Fd-dependent formate dehydrogenase enzyme activity assays using *T. paralvinellae* showed no activity (Hensley et al., 2016). In *E. coli*, formate and acetyl-CoA are made from pyruvate by pyruvate formate lyase (PFL) when the disposal of electrons on NADH is inhibited (Fig. 14). This reaction is *in lieu* of pyruvate dehydrogenase that forms acetyl-CoA, CO_2, and NADH. The formate from PFL is then transferred to FHL on the membrane for electron disposal as H_2 (McDowall et al., 2014). In *Thermococcus*, pyruvate cleavage and oxidation are catalyzed by pyruvate oxidoreductase and are Fd dependent rather than NAD^+ dependent. There is no bacterial PFL homolog in *T. paralvinellae* (Jung et al., 2014) and there was no evidence for this enzyme activity in *T. zilligii* or *T. litoralis* that produced formate (Xavier et al., 2000; Takács et al., 2008).

When fed ^{13}C-glucose, the labeled metabolite pattern of *T. zilligii* suggested that formate production occurred through a novel pentose phosphoketolase (PPK) pathway (Xavier et al., 2000). In this pathway, glucose-6-phosphate is oxidized to gluconate-6-phosphate, which is cleaved to form formate and ribulose-5-phosphate. Ribulose-5-

phosphate is isomerized into xylulose-5-phosphate, which is then split into acetyl-CoA and glyceraldehyde-3-phosphate, all using unknown mechanisms (Fig. 14). This pathway could partially divert glucose-6-phosphate around the Fd-dependent glyceraldehyde-3-phosphate oxidoreductase in the Embden-Meyerhof Pathway and the pyruvate oxidoreductase when Mbh is inhibited by high H_2. All these possible formate metabolisms can ameliorate H_2 inhibition with energetic costs to the cell and were included in our flux balance analysis to test their effect on growth (Fig. 14).

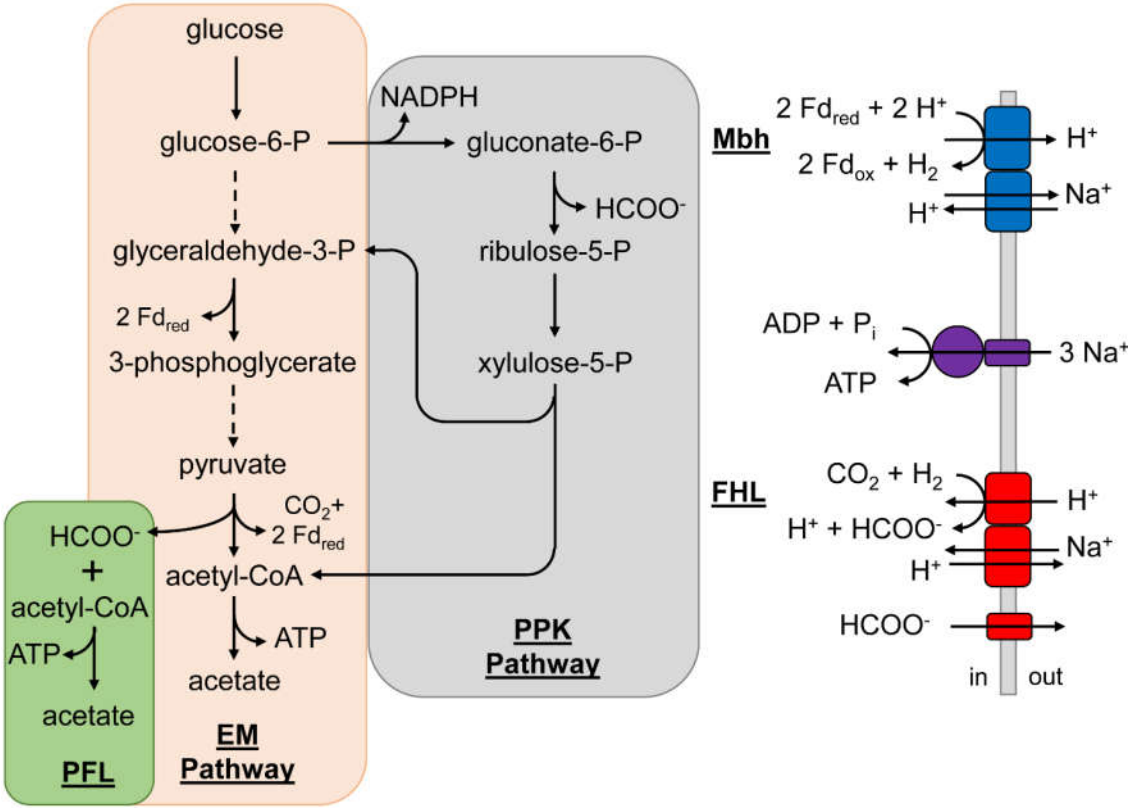

Figure 14 Glycolytic pathways using the archaeal Embden-Meyerhof (EM) pathway and the pentose phosphoketolase (PPK) pathway proposed by Xavier et al. (2000). These are juxtaposed with pyruvate formate lyase (PFL) in the cytoplasm and Fd-dependent hydrogenase (Mbh) with a H+/Na+ antiporter, ATP synthase, formate hydrogenlyase (FHL) with a H+/Na+ antiporter, and a formate uniporter on the cytoplasmic membrane.

To further assess the phenotypic implications of H_2 inhibition and the energetic costs of formate production, and account for other potential undetected mechanisms of formate production, a genome-scale metabolic network model of *T. paralvinellae* was constructed that accounts for 850 cellular reactions and 825 metabolites. The biomass objective function (BOF) was curated to simulate the growth rate of the cell as the cells grew on maltose. The flux rates of each reaction as well as the BOF were analyzed using flux balance analyses for four scenarios that tested formate metabolism during H_2 inhibition. The cells i) lacked any formate metabolism, ii) had FHL, iii) had FHL and PPK, and iv) had FHL and PFL. Every scenario where the cells have formate metabolism included FHL due to RNA-Seq results that show its upregulation upon H_2 inhibition and the formate transporter gene that is included with the FHL operon. With increasing H_2 inhibition, growth rates decreased for each modeling scenario; however, less so if the cells had a mechanism to generate formate (Fig. 15). The results showed that without any H_2 inhibition all the excess electrons from Fd were disposed of as H_2 with a modeled cellular growth rate of 0.374 h^{-1} (Fig. 15). In cells that lacked the alternate mechanism for electron disposal in the form of formate, the cell could not grow after 20% H_2 inhibition. If only the FHL was added to the model, where excess H_2 is oxidized on the membrane at the expense of H^+ influx through the FHL rather than Na^+ through the ATP synthase, the cells were resistant to H_2 up to 60% in the environment. If the PFL was added to the model that already had FHL, the cells were resistant to H_2 up to 80% in the environment as formate was produced from pyruvate which reduced the demand for Fd. The highest resistance to added H_2 occurred when both the PPK pathway and FHL were present. Under these conditions, there was less demand for Fd as an electron carrier as half of the

electrons from glucose were diverted to PPK pathway. Additionally, excess H_2 was oxidized by FHL on the membrane.

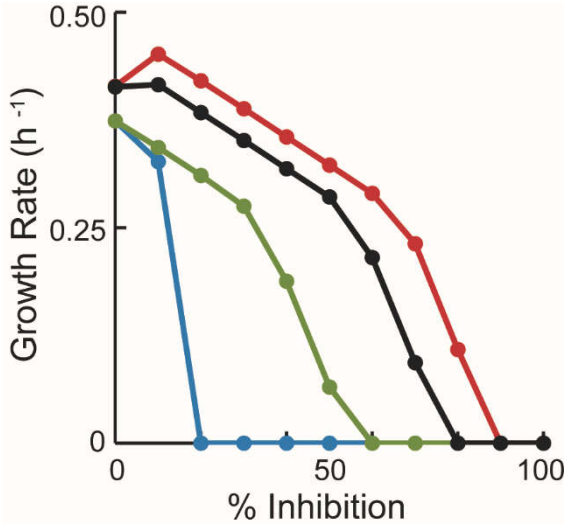

Figure 15 Biomass objective function simulations with *T. paralvinellae* metabolic network model as H_2 export (or exchange) limitation increased for cells lacking formate metabolism (●), cells with formate hydrogenlyase (FHL) only (●), cells with FHL and pyruvate formate lyase (●), and cells with FHL and the pentose phosphoketolase pathway (●).

3.4.4 Origin and role of FHL in *Thermococcus*

Membrane-bound, H_2-evolving hydrogenases have been proposed to be the origin of energy conservation in all respiratory organisms (Schut et al., 2013). They share an evolutionary history and structure with mitochondrial complex I and bacterial Nuo complexes (Andrews et al., 1997; Schut et al., 2013). The H^+/Na^+ antiporter and the hydrogenase in the complex can function together with a formate dehydrogenase or CO dehydrogenase for additional metabolic versatility (Schut et al., 2013). The question remains as to whether *fhl* was lost in many *Thermococcus* species through genetic drift or obtained by a few species through horizontal gene transfer. The *fhl* operon is found in distantly related *Thermococcus* such as *T. paralvinellae* and *T. onnurineus* (Hensley et al., 2014), which may be indicative of horizontal gene transfer. However, there is no

evidence of insertion elements near the operon nor G+C mol% differences that support this notion. A previous study showed that *Thermococcus* lacks a simple model of allopatric speciation (Price et al., 2015). Therefore, *Thermococcus* lineages with and without *fhl* and *codh* operons likely coexist in the same habitat and vary in relative abundances depending on environmental conditions.

It was suggested that formate oxidation to H_2 and CO_2 in *Thermococcus* represents a primitive metabolism that still occurs in modern subsurface environments (Kozhevnikova et al., 2016), but it is questionable if this is possible thermodynamically. Formate is in thermodynamic equilibrium with CO_2 and H_2 in most high-temperature (>100°C) subsurface environments (McCollom and Seewald, 2003). This accounts for relatively high formate concentrations in strongly reducing environments such as serpentinites, and the low concentrations in mildly reducing environments such as oil-field brines and formation water sedimentary basins. The highest formate concentrations reported for 105-114°C hydrothermal fluids were 158 μM and 669 μmol kg^{-1} from serpentinizing hydrothermal systems at Lost City and Mid-Cayman Rise vent sites, respectively (Lang et al., 2010; McDermott et al., 2015). These same serpentinite fluids had H_2 concentrations of 12.3 mmol kg^{-1} and 10.2 mM, respectively. Since formate oxidation to H_2 is endergonic under standard conditions ($\Delta G° = +1.3$ kJ mol^{-1}), it is unlikely that *Thermococcus* uses formate to make H_2 in serpentinite environments where H_2 concentrations greatly exceed those of formate. In oil-field waters, where hydrous pyrolysis of kerogen is the source of formate and H_2 is buffered by a pyrite-pyrrhotite-magnetite mineral assemblage, the calculated equilibrium formate concentrations are 5-76 μmol kg^{-1} (Carothers et al., 1978). *Thermococcus barophilus* Ch5, a close relative of

T. paralvinellae, had a Monod half-saturation constant (K_s) of 8 mM for formate and a minimum formate requirement of 1.1 mM for H_2 production from formate (Kozhevnikova et al., 2016). Therefore, it is unlikely that formate oxidation, from either internal or external sources, to H_2 and CO_2 is a common strategy for *Thermococcus* in nature.

In environments without S°, H_2 inhibition of *Thermococcus* could also be ameliorated by increasing the H_2 flux from the cells through syntrophic growth with a thermophilic hydrogenotroph such as a methanogen. This was demonstrated in microcosm incubations for a natural assemblage of *Thermococcus* and hyperthermophilic methanogens present in hydrothermal fluid samples (Topçuoğlu et al., 2016). This may explain the presence of thermophilic, hydrogenotrophic methanogens in marine sediments and petroleum reservoirs and may be a factor in natural gas production in those habitats.

3.5 Conclusion

This study showed that all seven hydrogenase operons are expressed in *T. paralvinellae*, including hydrogenases that are absent in closely related organisms. The two Mbhs are likely for energy generation on the cytoplasmic membrane, and the SH and perhaps Frh are anabolic hydrogenases. The role of CODH is unknown. FHL1 was likely active, even without added H_2, when formate was produced or oxidized. The *fhl1* operon expression levels and formate secretion rates increased when *T. paralvinellae* growth was inhibited by a high background of H_2 suggesting that this is an alternative electron disposal mechanism for the organism when electron disposal from Fd is not favorable. The electrons appear to be disposed of as formate using H_2 oxidation by FHL1 and

perhaps also a putative PFL or PPK pathway (Fig. 14). Further biochemical and genetic studies on formate metabolism in *Thermococcus* are needed to confirm the nature of the response. The combination of formate producing mechanisms provides cells with a growth advantage during H_2 inhibition over cells that have only one or none of the mechanisms.

CHAPTER 4

CHANGES IN GROWTH PARAMETERS AND GENE EXPRESSION IN THE HYPERTHERMOPHILE *METHANOCALDOCOCCUS JANNASCHII* DURING HYDROGEN-LIMITED AND SYNTROPHIC GROWTH

4.1 Introduction

Each year, approximately 1 Gt of CH_4 is produced globally through methanogenesis, largely by methanogens growing syntrophically with fermentative microbes that hydrolyze biopolymers (Thauer et al., 2008), but it is not known how much methanogenesis is from thermophilic syntrophy. Deep-sea hydrothermal vents are known habitats for thermophiles (Holden et al., 2012). Furthermore, it was estimated that 35% of all marine sediments are above 60°C (LaRowe et al., 2017) suggesting that these environments also provide a large global biotope for thermophiles. Microcosms containing low-temperature hydrothermal fluid as well as an archaeal coculture derived from a high-temperature oil pipeline each produced CH_4 through H_2 syntrophy at 80°C when supplemented with tryptone and yeast extract or yeast extract only, both without added H_2 (Davidova et al., 2012; Topçuoğlu et al., 2016). Both showed that CH_4 was produced from a mixed microbial community consisting of the hyperthermophilic H_2-producing heterotroph *Thermococcus* and the (hyper)thermophilic, hydrogenotrophic methanogens *Methanocaldococcus*, *Methanothermococcus*, and *Methanothermobacter*.

Molecular and culture-dependent analyses show that *Thermococcus* and thermophilic methanogens are collocated in hydrothermal vents (Takai et al., 2004; Nakagawa et al., 2005; Flores et al., 2011; Ver Eecke et al., 2012; Reveillaud et al., 2016;

Fortunato et al., 2018), produced waters from high-temperature petroleum reservoirs (Orphan et al., 2000; Bonch-Osmolovskaya et al., 2003; Nazina et al., 2006; Dahle et al., 2008; Kotlar et al., 2011; Lewin et al., 2014; Junzhang et al., 2014; Okpala et al., 2017), methane hydrate-bearing sediments (Inagaki et al., 2006), and mid-ocean ridge flanks (Ehrhardt et al., 2007). Thus, when high-temperature, organic-rich environments lack sufficient abiotic H_2 flux rates to support methanogen growth, collocated H_2-producing heterotrophs can be an alternate source of H_2. Therefore, it is important to understand how thermophilic methanogens respond kinetically and physiologically to H_2 limitation and grow through H_2 syntrophy.

In this study, *M. jannaschii* was grown in a chemostat under H_2-replete and H_2-limited conditions, and it was grown syntrophically in sealed bottles with the H_2-producing hyperthermophilic heterotroph *Thermococcus paralvinellae* using maltose and formate separately as the growth substrates. The purpose of this study was to measure specific growth rates and cell-specific CH_4 production rates for *M. jannaschii* with varying H_2 fluxes, to determine if *M. jannaschii* cell yield (amount of biomass produced per mole of CH_4 produced, Y_{CH4}) increases when cultures are shifted from H_2-replete to H_2-limited growth conditions, and if Y_{CH4} remains high or increases further during H_2 syntrophy. We previously showed that H_2 inhibited the growth of *T. paralvinellae*, which led to formate production as an alternative sink for electrons (Topçuoğlu et al., 2018). Therefore, this study also examined if H_2 syntrophy stimulates the growth rate or growth yield of *T. paralvinellae* or ameliorates its H_2 inhibition relative to its growth in monoculture. Furthermore, differential gene expression analysis using RNA-Seq was used to determine if changes occur in *M. jannaschii* for the expression of genes for

carbon assimilation, CH_4 production, or energy generation when H_2 decreases in availability. These data were then used to predict how a hyperthermophilic methanogen would behave in a high H_2 flux environment such as those found at some hydrothermal vents versus a low H_2-flux environment such as marine sedimentary environments and petroleum reservoirs.

4.2 Methods and materials

4.2.1 Growth media and culture conditions

Methanocaldococcus jannaschii DSM2661 (Jones *et al.*, 1983) and *Thermococcus paralvinellae* DSM 27261 (Hensley et al., 2014) were purchased from Deutsche Sammlung von Mikroorganismen und Zellkulturen (DSMZ). The growth medium for pure cultures of M. jannaschii was based on DSM medium 282 (Jones et al., 1983) and was composed of the following per liter: 30 g of NaCl, 3.40 g of $MgSO_4 \cdot 7H_2O$, 4.1 g of $MgCl_2 \cdot 6H_2O$, 0.33 g of KCl, 0.25 g of NH_4Cl, 0.14 g of K_2HPO_4, 0.14 g of $CaCl_2 \cdot 2H_2O$, 0.5 mg of $NiCl_2 \cdot 6H_2O$, 0.5 mg of $Na_2SeO_3 \cdot 5H_2O$, 1 g of $NaHCO_3$, 0.63 g of $Na_2S_2O_3$, 10 ml of DSM medium 141 trace elements solution, 10 ml of DSM medium 141 vitamins solution, and 50 µl of 0.5% (wt vol^{-1}) resazurin. For the cocultures of *M. jannaschii* and *T. paralvinellae* and monoculture of *T. paralvinellae,* the base medium was amended with 1 ml of 0.01% (wt vol^{-1}) each of $(NH_4)_2Fe(SO_4)_2 \cdot 6H_2O$ and $(NH_4)_2Ni(SO_4)_2$, 1 µM of $Na_2WO_4 \cdot 2H_2O$, 0.01% (wt vol^{-1}) of yeast extract (vitamin B_{12}-fortified; Difco). The primary carbon and energy source added for *T. paralvinellae* was either 0.05% (wt vol^{-1}) maltose (Sigma) or 0.1% (wt vol^{-1}) sodium formate (Fluka). All media were pH-balanced to 6.00 ± 0.05 and reduced with 0.025% (wt vol^{-1}) each of cysteine-HCl and $Na_2S \cdot 9H_2O$

before inoculation. To test if *M. jannaschii* can use formate, or yeast extract to grow in the absence of H_2 or if they stimulate growth in the presence of H_2, *M. jannaschii* was incubated in monoculture on the base medium amended with 0.1% formate and 0.01% yeast extract, and 0.01% yeast extract only as described above, each in serum bottles with 200 kPa of either H_2:CO_2 (80%:20%) or N_2:CO_2 (80%:20%) added to the headspace.

M. jannaschii was grown in monoculture at 82°C and high and low H_2 concentrations in a chemostat to measure its growth parameters and to generate biomass for gene expression analysis. A 2-L bioreactor with gas flow, temperature (± 0.1°C), and pH (± 0.1 unit) controls was used with 1.5 L of growth medium. For high H_2 conditions, the bioreactor was gassed with a mixture of CO_2 (20.5 ml min^{-1}) and H_2 (132 ml min^{-1}). For low H_2 conditions, the bioreactor was gassed with a mixture of CO_2 (20.5 ml min^{-1}), N_2 (130 ml of gas min^{-1}), and H_2 (2.5 ml min^{-1}). Pure gases were blended using a mass flow controller (Matheson Tri-Gas) and added to the bioreactor through a single submerged fritted bubbler. Aqueous H_2 and CH_4 concentrations were measured before and after inoculation by drawing 25 ml of medium from the bottom of the bioreactor directly into anoxic 60-ml serum bottles and measuring the headspace gas with a gas chromatograph. The aqueous H_2 concentrations in the bioreactor prior to inoculation were 80 μM for the high H_2 condition and 15-30 μM for the low H_2 condition (Table 13).

The media were inoculated with 50-100 ml of a logarithmic growth-phase culture of *M. jannaschii*. During growth, liquid samples were drawn from the bioreactor and cell concentrations were determined using phase-contrast light microscopy and a Petroff-Hausser counting chamber. *M. jannaschii* was grown in batch reactor mode until the culture reached late logarithmic growth phase, then the bioreactor was switched to

chemostat mode by pumping sterile growth medium into the bioreactor from a sealed 12-L reservoir that was degassed with N_2 through a submerged glass tube and heated to 75°C. Simultaneously and at the same rate, spent growth medium was pumped out of the bioreactor using a dual-channel peristaltic pump. The dilution rate of the chemostat matched the batch-phase growth rate of the organisms. The H_2 and CH_4 concentrations in the headspace of the bioreactor were measured with a gas chromatograph. Growth of *M. jannaschii* was stable in the chemostat after three volume replacements of the medium within the reactor and was monitored for an additional ~0.5 volume replacements to obtain kinetic data. The CH_4 production rate per cell (q) was calculated from the product of the CH_4 concentrations in the headspace, the gas flow rate, the medium dilution rate of the last three timepoints in chemostat growth and was normalized by the number of cells in the reactor. The cell yield per mole of CH_4 produced (Y_{CH4}) was calculated by dividing the number of methanogen cells in the reactor by the amount of CH_4 in the headspace at the last three timepoints in the chemostat growth. Then, the complete contents of the bioreactor were drained into ice-cooled centrifuge bottles, spun in a centrifuge at 10,000 × g and 4°C for 60 min, resuspended in 1 ml of TRIzol (Invitrogen), and frozen at -80°C until processed. Chemostats were run in triplicate for both conditions.

Attempts to grow *M. jannaschii* with *T. paralvinellae* in the chemostat when either maltose or formate was the energy source with and without stirring and gas flow of CO_2 (20.5 ml min^{-1}) and N_2 (130 ml min^{-1}) were unsuccessful. Therefore, *M. jannaschii* and *T. paralvinellae* were grown in coculture at 82°C in 2-L flasks containing 1.5 L of medium with 100 kPa of N_2:CO_2 (80%:20%) headspace and either maltose or formate as the energy source (Table 13). Separate logarithmic growth-phase cultures of *M.*

jannaschii and *T. paralvinellae* were combined to inoculate the bottles. The coculture was established immediately and did not require prior coculture transfers. At various times during growth, total cell concentrations in bottles were determined using a Petroff-Hausser counting chamber and phase-contrast light microscopy. The *M. jannaschii* cell concentration was determined by counting the number of autofluorescent cells using epifluorescence microscopy and ultraviolet light excitation (Doddema and Vogels, 1978). The concentration of *T. paralvinellae* cells was calculated by subtracting the concentration of *M. jannaschii* cells from the total cell concentration. For comparison, *T. paralvinellae* was also grown separately in bottles in monoculture on 0.5% maltose and separately on 0.1% sodium formate with 100 kPa of N_2:CO_2 headspace. Growth of the cells was measured as described above.

The growth rates (μ) of *M. jannaschii* and *T. paralvinellae* were determined by plotting cell concentration against time and fitting a logarithmic curve to the growth data. The total amounts of CH_4 and H_2 in the bottles were determined by gas chromatography. The concentrations of formate, acetate, butyrate, isovalerate, and 2-methylbutyrate were measured from aliquots of spent medium from each coculture and *T. paralvinellae* monoculture incubation at various time points using an ultra-high-pressure liquid chromatography (UHPLC) system as previously described (Hensley et al., 2016). Methanogen cell yields (Y_{CH4}) were determined from the linear slope of number of methanogen cells per bottle plotted against the amount of CH_4 per bottle (Ver Eecke et al., 2013). The rate of CH_4 production per cell is calculated from $\mu/(0.693\times Y_{CH4})$ as previously described (Ver Eecke et al., 2013). Similarly, *T. paralvinellae* cell yields based on acetate and formate produced (for maltose growth only) were determined from

the linear slope of *T. paralvinellae* cell concentration plotted against acetate or formate concentration. When the cocultures reached late logarithmic growth phase, the cells were harvested for transcriptome analysis as described above (*T. paralvinellae* cells were not harvested when grown in monoculture). Cocultures grown on maltose were grown in triplicate while cocultures grown on formate were grown in quadruplicate.

Table 13 Description of growth conditions. *M. jannaschii* was grown in monoculture in chemostats and in coculture with *T. paralvinellae* in 2-L bottles.

Experiment	Condition	Biological/Technical Replicates	Energy Source
M. jannaschii high H_2	Chemostat	3/1	80 μM H_2
M. jannaschii low H_2	Chemostat	3/1	15-30 μM H_2
T. paralvinellae maltose	Bottle	3/1	0.05% maltose
T. paralvinellae formate	Bottle	3/1	0.1% formate
Coculture maltose	Bottle	3/2	0.05% maltose
Coculture formate	Bottle	4/1	0.1% formate

4.2.2 RNA-Seq analysis

Total RNA was extracted from 13 cell pellets from each growth condition (Table 13) using a Direct-zol RNA extraction kit (Zymo). RNA quantity was determined using Qubit fluorometry. RNA integrity was checked using an Agilent 2100 bioanalyzer, a Nanodrop 2000 spectrophotometer, and gel electrophoresis of the RNA followed by staining with ethidium bromide. Removal of rRNA, library construction, multiplexing, and sequencing of the mRNA using an Illumina HiSeq2500 sequencer with 2×150 paired-ends was performed commercially by GENEWIZ, LLC (South Plainfield, NJ, USA) as described by the company. Sequencing depths ranged from 30,751,946 to 41,634,527 sequence reads per sample, with a median of 34,532,231 and a mean of 35,155,474 reads per sample. The RNA-Seq reads were mapped to both *M. jannaschii*

and *T. paralvinellae* genomes using BBSplit from BBMap package (https://sourceforge.net/projects/bbmap/). BBSplit is an aligner tool that bins sequencing reads by mapping to them multiple references simultaneously and separates the reads that map to multiple references to a special "ambiguous" file for each of them. For further analyses we removed all ambiguously mapped reads to both genomes and worked with only the reads that unambiguously map to *M. jannaschii* genome. 2-5% of the reads were lost in this step. For cocultures grown on maltose, 97% of the reads mapped unambiguously to the *T. paralvinellae* genome and 1.5% mapped to the *M. jannaschii* genome. For cocultures grown on formate, 67% of the reads mapped unambiguously to the *T. paralvinellae* genome and 29% mapped to the *M. jannaschii* genome. These proportions generally matched the proportions of *T. paralvinellae* and *M. jannaschii* cells in each coculture type based on cell concentration estimates.

The mapped reads for *M. jannaschii* were aligned to the *M. jannaschii* genome and sorted using the STAR aligner version 2.5.1b (Dobin et al., 2013). Aligned sequence reads were assigned to genomic features and quantified using featureCounts read summarization tool (Liao et al., 2014). The output of the analyses generated BAM files containing the sequence of every mapped read, its mapped location. An unsupervised *t*-distributed stochastic neighbor embedding (*t*-SNE) algorithm (Van Der Maaten and Hinton, 2008) and principal component analysis (PCA) was used to predict outliers among the total RNA sample replicates.

Genes that were differentially expressed were identified using ‘DESeq2’ in the Bioconductor software framework (www.bioconductor.org) in R (version 3.3 [http://www.r-project.org]) and on a Galaxy platform, respectively (Anders et al., 2010;

Goecks et al., 2010; Phipson et al., 2016). RLE (relative log expression)-normalization was performed by using the R package 'DESeq2'. The 'DESeq2' package allows for sequencing depth normalization between samples, estimates gene-wise dispersion across all samples and fits a negative binomial generalized linear model and applies Wald statistics to each gene. The genes were reported as differentially regulated if $\log_2FC > 1$ and the adjusted *p*-value was < 0.01. Heatmaps were plotted in R (version 3.3 [http://www.r-project.org]) using the 'pheatmap' package. The heatmap color scale represents the z-score, which is the number of standard deviations the mean score of the treatment is from the mean score of the entire population. The count files and raw sequences will be available in the NCBI Gene Expression Omnibus (GEO) database.

4.3 Results

4.3.1 Growth parameters for mono- and cocultures

In monoculture, the specific growth rate (μ) of *M. jannaschii* in the chemostat decreased from 1.05 h^{-1} ± 0.23 h^{-1} (± standard error) when grown on 80 μM $H_{2,aq}$ to 0.54 h^{-1} ± 0.17 h^{-1} when grown on 15-30 μM $H_{2,aq}$ (Fig. 16A). The growth rates of *M. jannaschii* decreased further when it was grown in coculture in bottles with *T. paralvinellae* to 0.12 h^{-1} ± 0.03 h^{-1} and 0.22 h^{-1} ± 0.06 h^{-1} when *T. paralvinellae* was grown on maltose and formate, respectively (Fig. 16A). Similarly, the cell-specific CH_4 production rate (*q*) decreased 3.75-fold when *M. jannaschii* was grown on 15-30 μM $H_{2,aq}$ relative to growth on 80 μM $H_{2,aq}$ (Fig. 16B). It was 31- and 21-fold lower when *M. jannaschii* was grown with *T. paralvinellae* on maltose and formate, respectively, relative to growth on high H_2 (Fig. 16B). However, the growth yield (Y_{CH4}) for *M. jannaschii*

increased 4.15-fold when cultures were grown on 15-30 μM $H_{2,aq}$ relative to growth on 80 μM $H_{2,aq}$ and was 13- and 10-fold higher than the growth yields for *M. jannaschii* when grown with *T. paralvinellae* on maltose and formate, respectively (Fig. 16C).

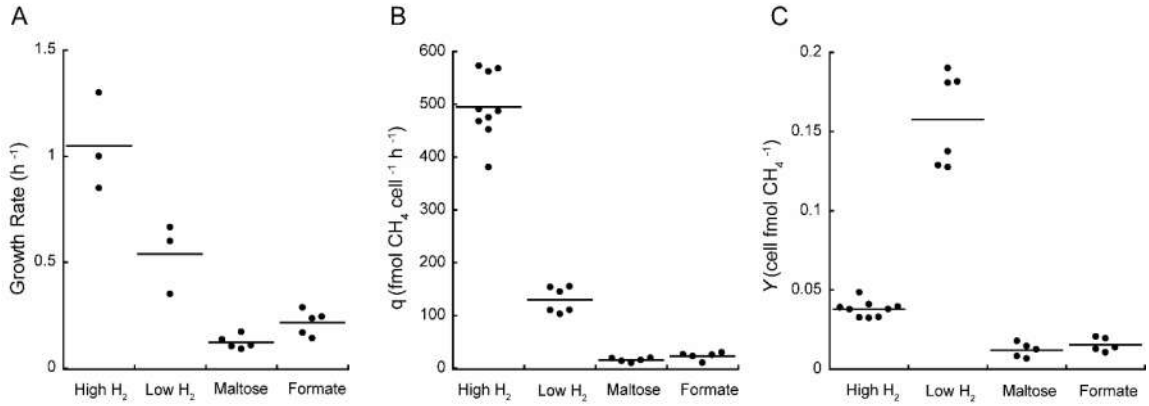

Figure 16 (A) Specific growth rate (μ), (B) cell-specific CH_4 production rate (q), and (C) cell yield (Y_{CH4}) for *M. jannaschii* grown in monoculture in the chemostat with high (80 μM) and low (15-30 μM) aqueous H_2 and grown in coculture with *T. paralvinellae* in bottles using maltose and formate as growth substrates. The horizontal bar represents the mean value.

There was no change in the specific growth rate of *T. paralvinellae* when it was grown with or without *M. jannaschii* or with change in carbon source (Fig. 17A). Furthermore, when grown on maltose, there was no change in the growth yield of *T. paralvinellae* when normalized to acetate production ($Y_{acetate}$) when grown in monoculture relative to growth in coculture with *M. jannaschii* (Fig. 17B). Similarly, the cell-specific acetate production rate (q) of *T. paralvinellae* remained unchanged when cells were grown with and without *M. jannaschii* (Fig. 18). However, when grown on maltose, *T. paralvinellae* only produced formate when grown in monoculture (Fig. 17C). There was no formate detected in the spent medium when *T. paralvinellae* was grown on maltose in coculture with *M. jannaschii*. There was no growth of *M. jannaschii* when it was incubated in monoculture in medium supplemented with 0.01% yeast extract, and 0.1% sodium formate and 0.01% yeast extract with N_2:CO_2 in the headspace. These

additions also did not stimulate the growth of *M. jannaschii* in monoculture when a H_2:CO_2 headspace was provided.

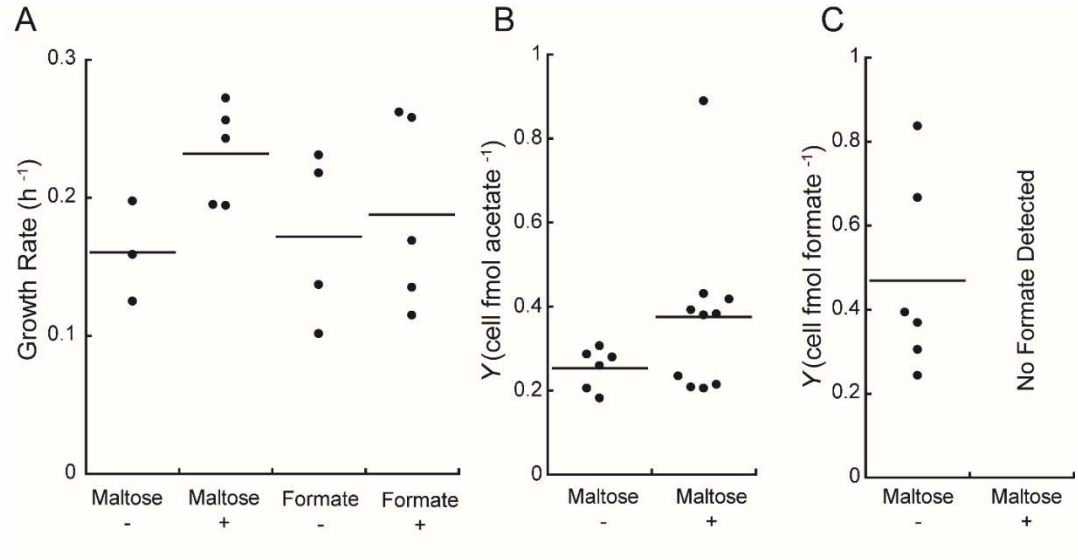

Figure 17 (A) Specific growth rate (μ) for *T. paralvinellae* in bottles grown in monoculture (-) and in coculture with *M. jannaschii* (+) on either maltose or formate. Cell yield (*Y*) for *T. paralvinellae* based on acetate (B) and formate (C) production for cells grown on maltose in monoculture (-) and in coculture with *M. jannaschii*. The horizontal bar represents the mean value.

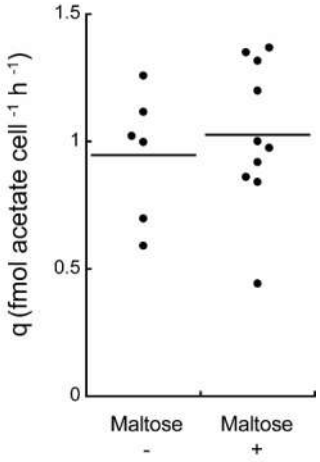

Figure 18 Cell-specific acetate production rate (*q*) for *T. paralvinellae* grown with and without *M. jannaschii* in bottles using maltose and formate as growth substrates.

4.3.2. Transcriptomic analyses

RNA-Seq mapped 1,866 transcripts to the *M. jannaschii* genome. The thirteen samples that span four growth conditions were analyzed based on *t*-Distributed Stochastic Neighbor Embedding (*t*-SNE) (Fig. 19A) and principal component analysis (PCA) results (Fig. 19B).

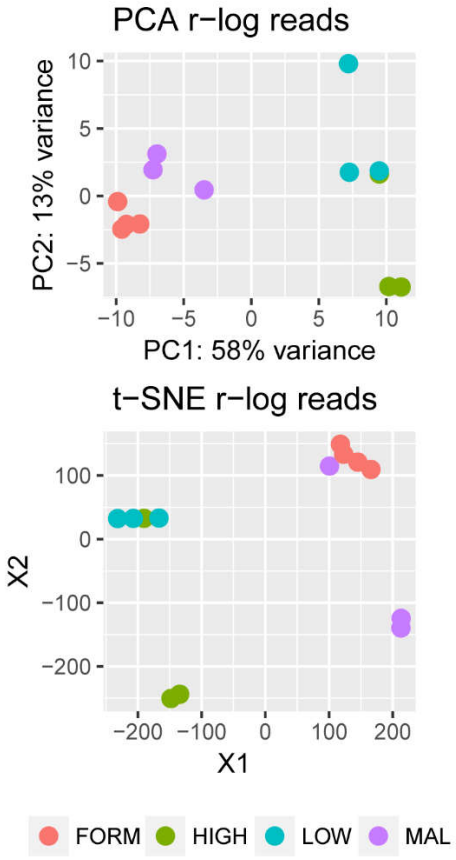

Figure 19 (A) Principal component analysis (PCA) (B) t-Distributed Stochastic Neighbor Embedding Analysis (t-SNE). Red and purple represent cocultures on formate and maltose, respectively. Blue and green represent monocultures with low H_2 and high H_2 conditions, respectively.

Pairwise comparisons of *M. jannaschii* grown in monoculture on high and low H_2 showed up to 12 genes to be differentially expressed (adjusted $p < 0.01$ and $\log_2FC > 1$) with 1 gene down-regulated and 11 genes up-regulated during growth on low H_2 relative

to growth on high H_2 (Table 14). Under low H_2 conditions, F_{420}-dependent methylene-tetrahydromethanopterin (H_4MPT) dehydrogenase (*mtd*, MJ_RS0555) gene expression increased 3.5-fold (Fig. 20A). There was no significant change in gene expression for H_2-dependent methylene-H_4MPT dehydrogenases (*hmd*, MJ_RS03820 and MJ_RS04180) (Fig. 20B, Fig. 21) or for any of the methyl-CoM reductase A I or II genes (*mcrA*, MJ_RS00415 and MJ_RS04540) (Fig. 22) for *M. jannaschii* grown on high and low H_2 in the chemostat. The genes that encode for a GTP binding protein (MJ_RS01180), bacteriohemerythrin (MJ_RS03980), radical SAM protein (MJ_RS04390), a signal recognition particle (MJ_RS05550), a transcriptional regulator (MJ_RS06225), and four hypothetical proteins were up-regulated on low H_2 while a gene that encodes for a histone (MJ_RS04990) was up-regulated on high H_2.

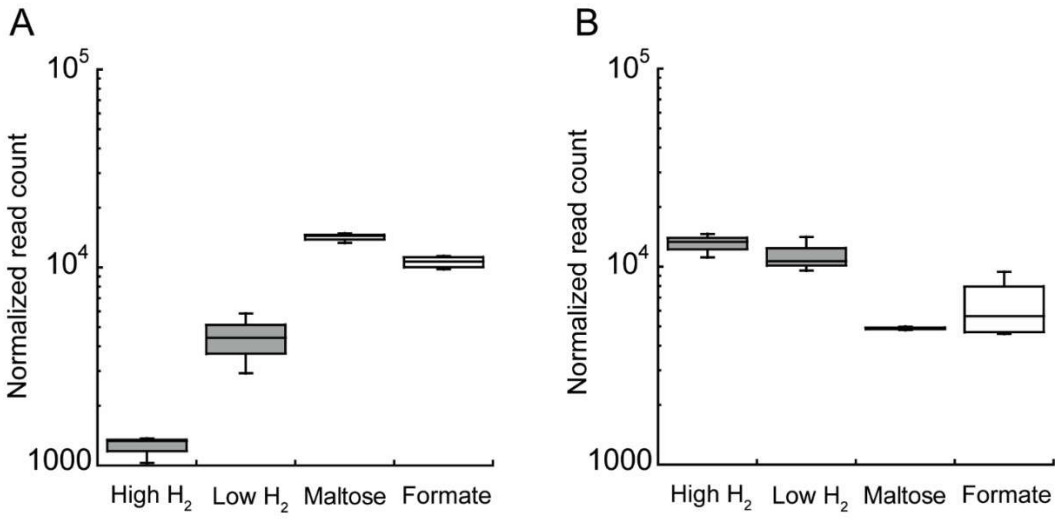

Figure 20 *M. jannaschii* transcript levels (relative log expression (RLE)-normalization) for F_{420}-dependent methylene-H_4MPT dehydrogenase (*mtd*, MJ_RS05555) (A) and H_2-dependent methylene-H_4MPT (*hmd*, MJ_RS04180) (B) for each growth condition.

Pairwise comparisons of *M. jannaschii* gene expression for cultures grown in monoculture and *M. jannaschii* grown in coculture with *T. paralvinellae* showed up to 338 genes to be differentially expressed (adjusted $p < 0.01$ and $\log_2FC > 1$) with 146 up-regulated genes and 192 down-regulated genes when grown in coculture relative to growth in monoculture on high and low H_2 (Table 15). F_{420}-dependent methylene-H_4MPT dehydrogenase (*mtd*, MJ_RS05555) gene expression was up-regulated 4.3-fold in coculture relative to *M. jannaschii* grown in monoculture conditions (Fig. 20A). In contrast, gene expression of H_2-dependent methylene-H_4MPT dehydrogenases (*hmd*X and *hmd*, MJ_RS03820 and MJ_RS04180) were downregulated 2.1-fold and 2.1-fold respectively, in *M. jannaschii* grown in coculture relative to *M. jannaschii* grown in monoculture (Fig. 20B, Fig. 21). There was no change in gene expression for the *mcr*I and *mcr*II genes (Fig. 22).

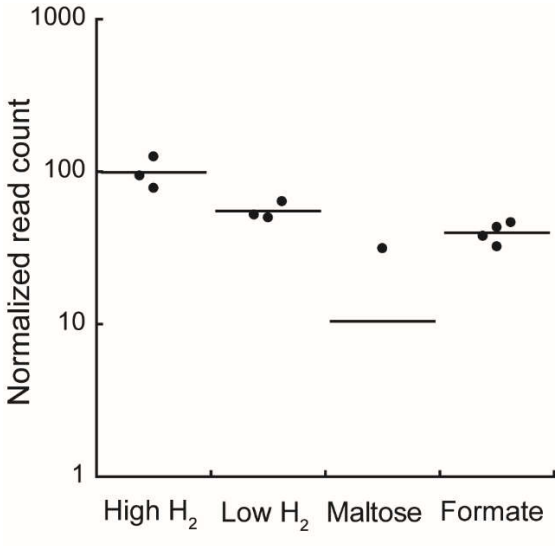

Figure 21 *M. jannaschii* transcript levels (relative log expression (RLE)-normalization) for H_2-dependent methylene-H_4MPT X (*hmd*X. MJ_RS03820) for each growth condition.

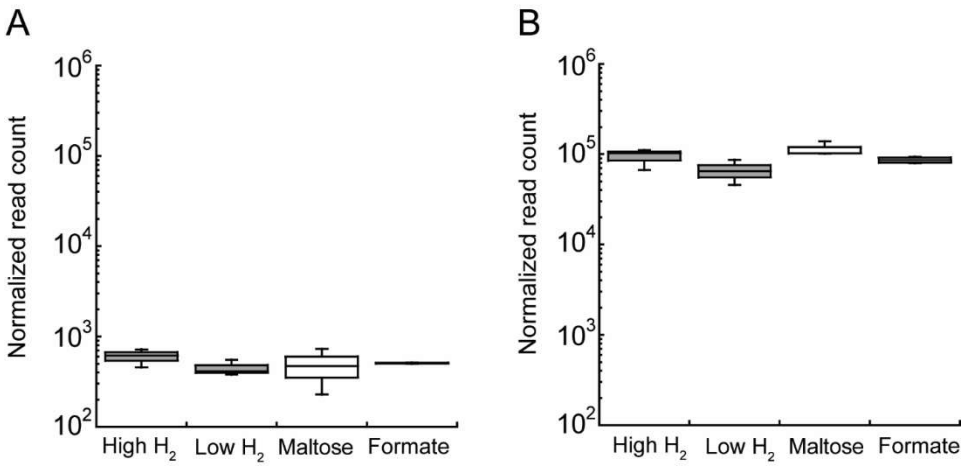

Figure 22 *M. jannaschii* transcript levels (relative log expression (RLE)-normalization) for (A) methyl-CoA reductase I subunit A (*mcrA*, MJ_RS00415) (B) methyl-CoA reductase II subunit A (*mcrA*, MJ_RS04540) for each growth condition.

Gene expression for a hypothetical protein with a predicted RNA-binding domain (MJ_RS03480) showed a 22.5-fold increase in cocultures relative to monocultures (Fig. 23). Expression of 6 to 9 *M. jannaschii* genes that encode for a V-type ATP synthase (MJ_RS01130-MJ_RS01165, MJ_RS03255) were down-regulated when cultures were grown in coculture relative to expression in *M. jannaschii* grown in monoculture (Fig. 24). Similarly, expression of 14 genes in a putative operon for membrane-bound, ferredoxin-dependent hydrogenase were also down-regulated in *M. jannaschii* cultures grown in cocultures relative to cultures grown in monoculture (Fig. 24). These genes include Eha subunits A and B (MJ_RS02795-02800), an oxidoreductase (MJ_RS02755), a dehydrogenase (MJ_RS02765), and a catalytic subunit (MJ_RS02730).

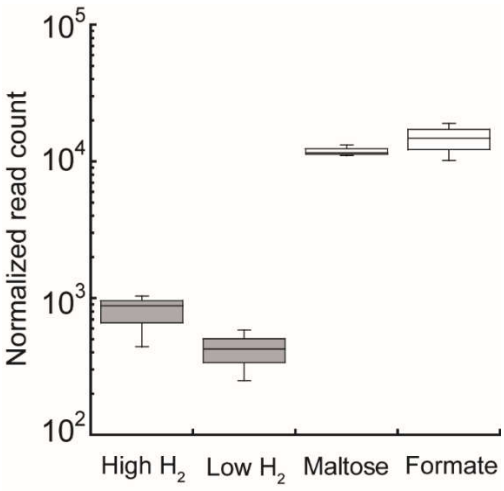

Figure 23 *M. jannaschii* transcript levels (relative log expression (RLE)-normalization) for MJ_RS03480, a hypothetical protein with a predicted RNA-binding domain.

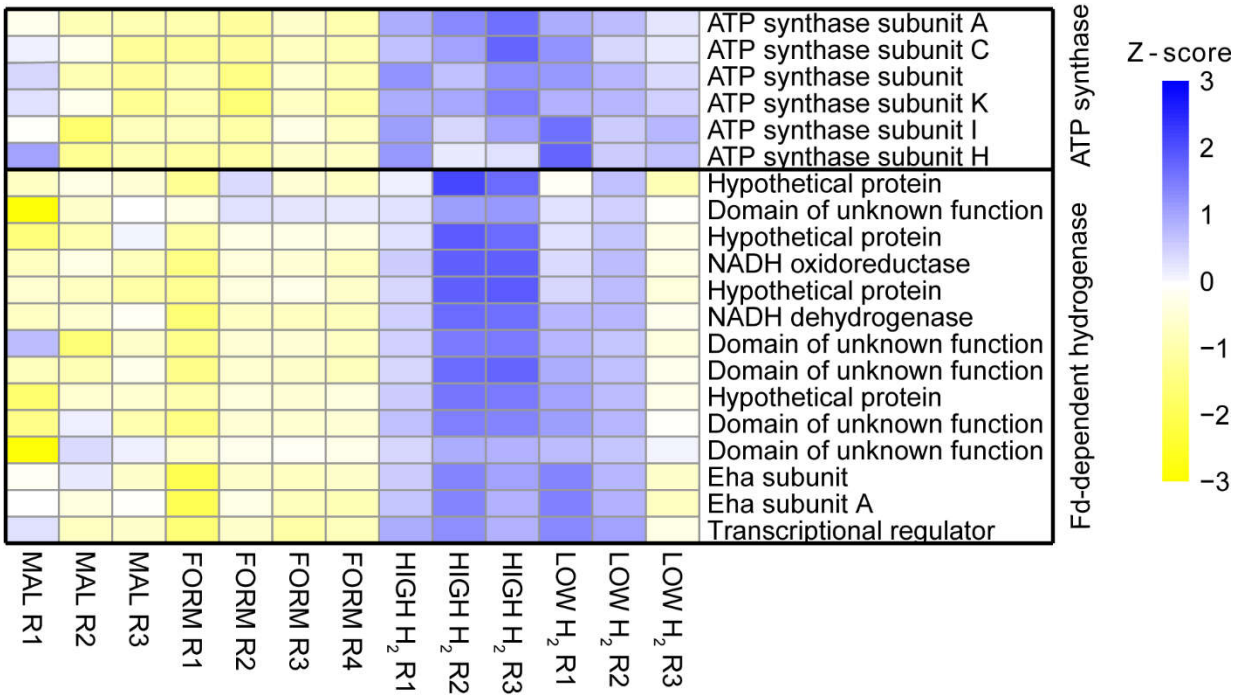

Figure 24 Differential gene expression analysis and RNA-Seq heat map for the *M. jannaschii* membrane-bound ATP synthase genes (MJ_RS01135, MJ_RS01145, MJ_RS01150-65), and the *M. jannaschii* membrane-bound, ferredoxin-dependent hydrogenase genes (MJ_RS02730, MJ_RS02745-02800) for each growth condition.

Table 14 Coding sequences that showed more than two-fold differences in gene expression for high H_2 growth versus low H_2 growth. Expression counts are normalized for size factor.

Coding sequence	Low H_2			High H_2			
	L1	L2	L3	H1	H2	H3	Log_2FC
MJ_RS01685	1370.6	1423.8	2327.9	752.2	447.4	350.9	-1.72
MJ_RS01910	152.9	67.1	210.3	29.7	45.2	32.7	-2.01
MJ_RS03980	2667.1	3121.7	1696.3	858.6	1116.0	804.2	-1.43
MJ_RS09325	326.1	475.5	607.8	240.8	165.0	173.3	-1.28
MJ_RS04390	429.0	447.6	575.4	217.7	79.4	78.1	-1.94
MJ_RS04990	23238.4	23022.4	13108.6	36915.9	55159.0	65542.9	1.41
MJ_RS05550	1059.9	1524.5	1374.3	479.2	465.7	443.3	-1.51
MJ_RS05555	27258.7	35536.4	16861.6	6294.1	8235.9	8493.7	-1.79
MJ_RS06225	1419.6	1450.8	2623.0	846.3	694.3	548.4	-1.39
MJ_RS06835	2919.1	2682.6	3236.1	1016.2	962.0	1140.9	-1.50
MJ_RS06840	2915.3	2684.4	3246.9	1087.1	723.6	910.8	-1.70
MJ_RS06845	1224.4	1766.9	1200.9	352.2	512.1	642.2	-1.48

Table 15 Coding sequences that showed more than two-fold differences in gene expression for coculture growth versus monoculture growth. Expression counts are normalized for size factor.

	Coculture							**Monoculture**						
Coding sequence	0.05% Maltose			0.1% formate				High H_2			Low H_2			Log_2 FC
	M1	M2	M3	F1	F2	F3	F4	H1	H2	H3	L1	L2	L3	
MJ_RS00060	415.5	595.8	456.8	473.3	610.1	440.1	300.9	151.3	258.7	268.2	154.7	216.8	236.0	1.12
MJ_RS00100	519.4	1160.2	1636.8	742.9	1261.3	538.9	470.0	411.7	447.4	433.8	394.6	304.1	316.6	1.20
MJ_RS00125	207.7	188.1	342.6	166.8	214.3	154.5	183.2	84.1	100.8	95.3	83.7	75.1	75.3	1.13
MJ_RS00165	519.4	972.1	685.2	388.9	620.6	435.1	450.1	211.0	234.2	237.5	221.8	226.6	238.6	1.23
MJ_RS00180	1558.1	1630.5	1103.9	1513.9	1675.0	1174.2	1274.9	2657.8	2975.0	3780.4	2937.0	2856.9	3954.6	-1.17
MJ_RS00225	51.9	125.4	76.1	99.9	99.2	95.5	85.4	44.8	43.8	28.6	34.5	47.3	46.7	1.20
MJ_RS00230	415.5	282.2	532.9	344.3	296.6	282.3	229.6	101.1	178.0	116.6	106.7	145.1	120.5	1.28
MJ_RS00235	2025.5	2822.1	3273.6	3308.0	3665.7	2788.5	1918.1	359.1	719.9	568.7	401.3	538.7	438.7	2.50
MJ_RS00250	519.4	125.4	152.3	349.1	473.9	316.4	322.4	117.4	190.3	148.4	88.3	159.8	94.5	1.34
MJ_RS00255	207.7	125.4	0.0	128.0	91.8	64.8	62.2	287.8	212.2	251.0	261.6	317.7	313.9	-1.64
MJ_RS00260	103.9	31.4	152.3	60.1	73.9	78.9	75.4	164.7	210.6	256.1	157.5	179.9	129.5	-1.31
MJ_RS00300	0.0	0.0	38.1	26.2	19.0	49.0	41.4	60.6	78.1	99.6	54.9	65.1	66.5	-1.12
MJ_RS00430	0.0	62.7	76.1	195.9	135.1	166.9	155.0	52.9	32.7	28.6	54.3	31.8	106.6	1.41
MJ_RS00435	0.0	62.7	38.1	225.0	157.3	157.8	185.7	46.7	49.3	51.1	48.5	35.6	77.7	1.55
MJ_RS00440	51.9	31.4	0.0	67.9	52.8	73.1	93.7	21.3	23.9	20.4	19.0	14.9	41.4	1.49
MJ_RS00475	259.7	94.1	152.3	183.3	139.3	201.8	203.1	86.5	80.1	60.5	50.5	63.1	78.3	1.36
MJ_RS00490	415.5	689.8	609.1	283.2	311.4	177.7	178.2	945.8	1031.0	1320.8	655.4	886.0	920.5	-1.52
MJ_RS00535	207.7	439.0	342.6	429.6	350.4	448.4	383.0	173.3	178.6	167.4	176.7	198.2	180.0	1.14
MJ_RS00540	831.0	1003.4	1180.0	873.8	813.8	777.3	765.1	207.5	289.5	298.4	260.8	274.4	194.2	1.76
MJ_RS00615	51.9	62.7	76.1	39.8	32.7	47.3	32.3	76.8	59.9	55.7	79.3	84.4	169.8	-1.11
MJ_RS00630	1194.5	878.0	989.7	911.6	942.5	808.8	810.7	316.5	506.9	498.1	326.1	470.0	312.4	1.16
purP	1142.6	1128.8	1294.2	1896.0	1303.5	1518.0	1584.9	5046.5	4464.4	2417.7	3348.8	4669.4	1467.0	-1.32
MJ_RS00710	3168.1	3511.9	3768.5	3630.0	3799.7	2970.4	3349.6	849.4	1397.8	1151.1	782.8	1181.7	568.0	1.81
MJ_RS00720	51.9	0.0	38.1	38.8	38.0	59.0	46.4	82.9	55.2	58.4	114.5	121.4	160.7	-1.18
MJ_RS00730	0.0	31.4	38.1	25.2	24.3	32.4	32.3	5.9	10.1	16.9	5.8	6.4	11.3	1.60
MJ_RS09285	259.7	125.4	342.6	128.0	108.7	162.8	165.0	401.6	420.4	417.5	298.5	387.7	378.2	-1.32
MJ_RS00815	27544 54.5	2541703 .3	2220143. 5	937056. 2	1425908 .5	949855. 6	1049826. 0	32978 6.3	715134. 3	895359.2	44004 0.4	481388. 9	518183.6	1.59
MJ_RS00825	27827 0.7	277725. 4	193373.7	102413. 2	188071. 1	107873. 0	121877.8	29600. 5	70341.9	81325.0	39350. 0	41994.8	56181.0	1.77
MJ_RS00835	779.0	878.0	799.4	1243.3	1168.4	1072.9	1012.1	570.2	558.8	480.5	527.2	536.7	364.1	1.04
MJ_RS00975	51.9	31.4	0.0	22.3	36.9	34.0	31.5	64.7	50.3	47.2	83.5	64.0	64.6	-1.01
MJ_RS01025	103.9	125.4	76.1	103.8	153.0	70.6	92.8	17.0	31.2	29.3	21.3	26.1	28.3	2.04
MJ_RS01050	0.0	62.7	38.1	51.4	54.9	41.5	43.9	101.8	69.8	86.8	102.3	127.3	215.5	-1.32
MJ_RS01090	103.9	31.4	38.1	16.5	19.0	12.5	11.6	44.4	40.2	33.7	43.5	43.9	64.1	-1.37

MJ_RS01110	103.9	313.6	266.5	228.9	240.6	285.7	279.3	515.1	691.1	753.3	509.7	375.4	244.5	-1.02
MJ_RS01135	2025.5	1442.4	1408.4	1345.1	1236.0	1618.5	1364.4	3520.2	4409.8	5107.7	3582.3	3191.8	2505.4	-1.35
MJ_RS01145	831.0	721.2	456.8	464.5	472.9	564.7	518.9	1074.1	1232.5	1720.5	1361.2	955.6	865.6	-1.14
MJ_RS01150	727.1	344.9	304.5	344.3	260.7	414.4	344.0	1113.2	841.1	1183.6	1074.7	899.9	698.8	-1.43
MJ_RS01155	882.9	627.1	304.5	377.3	234.3	463.4	363.1	1339.8	1434.8	1948.8	1286.4	1237.3	1036.4	-1.71
MJ_RS01160	1402.3	658.5	1027.8	1012.5	917.2	1279.7	1064.3	2425.6	1782.5	2377.1	3149.9	1904.3	2116.4	-1.13
MJ_RS01165	415.5	125.4	152.3	139.7	136.2	177.7	169.9	448.0	271.3	281.7	600.8	326.6	346.9	-1.20
MJ_RS01170	259.7	250.9	152.3	164.9	172.0	149.5	141.7	489.7	384.3	586.3	495.2	432.3	878.5	-1.71
MJ_RS01195	0.0	0.0	38.1	29.1	19.0	24.1	9.9	58.0	39.0	45.6	50.1	61.6	96.8	-1.55
MJ_RS01240	0.0	62.7	76.1	57.2	71.8	53.1	59.7	26.5	17.0	13.3	23.8	16.0	25.2	1.55
MJ_RS01275	51.9	156.8	190.3	177.5	176.3	175.2	168.3	75.9	61.3	59.8	78.1	62.0	80.5	1.30
MJ_RS01290	259.7	250.9	228.4	168.7	207.9	266.6	268.6	407.2	604.1	650.9	409.2	419.1	428.3	-1.07
MJ_RS01295	0.0	31.4	76.1	44.6	61.2	48.2	55.5	186.5	152.6	172.5	180.4	168.7	180.8	-1.75
MJ_RS01305	155.8	376.3	342.6	284.2	298.7	216.7	244.5	696.9	528.4	539.4	603.1	597.9	581.5	-1.15
MJ_RS01310	571.3	1003.4	799.4	553.8	661.8	599.6	583.6	1420.3	1470.3	1663.5	1406.0	1394.4	1515.3	-1.21
MJ_RS01320	51.9	250.9	304.5	46.6	70.7	33.2	44.8	15.8	19.1	18.6	17.6	29.3	37.2	1.91
MJ_RS01350	103.9	125.4	114.2	87.3	89.7	85.5	84.5	193.3	162.5	248.0	196.1	181.8	232.2	-1.19
MJ_RS01375	0.0	0.0	76.1	15.5	25.3	30.7	26.5	78.6	76.3	94.8	74.2	73.4	78.7	-1.68
MJ_RS01385	259.7	188.1	114.2	162.9	106.6	160.3	172.4	510.1	304.2	277.8	592.1	499.9	459.8	-1.50
porA	882.9	909.3	456.8	294.8	503.5	587.9	357.3	854.8	945.3	982.6	2230.7	1322.2	807.3	-1.15
MJ_RS01410	51.9	250.9	228.4	66.9	91.8	136.2	82.1	294.4	328.9	268.0	781.8	403.2	242.1	-1.78
MJ_RS01415	207.7	219.5	76.1	51.4	65.4	108.8	51.4	208.0	175.9	160.3	593.0	293.1	151.2	-1.56
MJ_RS01445	0.0	125.4	152.3	104.7	121.4	132.0	125.2	34.6	45.9	30.0	32.5	46.7	56.5	1.53
MJ_RS01455	103.9	344.9	304.5	323.9	310.3	239.2	316.6	644.4	699.0	709.3	505.6	600.0	395.4	-1.02
MJ_RS01480	0.0	62.7	0.0	21.3	25.3	14.9	19.1	52.4	29.6	33.4	49.0	48.1	100.9	-1.35
MJ_RS01510	5609.0	4797.6	3882.7	5525.0	4978.7	4790.6	4615.4	1810.0	2937.3	3269.7	1613.6	2853.2	1646.5	1.05
MJ_RS01515	0.0	31.4	0.0	17.5	6.3	16.6	23.2	31.5	33.1	36.9	30.0	31.6	41.4	-1.09
MJ_RS01535	0.0	0.0	114.2	35.9	35.9	28.2	37.3	112.2	95.8	65.3	63.6	135.7	80.6	-1.42
MJ_RS01545	0.0	62.7	76.1	41.7	59.1	52.3	40.6	103.3	75.1	88.4	228.6	96.3	90.4	-1.22
MJ_RS01560	0.0	0.0	38.1	16.5	16.9	21.6	29.8	58.0	39.0	33.7	44.5	44.7	65.1	-1.18
MJ_RS01570	51.9	31.4	76.1	49.5	41.2	78.1	79.6	161.0	141.6	115.4	134.7	123.3	162.6	-1.18
MJ_RS01610	467.4	1191.6	1218.1	659.5	704.0	423.5	450.1	363.0	221.8	169.0	319.1	419.9	404.4	1.15
MJ_RS01665	103.9	62.7	152.3	38.8	40.1	36.5	31.5	208.8	98.0	111.5	221.0	181.9	366.1	-2.12
MJ_RS01675	2648.7	3041.6	3349.8	2528.3	1229.6	2440.6	1637.9	6560.7	8474.3	6726.0	5228.8	5455.6	2590.8	-1.30
MJ_RS01680	779.0	439.0	609.1	749.7	728.3	1118.6	1340.3	340.2	392.0	399.7	318.4	401.6	397.4	1.21
MJ_RS01705	0.0	94.1	76.1	61.1	57.0	54.0	49.7	100.8	76.9	85.2	115.7	103.5	211.8	-1.04
MJ_RS01720	0.0	219.5	114.2	7.8	9.5	14.9	15.7	4.0	6.1	6.4	4.2	7.5	19.6	2.38
MJ_RS01755	0.0	0.0	38.1	9.7	7.4	6.6	9.1	9.7	24.8	38.5	17.9	18.1	27.6	-1.40
MJ_RS01845	0.0	0.0	38.1	9.7	5.3	14.1	7.5	19.4	21.1	19.0	29.7	22.1	55.1	-1.54
MJ_RS01865	103.9	282.2	0.0	67.9	87.6	53.1	30.7	277.1	174.5	198.3	270.0	279.7	402.4	-1.89
MJ_RS01870	51.9	156.8	114.2	43.6	66.5	33.2	25.7	138.2	63.5	69.2	148.5	140.2	233.7	-1.31

MJ_RS01900	363.5	689.8	647.1	614.9	562.6	759.0	673.9	225.3	189.3	131.7	225.8	309.8	303.3	1.45
MJ_RS01910	0.0	0.0	0.0	1.0	2.1	0.8	5.8	4.9	7.3	5.3	24.7	11.1	36.4	-2.26
MJ_RS01915	103.9	62.7	0.0	25.2	39.1	31.6	36.5	66.1	66.4	90.2	171.1	102.9	263.6	-1.85
MJ_RS01965	934.8	878.0	456.8	803.0	966.8	728.3	709.5	2071.6	2580.8	2989.6	2463.1	1852.7	2265.8	-1.59
MJ_RS01995	51.9	31.4	38.1	27.2	27.4	26.6	25.7	70.3	79.3	86.1	56.9	67.6	78.2	-1.43
MJ_RS02005	311.6	188.1	342.6	220.1	174.2	246.6	202.3	458.4	619.9	646.1	544.3	398.1	565.6	-1.29
MJ_RS02010	155.8	94.1	190.3	81.5	49.6	78.9	95.3	243.9	284.3	313.3	342.0	193.1	301.2	-1.73
MJ_RS02015	103.9	125.4	76.1	101.8	95.0	142.0	112.7	430.6	502.8	486.7	545.7	338.2	453.8	-2.03
MJ_RS02020	207.7	250.9	418.7	194.0	206.9	146.2	135.1	514.7	433.6	442.0	479.8	458.8	471.5	-1.31
MJ_RS02025	1298.4	2069.5	2398.1	1461.5	1716.2	1738.1	1995.2	785.1	1018.4	917.3	752.4	1002.3	884.0	1.01
MJ_RS02030	1246.5	1975.5	2207.8	1605.0	1712.0	2254.6	2440.3	311.3	584.6	527.5	321.2	568.5	378.8	2.11
MJ_RS02100	1194.5	2069.5	2436.2	702.1	775.8	769.8	817.3	237.4	69.4	88.4	211.2	271.3	661.1	2.26
MJ_RS02115	623.2	344.9	799.4	750.6	527.7	734.1	622.5	2133.0	1943.1	2324.0	2203.0	1716.8	1643.7	-1.64
MJ_RS02130	1765.8	1317.0	1827.2	1617.6	1399.6	1088.7	1092.5	646.0	607.3	497.7	560.4	875.3	637.1	1.14
MJ_RS02285	0.0	31.4	0.0	20.4	20.1	18.3	25.7	53.0	43.0	43.7	42.1	57.7	72.3	-1.33
MJ_RS02405	0.0	0.0	38.1	9.7	11.6	7.5	13.3	31.0	20.7	19.9	24.9	21.5	47.8	-1.37
MJ_RS02415	103.9	188.1	228.4	148.4	133.0	134.5	127.7	358.9	228.3	235.2	289.7	276.7	308.3	-1.02
MJ_RS02420	675.2	313.6	342.6	375.3	443.3	432.6	466.7	916.1	947.6	1207.9	891.6	797.4	661.3	-1.08
MJ_RS02440	103.9	219.5	152.3	264.8	323.0	222.6	274.4	460.3	513.4	645.6	747.5	491.8	600.4	-1.19
rps14P	259.7	250.9	228.4	220.1	183.7	124.6	135.9	249.0	363.8	484.6	442.5	259.9	370.5	-1.01
MJ_RS02550	727.1	815.3	685.2	517.9	608.0	709.2	702.1	1400.3	2038.8	2293.3	1300.5	1499.9	936.3	-1.24
MJ_RS02640	51.9	376.3	266.5	226.9	283.9	230.9	180.7	544.5	532.0	597.3	394.4	497.3	531.4	-1.15
MJ_RS02705	1713.9	2383.1	2474.3	4606.6	3525.3	3731.0	4039.3	1067.0	1557.7	1654.3	1255.0	1040.6	1068.3	1.37
MJ_RS02710	467.4	595.8	1142.0	1762.1	1165.2	1190.0	1250.8	487.2	606.5	598.9	670.2	450.3	526.6	1.03
MJ_RS02730	207.7	250.9	228.4	141.6	383.1	230.9	205.6	337.3	1115.2	862.8	280.9	455.4	182.0	-1.18
MJ_RS02745	0.0	31.4	76.1	50.4	126.7	116.3	102.0	121.6	403.2	442.0	122.2	161.7	70.6	-1.37
MJ_RS02750	51.9	94.1	266.5	88.3	183.7	181.9	164.1	339.2	1545.8	1344.9	333.6	460.6	177.5	-2.22
MJ_RS02755	311.6	439.0	304.5	179.4	408.5	382.0	324.9	886.2	2472.6	2468.1	778.3	1051.2	444.9	-2.02
MJ_RS02760	103.9	94.1	76.1	63.0	121.4	129.5	103.6	216.5	588.8	597.8	216.5	269.9	113.7	-1.72
MJ_RS02765	207.7	219.5	304.5	98.9	207.9	196.8	181.5	493.1	1282.2	1190.7	625.7	634.2	294.4	-1.99
MJ_RS02770	519.4	94.1	190.3	116.4	212.2	210.1	186.5	426.8	918.6	927.4	549.0	478.7	231.5	-1.57
MJ_RS02775	259.7	250.9	418.7	161.0	320.9	311.4	263.6	736.6	2126.9	2285.5	1108.0	919.5	431.6	-2.19
MJ_RS02780	51.9	156.8	152.3	106.7	175.2	157.8	179.9	412.0	1034.4	1015.1	654.3	479.6	200.9	-2.09
MJ_RS02785	51.9	219.5	76.1	47.5	122.4	115.4	118.5	383.4	791.5	747.6	573.3	418.4	176.0	-2.28
MJ_RS02790	0.0	219.5	152.3	45.6	83.4	89.7	81.2	248.5	557.8	486.9	414.6	311.5	134.0	-2.06
MJ_RS02795	363.5	470.3	266.5	97.0	268.1	245.8	259.4	599.9	1131.4	873.5	1105.8	714.2	263.2	-1.58
MJ_RS02800	363.5	282.2	342.6	94.1	297.6	218.4	208.9	568.4	967.9	657.3	992.6	668.8	224.5	-1.51
MJ_RS02805	779.0	313.6	342.6	135.8	339.9	231.7	290.1	1365.6	1837.3	1253.0	1990.1	1468.4	448.8	-2.15
MJ_RS02850	207.7	439.0	190.3	464.5	486.6	469.2	518.1	258.4	161.9	112.5	242.0	206.5	220.3	1.11
MJ_RS02860	51.9	62.7	0.0	100.9	112.9	131.2	126.0	46.4	44.8	30.0	45.7	46.1	51.8	1.28
MJ_RS02865	0.0	250.9	266.5	226.9	258.6	275.7	304.2	113.4	107.7	79.5	110.1	94.9	110.0	1.31

MJ_RS02940	259.7	94.1	228.4	166.8	109.8	168.6	126.8	382.1	490.4	490.4	350.4	323.5	254.2	-1.36
MJ_RS02945	51.9	94.1	76.1	98.0	68.6	101.3	67.1	227.7	219.8	190.1	205.5	177.0	149.5	-1.23
MJ_RS02995	0.0	250.9	76.1	68.9	61.2	73.9	115.2	331.1	242.9	290.6	194.9	52.2	121.8	-1.21
MJ_RS03005	51.9	125.4	38.1	44.6	36.9	40.7	38.1	82.6	81.4	89.3	79.0	71.5	143.7	-1.09
MJ_RS03015	0.0	31.4	0.0	6.8	11.6	6.6	16.6	22.9	18.3	24.7	20.4	18.7	23.8	-1.02
MJ_RS03035	51.9	62.7	38.1	43.6	42.2	46.5	53.1	88.5	71.8	92.1	106.2	99.9	139.1	-1.09
MJ_RS03055	51.9	0.0	0.0	27.2	17.9	26.6	24.9	39.1	38.6	41.9	61.6	39.3	86.7	-1.12
MJ_RS03060	259.7	282.2	228.4	161.0	136.2	170.2	222.1	342.5	439.3	499.8	340.8	383.1	295.7	-1.05
MJ_RS03075	155.8	125.4	304.5	422.8	160.4	176.0	148.4	572.2	641.8	493.6	379.8	456.8	393.6	-1.16
MJ_RS03095	207.7	0.0	266.5	68.9	83.4	68.1	63.0	414.8	494.7	547.4	385.1	411.3	611.4	-2.58
MJ_RS03100	311.6	156.8	380.7	85.3	111.9	93.8	88.7	917.1	1045.4	1182.5	722.0	734.5	939.8	-2.82
MJ_RS03105	1713.9	1881.4	1636.8	1960.0	1946.3	1057.1	1088.4	723.5	890.6	635.6	612.5	850.4	750.6	1.10
MJ_RS03260	51.9	31.4	114.2	63.0	48.6	62.3	41.4	151.7	92.5	116.6	170.8	128.4	95.2	-1.20
MJ_RS03285	259.7	282.2	190.3	331.7	343.0	284.0	335.7	165.6	132.9	88.9	156.9	181.9	165.2	1.05
MJ_RS03310	467.4	595.8	609.1	576.1	480.2	700.9	690.5	259.6	259.5	165.4	229.6	249.5	209.8	1.39
MJ_RS03330	103.9	188.1	76.1	162.9	203.7	255.8	315.8	79.9	61.5	46.7	61.7	85.2	90.4	1.58
MJ_RS03335	103.9	62.7	152.3	217.2	207.9	246.6	272.7	90.3	67.8	57.7	61.6	90.6	110.4	1.40
MJ_RS03380	51.9	0.0	38.1	48.5	68.6	70.6	75.4	24.2	17.5	17.4	25.2	22.3	33.9	1.40
MJ_RS03395	0.0	0.0	0.0	48.5	47.5	39.0	34.8	87.1	96.4	96.9	63.8	81.5	70.7	-1.11
MJ_RS03420	0.0	31.4	0.0	32.0	43.3	29.9	34.8	52.5	52.4	54.3	57.7	69.7	136.5	-1.10
MJ_RS09320	0.0	156.8	114.2	74.7	46.4	72.2	92.0	201.3	216.1	171.5	128.0	197.4	203.8	-1.33
MJ_RS03470	51.9	407.6	380.7	265.7	353.6	227.5	201.4	85.4	136.2	112.7	78.2	128.5	103.3	1.33
MJ_RS03480	13191.6	11570.6	11001.0	15261.0	10141.0	14246.5	18949.7	439.9	881.4	1033.4	423.7	584.5	249.4	4.49
MJ_RS03490	51.9	156.8	0.0	36.9	34.8	34.0	49.7	114.3	82.8	105.6	97.8	100.1	146.1	-1.38
MJ_RS03495	623.2	815.3	1065.8	647.8	541.5	631.9	639.1	1461.9	2071.3	1734.9	1076.7	1965.7	1045.0	-1.20
MJ_RS03510	103.9	188.1	190.3	79.5	69.7	59.8	65.5	240.1	125.4	150.7	243.6	252.7	376.3	-1.46
MJ_RS03515	1817.7	2289.0	2854.9	3071.4	2653.5	2370.0	2354.1	889.9	1196.8	1114.7	887.9	1190.2	731.3	1.33
MJ_RS03525	103.9	501.7	418.7	205.6	169.9	105.5	127.7	97.9	55.0	49.5	72.8	101.0	182.4	1.18
MJ_RS03540	103.9	94.1	76.1	32.0	43.3	48.2	52.2	94.5	59.7	90.0	94.4	92.1	149.1	-1.00
MJ_RS03545	155.8	188.1	266.5	251.2	235.4	166.9	175.7	452.6	276.2	320.6	551.0	415.5	471.4	-1.00
MJ_RS03570	51.9	94.1	38.1	80.5	83.4	72.2	66.3	147.0	128.2	135.4	139.5	154.3	205.8	-1.02
MJ_RS03645	0.0	62.7	76.1	79.5	114.0	31.6	38.1	13.5	22.1	23.1	15.2	14.6	19.0	1.83
MJ_RS03650	0.0	62.7	0.0	42.7	47.5	32.4	39.0	93.4	73.3	82.9	86.9	96.3	145.3	-1.29
MJ_RS03685	51.9	0.0	0.0	27.2	31.7	27.4	19.1	77.2	50.5	53.8	82.6	67.1	76.9	-1.41
MJ_RS03710	103.9	31.4	76.1	52.4	77.0	63.1	78.7	180.2	122.2	120.5	124.0	124.8	188.4	-1.08
MJ_RS03720	259.7	188.1	152.3	72.7	106.6	83.9	118.5	272.1	214.1	192.6	219.6	245.0	291.7	-1.14
MJ_RS03725	415.5	344.9	342.6	154.2	203.7	186.8	197.3	772.1	715.0	818.1	575.5	724.7	523.4	-1.66
MJ_RS03730	311.6	125.4	190.3	68.9	109.8	73.1	105.3	386.6	251.6	262.2	432.2	496.4	789.0	-1.98
MJ_RS03735	0.0	0.0	0.0	36.9	54.9	28.2	36.5	82.2	76.7	93.4	75.6	87.4	113.2	-1.32

MJ_RS03775	980439.5	978075.1	811522.5	387782.5	661575.8	382269.2	434893.1	108314.5	295432.6	336238.7	146626.8	164120.4	195537.2	1.67
MJ_RS03785	3529800.5	3266824.6	2921960.7	1156300.7	1820402.3	1141648.3	1273683.8	396594.1	902399.9	1106603.1	522575.5	593058.1	646991.9	1.64
MJ_RS03810	51.9	156.8	304.5	108.6	83.4	98.8	110.2	207.7	264.8	259.7	210.6	236.7	231.1	-1.12
MJ_RS03815	103.9	0.0	0.0	20.4	15.8	34.0	33.2	62.2	85.6	88.2	36.2	53.1	45.8	-1.25
MJ_RS03820	0.0	31.4	0.0	37.8	46.4	43.2	32.3	125.4	93.9	78.1	49.9	52.0	63.8	-1.05
MJ_RS03825	155.8	125.4	76.1	76.6	83.4	103.0	60.5	176.2	238.0	253.1	151.2	182.1	184.8	-1.23
MJ_RS03845	207.7	156.8	190.3	196.9	214.3	165.3	152.5	479.1	507.3	544.0	427.9	279.9	276.3	-1.20
MJ_RS03890	103.9	721.2	532.9	381.1	1802.8	497.4	393.7	228.8	275.3	238.4	286.6	167.8	149.1	1.55
MJ_RS03895	727.1	1693.3	1218.1	1126.9	5720.7	1694.9	1314.7	531.4	712.4	647.2	830.0	340.1	307.0	1.80
MJ_RS03900	155.8	439.0	228.4	307.4	1154.7	351.3	359.7	145.6	132.9	100.8	226.6	89.5	46.2	1.86
MJ_RS03910	2804.5	4045.0	2854.9	3284.8	10399.6	3766.7	2548.1	1706.6	2176.8	1605.5	3552.6	1447.7	505.3	1.22
MJ_RS03915	5349.4	8372.2	6433.1	6796.4	23239.5	8091.5	5630.0	3236.7	4312.4	3248.8	7065.5	3043.2	722.0	1.34
MJ_RS03920	4881.9	8873.9	6433.1	4497.0	17620.1	5660.9	4132.1	2460.9	3976.6	3361.1	6095.6	2523.5	501.1	1.24
MJ_RS03950	4985.8	6522.2	6471.2	5698.6	9484.5	4297.4	4019.4	2185.6	2837.7	2125.0	3926.0	2984.0	961.7	1.24
MJ_RS03980	934.8	1379.7	1065.8	723.5	1767.9	675.1	733.6	140.5	180.0	129.6	431.3	514.0	293.9	1.88
MJ_RS04015	155.8	815.3	342.6	199.8	235.4	284.0	280.2	70.3	101.9	107.4	75.1	112.7	88.6	1.71
MJ_RS04020	103.9	282.2	380.7	120.3	164.7	181.0	164.1	40.9	52.1	46.5	40.0	55.0	45.1	1.89
MJ_RS04030	259.7	250.9	342.6	107.6	91.8	93.0	102.8	51.3	40.2	32.8	24.3	61.7	39.5	1.74
MJ_RS04035	415.5	783.9	989.7	419.0	313.5	292.3	299.2	205.3	217.1	215.7	107.8	270.8	190.4	1.19
MJ_RS04070	727.1	1160.2	1408.4	885.4	740.9	799.7	848.0	276.3	426.7	403.6	297.4	454.1	300.0	1.33
MJ_RS04075	934.8	1254.3	685.2	837.9	641.7	685.9	588.5	201.4	247.5	224.0	194.9	319.8	181.2	1.75
MJ_RS04080	7219.0	9124.8	9706.8	12003.4	9576.3	8700.2	8892.5	2926.2	3845.1	3139.6	2965.1	4626.7	2193.2	1.51
MJ_RS04140	727.1	1034.8	532.9	614.9	620.6	610.4	684.7	239.9	368.5	224.5	217.3	390.9	321.8	1.19
MJ_RS04145	363.5	501.7	304.5	425.7	405.3	430.2	567.0	132.4	115.5	87.0	117.4	164.9	155.1	1.79
MJ_RS04175	0.0	94.1	38.1	45.6	55.9	44.8	45.6	101.5	81.6	94.4	79.6	102.1	140.9	-1.06
MJ_RS04180	4881.9	4797.6	4986.6	9404.3	4589.2	6483.9	4760.4	14656.0	13331.3	11160.1	9560.6	14141.5	10680.1	-1.09
MJ_RS04205	51.9	31.4	38.1	69.8	74.9	88.9	111.1	25.2	54.2	35.5	29.9	31.0	34.6	1.20
MJ_RS04230	51.9	94.1	0.0	13.6	20.1	19.9	18.2	61.1	31.5	31.6	41.1	70.9	89.8	-1.40
MJ_RS04255	51.9	31.4	38.1	19.4	21.1	21.6	19.1	46.6	37.7	38.9	35.5	47.7	54.7	-1.05
MJ_RS04260	0.0	31.4	0.0	1.9	7.4	5.0	9.1	34.0	19.3	23.4	26.3	30.2	38.8	-2.17
MJ_RS04290	519.4	595.8	1142.0	614.9	530.9	694.2	804.9	328.5	402.2	333.0	271.7	357.4	204.3	1.12
MJ_RS04330	103.9	31.4	114.2	52.4	68.6	45.7	68.8	119.6	149.3	134.4	107.5	154.6	89.1	-1.06
MJ_RS04380	51.9	62.7	114.2	96.0	92.9	91.3	88.7	199.8	183.4	216.9	150.7	197.4	223.1	-1.10
MJ_RS09325	51.9	62.7	114.2	202.7	255.4	195.1	150.9	39.4	26.6	27.9	52.7	78.3	105.3	1.62
MJ_RS04390	155.8	156.8	304.5	477.1	487.6	399.4	290.9	35.6	12.8	12.6	69.4	73.7	99.7	2.75
MJ_RS09330	259.7	282.2	190.3	547.9	496.1	364.6	279.3	39.8	6.7	7.3	92.5	65.1	69.9	2.92
MJ_RS04395	162558.3	155999.1	155840.9	228882.6	165805.8	177880.8	175952.6	79914.0	91522.2	104158.4	103433.0	88903.7	50627.1	1.02

MJ_RS04410	103.9	125.4	152.3	484.9	345.1	245.8	233.8	1280.3	1194.5	865.1	846.7	964.3	712.3	-1.81
MJ_RS04460	207.7	188.1	380.7	535.3	563.6	577.1	641.6	231.4	259.5	198.8	202.5	273.7	264.8	1.06
MJ_RS04485	727.1	1473.8	1408.4	345.3	505.6	214.2	245.4	242.7	240.2	267.1	186.3	243.3	290.8	1.43
MJ_RS04500	415.5	439.0	456.8	315.2	491.9	399.4	424.4	205.3	65.5	74.0	147.1	193.1	347.9	1.28
MJ_RS04625	3531.6	2100.9	1522.6	2037.6	1068.1	2156.6	1864.2	9894.2	9868.2	7923.4	7198.4	7713.3	4057.1	-1.96
MJ_RS04630	1506.1	1034.8	1370.4	1061.9	516.1	1148.5	1038.6	5747.4	5634.4	4020.7	3889.7	4361.5	2327.2	-2.03
MJ_RS04660	882.9	627.1	571.0	219.2	210.0	164.4	152.5	585.4	707.3	715.3	1161.9	737.0	770.7	-1.16
MJ_RS04860	51.9	31.4	38.1	52.4	78.1	88.0	81.2	40.1	38.6	31.6	28.0	33.5	31.2	1.09
MJ_RS04940	259.7	313.6	380.7	257.0	255.4	372.9	335.7	985.4	1257.6	1338.0	1087.8	904.9	434.0	-1.70
MJ_RS04965	467.4	1222.9	1370.4	1389.7	1361.6	1285.5	1322.1	287.5	354.1	265.7	304.2	371.7	326.0	1.99
MJ_RS04970	571.3	1379.7	1218.1	1263.7	1432.3	1426.6	1183.7	380.8	409.9	399.9	285.4	447.2	294.7	1.76
MJ_RS04990	3479.7	2445.8	2055.5	1772.8	2782.2	2688.0	2318.5	6041.4	8897.9	10565.3	3757.7	3790.9	2271.0	-1.24
MJ_RS04995	0.0	0.0	0.0	9.7	5.3	3.3	5.0	10.8	27.4	32.1	13.8	16.7	16.1	-1.71
MJ_RS05035	259.7	407.6	494.9	387.0	608.0	394.4	346.5	182.4	59.5	59.5	211.8	204.5	303.2	1.30
MJ_RS05040	103.9	125.4	152.3	171.7	225.9	212.6	225.5	51.6	23.1	19.2	71.7	65.3	127.6	1.64
MJ_RS05080	51.9	188.1	152.3	144.5	80.2	88.9	67.1	19.2	24.3	23.6	29.7	24.7	31.1	1.98
MJ_RS05085	467.4	344.9	152.3	217.2	288.1	330.5	279.3	523.6	628.8	570.1	450.7	729.3	528.2	-1.01
MJ_RS05135	519.4	282.2	152.3	406.4	391.6	385.3	366.4	715.9	988.4	1026.3	406.7	887.3	648.7	-1.08
MJ_RS05165	51.9	188.1	114.2	104.7	100.3	103.0	103.6	234.9	190.7	218.0	198.9	207.7	231.4	-1.04
MJ_RS05170	467.4	439.0	609.1	406.4	277.6	460.0	374.7	1312.7	1037.5	1297.9	1125.1	957.1	857.9	-1.44
MJ_RS05175	571.3	564.4	571.0	617.8	657.6	590.4	564.5	1285.6	1662.0	1828.4	774.4	988.6	731.3	-1.02
MJ_RS05225	103.9	94.1	190.3	253.1	63.3	176.9	132.6	466.6	301.1	275.1	373.1	308.9	271.3	-1.14
MJ_RS05325	0.0	94.1	114.2	38.8	42.2	44.0	40.6	89.5	102.9	123.4	99.4	109.8	151.2	-1.37
MJ_RS05365	363.5	501.7	723.2	676.9	451.7	485.0	756.0	406.6	270.3	231.8	250.9	225.1	194.6	1.13
MJ_RS05375	51.9	94.1	38.1	38.8	40.1	36.5	35.6	79.5	88.3	101.5	87.6	61.6	84.9	-1.10
MJ_RS05415	363.5	344.9	342.6	334.6	219.5	326.4	234.6	671.9	633.5	745.0	698.0	647.4	469.4	-1.15
MJ_RS05455	2025.5	1912.8	1560.7	4053.8	1942.1	3820.7	4034.3	1438.0	1759.2	2296.7	932.2	1251.9	689.8	1.01
MJ_RS05470	207.7	250.9	228.4	208.5	176.3	181.0	177.4	402.1	326.1	414.3	414.5	353.9	379.6	-1.01
MJ_RS05490	779.0	1034.8	456.8	659.5	632.2	662.7	621.7	1427.7	1389.5	1545.3	1369.3	1401.3	1755.6	-1.15
MJ_RS05495	0.0	62.7	0.0	9.7	13.7	11.6	10.8	46.3	33.3	28.6	39.2	42.5	64.3	-1.82
MJ_RS05520	727.1	407.6	571.0	862.2	689.2	724.9	891.9	372.4	229.9	202.5	424.4	400.6	388.2	1.10
MJ_RS05525	103.9	94.1	38.1	232.8	190.0	239.2	273.5	79.2	55.2	41.9	71.5	80.0	90.0	1.52
MJ_RS05530	207.7	62.7	152.3	86.3	78.1	98.8	110.2	38.7	25.4	22.9	30.6	46.1	69.7	1.35
MJ_RS05550	467.4	940.7	837.4	325.9	350.4	238.3	223.0	78.4	75.1	71.5	171.4	251.0	238.1	1.62
MJ_RS05555	13295.5	14392.7	14807.6	9795.1	11398.1	10263.1	11114.8	1030.1	1328.6	1369.2	4407.8	5851.4	2921.2	2.11
MJ_RS09345	0.0	0.0	38.1	11.6	17.9	18.3	14.9	53.9	53.2	54.3	45.9	54.4	73.7	-1.84
MJ_RS05720	207.7	125.4	228.4	105.7	140.4	142.8	144.2	305.5	281.0	286.5	247.3	363.9	380.2	-1.17
MJ_RS05870	311.6	501.7	532.9	385.0	395.8	427.7	460.9	818.1	972.7	1152.7	883.2	839.4	684.4	-1.07
MJ_RS05885	103.9	125.4	114.2	135.8	103.4	172.7	126.0	468.1	404.6	556.8	461.9	338.8	299.5	-1.67
MJ_RS05900	779.0	972.1	875.5	627.5	724.1	445.9	416.9	325.0	372.3	311.9	255.1	394.0	268.1	1.01

MJ_RS05930	103.9	376.3	114.2	170.7	135.1	176.0	157.5	720.3	524.5	579.7	691.5	552.9	585.1	-1.88
MJ_RS05940	415.5	752.6	951.6	991.1	907.7	976.6	1090.8	342.5	267.2	245.1	316.3	317.4	327.1	1.61
MJ_RS05975	155.8	188.1	114.2	168.7	191.0	121.2	158.3	436.8	359.1	335.8	369.7	330.2	302.0	-1.16
MJ_RS05995	103.9	31.4	38.1	33.0	17.9	38.2	40.6	125.1	108.1	124.1	98.0	103.2	94.2	-1.69
MJ_RS06000	51.9	0.0	0.0	22.3	8.4	26.6	22.4	56.3	51.9	69.4	54.4	49.9	49.5	-1.47
MJ_RS06110	207.7	188.1	418.7	268.6	194.2	191.8	195.6	86.7	73.9	45.8	66.7	115.6	124.9	1.39
MJ_RS06125	51.9	156.8	38.1	143.5	157.3	126.2	112.7	295.1	240.4	301.6	281.2	261.2	319.4	-1.12
MJ_RS06135	311.6	62.7	76.1	105.7	134.0	144.5	160.8	346.9	306.8	419.4	361.1	286.6	316.8	-1.32
MJ_RS06170	103.9	0.0	38.1	52.4	79.2	44.8	48.1	22.0	13.8	9.2	18.5	24.9	36.0	1.38
MJ_RS06180	9504.2	12103.6	10886.8	11244.0	10067.1	8592.3	8987.0	3958.4	6065.1	5130.6	4564.1	4539.5	2796.1	1.18
MJ_RS06185	779.0	721.2	532.9	644.9	559.4	614.5	557.9	212.2	350.4	240.0	263.3	297.9	198.6	1.23
MJ_RS06205	3375.8	3386.5	2360.1	1445.0	2076.1	2122.5	2236.4	464.9	290.8	346.3	790.1	674.5	787.4	2.10
MJ_RS06210	415.5	313.6	266.5	239.5	308.2	338.8	257.0	134.7	78.7	68.3	151.0	197.3	257.2	1.00
MJ_RS06230	2856.5	2038.2	2245.9	2284.9	1955.8	2186.5	2130.3	5651.5	6118.5	6142.4	3740.0	4562.0	1669.6	-1.06
MJ_RS06265	571.3	156.8	76.1	187.2	218.5	300.6	308.4	514.3	709.4	765.7	462.2	661.1	413.6	-1.22
MJ_RS06325	882.9	1285.6	989.7	1004.7	955.2	897.7	853.8	298.0	378.8	377.7	323.8	420.8	410.0	1.38
MJ_RS06330	311.6	31.4	152.3	112.5	96.0	89.7	64.7	714.2	579.7	643.1	616.0	663.6	471.9	-2.67
MJ_RS06355	9452.3	7494.2	7575.1	7591.7	7293.3	7600.8	7451.9	13062.4	26008.8	29556.8	12393.4	14148.1	8422.2	-1.15
MJ_RS06390	51.9	62.7	0.0	17.5	32.7	20.8	24.9	78.3	51.9	60.9	92.7	97.6	236.8	-2.03
MJ_RS06395	467.4	344.9	418.7	361.7	312.4	318.0	326.6	676.5	527.6	656.2	807.7	530.1	1068.5	-1.05
MJ_RS06445	0.0	470.3	304.5	44.6	32.7	8.3	16.6	3.2	5.5	4.1	5.3	4.1	7.3	4.52
MJ_RS06450	155.8	1630.5	1751.0	450.0	432.7	83.0	104.4	30.1	66.1	71.5	36.1	30.9	35.0	3.84
MJ_RS06455	675.2	972.1	1522.6	414.1	785.3	270.7	321.6	206.4	17.4	14.4	103.9	105.2	114.0	2.90
MJ_RS06520	0.0	0.0	0.0	3.9	2.1	6.6	4.1	14.8	13.6	18.1	16.6	18.6	27.1	-2.00
MJ_RS06525	0.0	62.7	114.2	27.2	15.8	31.6	36.5	115.3	103.5	110.4	94.2	103.3	142.0	-1.89
MJ_RS06550	0.0	0.0	76.1	47.5	28.5	49.8	47.2	90.6	73.7	90.9	88.8	76.8	122.9	-1.10
MJ_RS06575	727.1	1034.8	1370.4	1096.9	1481.9	1003.1	1118.2	556.9	699.2	656.6	478.1	570.2	314.4	1.06
MJ_RS06580	51.9	62.7	76.1	69.8	119.3	85.5	96.2	51.0	53.0	44.7	38.1	47.9	27.1	1.04
MJ_RS06605	1298.4	1191.6	1408.4	1298.6	1300.3	1042.2	1097.5	461.9	755.4	704.3	460.4	546.9	454.3	1.11
MJ_RS06640	363.5	501.7	380.7	353.0	288.1	307.3	333.2	1060.8	832.5	711.4	1123.1	885.1	856.1	-1.44
MJ_RS06650	155.8	156.8	152.3	130.9	141.4	166.9	150.0	329.5	344.1	368.7	408.6	306.9	242.6	-1.17
MJ_RS06665	363.5	501.7	380.7	141.6	116.1	70.6	91.2	39.5	9.1	9.8	30.9	33.5	27.2	3.03
MJ_RS06670	51.9	282.2	190.3	94.1	116.1	110.4	72.9	292.0	365.8	450.7	298.8	201.7	307.6	-1.52
MJ_RS06675	0.0	31.4	152.3	15.5	27.4	28.2	17.4	95.0	104.7	93.2	82.0	80.0	254.9	-2.17
MJ_RS06685	207.7	125.4	38.1	46.6	46.4	49.8	35.6	121.5	74.5	97.8	97.2	104.9	143.2	-1.01
MJ_RS06840	882.9	940.7	571.0	713.8	612.2	633.6	689.7	177.9	116.7	146.8	471.4	442.0	562.5	1.15
MJ_RS06845	779.0	940.7	799.4	844.7	565.7	875.3	965.7	57.6	82.6	103.5	198.0	290.9	208.1	2.39
MJ_RS06850	17086.8	15960.5	15683.1	11763.8	9877.1	12633.9	13483.9	735.3	1113.6	1281.0	2155.6	2642.0	1627.8	3.11
MJ_RS09360	415.5	689.8	456.8	400.5	387.4	634.4	718.7	149.7	190.1	163.8	144.0	250.4	196.6	1.55

MJ_RS06855	1454.2	1818.7	1560.7	1395.6	1457.6	1515.5	1818.6	261.7	321.0	381.3	410.7	571.1	415.6	2.00
MJ_RS06860	207.7	376.3	456.8	354.0	312.4	282.3	347.3	123.1	135.5	149.1	135.8	188.8	198.6	1.09
MJ_RS06995	51.9	31.4	38.1	37.8	51.7	61.5	42.3	117.2	140.4	140.9	242.5	129.3	118.1	-1.63
MJ_RS07000	51.9	219.5	76.1	92.1	104.5	91.3	62.2	157.4	160.1	147.5	578.1	192.2	205.9	-1.35
MJ_RS07045	311.6	313.6	494.9	450.0	561.5	394.4	404.5	180.5	199.9	235.7	202.8	204.0	222.5	1.08
MJ_RS07180	51.9	0.0	0.0	37.8	29.6	29.9	24.9	70.6	77.1	100.8	74.8	83.5	84.5	-1.46
MJ_RS07190	103.9	94.1	114.2	174.6	149.9	202.6	155.0	469.3	592.5	550.6	324.4	442.3	334.8	-1.49
MJ_RS07195	2129.4	1787.3	1598.8	2075.4	1181.1	1787.0	1356.1	7276.0	6673.5	7454.4	4105.1	4356.9	2739.1	-1.69
MJ_RS07230	103.9	188.1	114.2	122.2	122.4	112.1	97.0	236.8	251.2	342.9	233.8	238.1	303.7	-1.21
MJ_RS07245	0.0	0.0	0.0	2.9	3.2	5.8	3.3	22.5	18.1	21.5	16.5	21.3	39.5	-2.49
MJ_RS07270	1402.3	1505.1	1332.3	1626.4	1319.3	1655.8	1553.4	554.2	916.1	790.6	564.4	631.2	392.8	1.22
MJ_RS07275	207.7	533.1	266.5	563.5	456.0	513.2	485.7	214.4	233.7	161.7	173.9	238.4	143.2	1.27
MJ_RS07310	207.7	407.6	456.8	277.4	239.6	244.1	265.3	641.2	533.2	642.4	698.8	527.7	773.9	-1.22
MJ_RS07315	103.9	62.7	114.2	33.0	31.7	39.0	31.5	162.0	83.8	87.9	145.0	113.9	221.1	-1.77
MJ_RS07430	0.0	31.4	38.1	57.2	73.9	94.7	87.0	23.8	16.2	10.8	23.6	25.5	28.0	1.73
MJ_RS07495	51.9	0.0	0.0	65.0	50.7	97.2	89.5	95.8	161.5	165.1	97.8	112.4	249.4	-1.15
MJ_RS07595	571.3	439.0	494.9	324.9	335.6	201.8	194.8	787.4	567.9	309.2	691.6	935.8	739.5	-1.04
MJ_RS07715	4518.4	3543.3	4073.0	1091.0	782.1	1638.4	1821.1	332.9	687.7	868.0	608.3	907.2	597.0	1.87
MJ_RS07720	3220.0	2383.1	2626.5	1120.1	1088.2	1795.4	2003.5	275.0	393.0	454.2	400.5	563.0	490.7	2.20
MJ_RS07750	103.9	62.7	152.3	185.2	152.0	176.9	219.7	81.8	88.7	72.1	64.7	72.8	66.6	1.22
MJ_RS07770	207.7	439.0	685.2	322.0	368.4	391.1	379.6	185.6	143.7	123.2	145.0	185.5	148.8	1.30
MJ_RS07775	207.7	156.8	532.9	391.8	371.5	343.8	329.1	211.4	140.6	109.7	137.8	186.7	177.8	1.11
MJ_RS07780	4206.8	4578.1	6090.5	5366.9	5714.3	4046.6	4079.9	1246.0	1422.2	951.4	910.3	995.3	773.1	2.21
MJ_RS07785	155.8	156.8	304.5	139.7	149.9	142.0	103.6	350.7	248.8	320.0	318.7	229.7	258.0	-1.02
MJ_RS07835	986.8	564.4	685.2	579.9	573.1	425.2	362.2	1519.6	1287.2	1289.5	1149.8	1378.6	1253.7	-1.28
MJ_RS07940	727.1	2822.1	2664.6	989.2	1260.2	723.3	745.2	453.3	411.5	351.3	321.8	706.6	556.0	1.57
MJ_RS07970	986.8	846.6	837.4	758.4	451.7	801.3	689.7	176.3	110.4	117.3	295.8	268.1	196.6	1.94
MJ_RS07975	103.9	407.6	456.8	264.8	259.6	235.0	230.4	110.1	53.4	52.2	109.5	127.7	177.6	1.37
MJ_RS08040	259.7	282.2	266.5	390.8	487.6	380.3	373.0	147.7	109.8	96.4	123.5	116.4	119.6	1.69
MJ_RS08070	51.9	344.9	342.6	230.8	325.1	260.7	248.7	30.9	118.3	193.8	22.6	57.6	41.0	1.77
MJ_RS08085	0.0	0.0	0.0	10.7	4.2	11.6	9.9	28.3	27.8	20.4	120.5	14.1	44.8	-2.26
MJ_RS08090	0.0	62.7	38.1	15.5	20.1	44.0	29.0	73.2	102.3	77.2	320.7	45.3	118.0	-2.11
MJ_RS08095	51.9	31.4	0.0	11.6	10.6	21.6	16.6	42.8	82.2	74.4	162.1	37.6	77.1	-2.32
MJ_RS08110	0.0	0.0	38.1	8.7	6.3	11.6	5.8	22.9	32.5	31.4	66.3	22.1	31.4	-2.01
MJ_RS08115	0.0	0.0	0.0	11.6	9.5	21.6	20.7	48.3	59.9	43.3	108.9	28.2	43.6	-1.90
MJ_RS08130	103.9	188.1	114.2	139.7	112.9	102.1	117.7	300.9	208.6	299.3	383.8	299.4	379.0	-1.37
MJ_RS08135	103.9	62.7	38.1	61.1	81.3	68.1	49.7	231.4	177.9	197.2	167.0	208.5	180.2	-1.58
MJ_RS08140	0.0	0.0	76.1	26.2	26.4	27.4	19.1	70.3	43.4	45.3	76.1	71.5	136.0	-1.57
MJ_RS08175	0.0	62.7	76.1	49.5	52.8	49.8	45.6	32.1	14.4	12.6	26.0	29.5	28.7	1.05
MJ_RS08240	1610.0	689.8	609.1	907.7	1106.1	854.5	792.4	2320.2	2354.8	2807.5	2235.9	1452.4	1047.5	-1.14
MJ_RS08245	103.9	31.4	152.3	42.7	31.7	26.6	19.1	100.8	69.2	68.3	93.3	87.7	149.6	-1.36

MJ_RS08275	0.0	62.7	38.1	12.6	9.5	13.3	15.7	38.1	39.2	34.1	29.1	25.9	25.9	-1.19
MJ_RS08280	0.0	31.4	38.1	15.5	24.3	19.9	17.4	64.4	61.3	51.5	42.9	43.3	50.7	-1.43
MJ_RS09390	103.9	0.0	0.0	27.2	28.5	34.0	37.3	73.0	87.5	68.0	53.7	52.0	57.1	-1.04
MJ_RS08285	51.9	125.4	114.2	98.9	85.5	106.3	98.6	200.7	298.5	251.7	161.4	185.6	191.6	-1.13
MJ_RS08290	0.0	62.7	38.1	31.0	31.7	20.8	28.2	120.5	88.9	77.6	76.8	111.3	134.4	-1.85
MJ_RS08340	207.7	125.4	418.7	93.1	87.6	49.8	39.8	531.3	668.2	787.4	428.9	71.9	285.6	-1.87
MJ_RS08425	155.8	31.4	152.3	143.5	114.0	125.4	146.7	54.1	68.2	49.0	45.6	47.0	52.8	1.30
MJ_RS08540	986.8	1097.5	951.6	825.3	1125.1	701.7	620.0	347.9	549.7	493.8	290.8	326.4	319.6	1.18
MJ_RS08545	779.0	533.1	723.2	890.3	770.5	856.2	825.6	269.8	345.3	299.3	249.2	297.2	291.1	1.46
MJ_RS08550	779.0	564.4	875.5	1014.4	857.0	745.7	794.1	305.6	347.0	232.0	275.4	297.2	245.6	1.54
MJ_RS08585	467.4	470.3	571.0	599.3	485.5	637.8	661.5	257.4	299.5	331.0	275.4	260.1	205.8	1.09
MJ_RS08590	415.5	344.9	532.9	656.6	581.6	686.8	712.9	316.0	271.9	257.7	300.9	344.5	277.6	1.05
MJ_RS08680	0.0	94.1	38.1	25.2	29.6	43.2	54.7	24.7	6.1	5.7	17.1	18.6	21.1	1.35
MJ_RS08725	0.0	62.7	38.1	23.3	20.1	21.6	16.6	255.1	157.5	170.2	141.8	193.0	160.1	-3.09
MJ_RS08730	51.9	62.7	38.1	67.9	58.1	65.6	48.9	327.5	175.5	177.5	212.9	275.1	279.2	-2.02
MJ_RS08785	103.9	0.0	114.2	59.2	49.6	48.2	59.7	146.6	83.2	116.6	128.9	124.5	116.4	-1.12
MJ_RS08900	259.7	188.1	266.5	64.0	50.7	37.4	41.4	208.5	227.3	235.9	188.3	273.4	268.6	-1.41
MJ_RS08995	0.0	156.8	190.3	116.4	128.8	128.7	116.0	44.3	40.4	43.1	43.5	47.4	49.6	1.45
MJ_RS09015	0.0	0.0	76.1	13.6	8.4	27.4	21.6	6.1	4.9	3.9	7.5	8.4	9.2	1.46
MJ_RS09020	103.9	31.4	38.1	147.4	126.7	168.6	122.7	43.7	31.2	29.1	60.8	50.8	60.1	1.46
MJ_RS09025	0.0	31.4	190.3	191.1	127.7	132.0	131.0	60.6	43.0	36.2	71.7	61.9	65.7	1.25
MJ_RS09030	0.0	62.7	0.0	69.8	74.9	57.3	71.3	11.9	13.6	11.9	13.5	15.8	16.0	2.21
MJ_RS09035	0.0	0.0	114.2	18.4	33.8	29.9	26.5	7.2	4.3	5.0	9.6	8.8	13.6	1.79
MJ_RS09040	0.0	0.0	38.1	8.7	9.5	8.3	11.6	3.1	1.2	2.5	3.4	4.0	4.0	1.68
MJ_RS09415	51.9	125.4	0.0	65.0	50.7	94.7	95.3	16.2	37.3	54.3	31.6	29.6	24.2	1.22
MJ_RS09235	571.3	407.6	609.1	540.2	487.6	893.5	940.8	260.9	216.1	217.8	225.0	289.7	309.9	1.39
MJ_RS09240	51.9	0.0	152.3	193.0	130.9	355.4	410.3	78.6	66.6	87.0	78.5	76.3	98.6	1.41

4.4 Discussion

Microorganisms in nature live in complex communities and impact their environment through interspecies metabolic interactions. Next-generation sequencing technology used in tandem with kinetic measurements of growth rates and metabolic activities in mixed cultures can help us elucidate how microbes interact with one another and impact their environment (Embree et al., 2015, Wolf et al., 2018). This study modeled H_2 syntrophy among two hyperthermophilic archaea through kinetic and metabolic measurements while also leveraging dual-RNA-Seq analyses.

Most of what is known about the kinetics and physiology of methanogenesis at varying H_2 concentrations and during syntrophy comes from studies of the thermophile *Methanothermobacter thermoautotrophicus* and the mesophile *Methanococcus maripaludis*. Growth rates of both organisms decreased when they were H_2-limited relative to H_2-replete growth. However, growth yields (Y_{CH4}) increased when the cultures were H_2-limited (Schönheit et al., 1980; Morgan et al., 1997; Costa et al., 2013). Growth yields have not been measured for any methanogen during H_2 syntrophy or for hyperthermophilic methanogens under varying H_2 concentrations.

To determine *M. jannaschii* metabolism and kinetics under H_2-replete and H_2-limited growth conditions, continuous growth in chemostats was established. The decrease in specific growth rate and cell-specific CH_4 production rate of *M. jannaschii* when grown in monoculture under H_2-limited conditions show that growth and methanogenesis rates are limited by H_2 concentration. However, the growth yield for *M. jannaschii* was the highest when the cells were grown under H_2-limited conditions, as seen with *M. thermoautotrophicus* and *M. maripaludis*, but there is no consensus on a

physiological explanation (Schönheit et al., 1980; Morgan et al., 1997; Costa et al., 2013). During methanogenesis, methyl-H_4MPT is either converted to methyl-CoM for production of CH_4 and energy generation on the cytoplasmic membrane or to acetyl-CoA for biosynthetic reactions (Fig. 25). Depending on the H_2 concentration, hydrogenotrophic methanogens decide between maximum growth rate and maximum growth yield. This pattern might be explained by a rate-yield tradeoff in energy limited environments that shows a negative relationship between growth rate and yield and is suggested to be integral to evolution and the coexistence of species (Lipson, 2015).

In cocultures of *M. jannaschii* and *T. paralvinellae*, methanogens are expected to be optimized for H_2 consumption where removal of H_2 from the environment is required for syntrophy (Morgan et al., 1997). However, while *M. jannaschii* was capable of growth and methanogenesis solely on the H_2 produced by *T. paralvinellae*, the growth and CH_4 production rates and the growth yield of *M. jannaschii* decreased in coculture compared to when *M. jannaschii* was grown in monoculture under H_2-replete and H_2-limited conditions. Excess H_2 was previously shown to inhibit the growth of *T. paralvinellae*, which led to formate production as an alternate sink for electrons (Topçuoğlu et al., 2018). When *T. paralvinellae* was grown with *M. jannaschii*, H_2 syntrophy did not stimulate the growth rate or growth yield of *T. paralvinellae.* However, *T. paralvinellae* only produced formate when grown in monoculture while no formate was detected during growth in coculture suggesting that all electrons are being diverted to H_2 production.

During CO_2 fixation and methanogenesis (Fig. 25), expression of genes in *M. thermoautotrophicum* for H_2-dependent methylene-H_4MPT dehydrogenase (*hmd*) and

methyl-CoM reductase II (*mcr*II) decreased while expression of cofactor F_{420}-dependent methylene-H_4MPT (*mtd*) and the isozyme methyl-CoM reductase I (*mcr*I) increased when growth was H_2 limited relative to H_2-replete growth (Morgan et al., 1997). During H_2 syntrophy, the *M. thermoautotrophicum* proteome had more Mtd and F_{420}-dependent methylene-H_4MPT reductase (Mer) and less Hmd relative to monoculture growth on high H_2 (Enoki et al., 2011). Using gene expression and proteomic analyses, only *mcr*I was shown to be expressed in *M. thermoautotrophicum* during syntrophy while both *mcr*I and *mcr*II were shown to be expressed in pure culture (Luo et al., 2002; Enoki et al., 2011). In *M. maripaludis*, expression of *hmd* decreased and *mtd* increased during H_2-limited growth relative to H_2-replete growth (Hendrickson et al., 2007; Costa et al., 2013). During H_2 syntrophy, there were no significant changes in gene expression or protein abundance for Hmd and Mtd in *M. maripaludis* relative to a H_2-limited monoculture (Walker et al., 2012). The proteome of the hyperthermophile *Methanocaldococcus jannaschii* contained a lower abundance of Hmd and higher abundances of Mtd and four flagellar proteins in early logarithmic growth phase when grown in batch phase under H_2 limited conditions relative to H_2-replete conditions, but both Hmd and Mtd were found at high relative abundances in late logarithmic growth phase when grown on high H_2 (Mukhopadhyay et al., 2000).

In this study, RNA-Seq was used to determine changes in gene expression profiles in *M. jannaschii* for carbon assimilation, CH_4 production, and energy generation pathways when there were changes in H_2 availability. When *M. jannaschii* was grown under H_2-limited conditions, *mtd* expression was significantly upregulated, suggesting a preference for F_{420} as an electron carrier in the methanogenesis pathway under H_2-limited

conditions. The increase in cell yield under H_2-limited conditions was not supported by a change in the expression of genes in the carbon assimilation and methanogenesis pathways. No significant changes were detected in the expression of methyl-CoM reductase I and II and methyl-H_4MPT:CoM methyltransferase, which catalyze the last two steps of methanogenesis (Fig. 25). Moreover, there was no change in expression of the carbon monoxide dehydrogenase/acetyl-CoA synthase genes, which encode for the enzyme that converts methyl-MPT to acetyl-CoA. It is possible that high intracellular H_2 concentrations lead to an excess of reduced ferredoxin being produced by the cell by the electron bifurcating hydrogenase-heterodisulfide reductase, and that the cell recycles the ferredoxin on the membrane with a hydrogenase by producing H_2 that can be re-used by the cell, translocates H^+ or Na^+ to the outside of the cell, and produces more ATP on the membrane by oxidative phosphorylation (reaction 13). However, under H_2-limited conditions, the cell must direct more of its methyl-H_4MPT towards biosynthesis. Furthermore, there was no change in the expression of the genes for flagella. This difference from what was previously observed for *M. jannaschii* using proteomics (Mukhopadhyay et al., 2000) may be due to the use of a chemostat in this study instead of a batch reactor as was previously used.

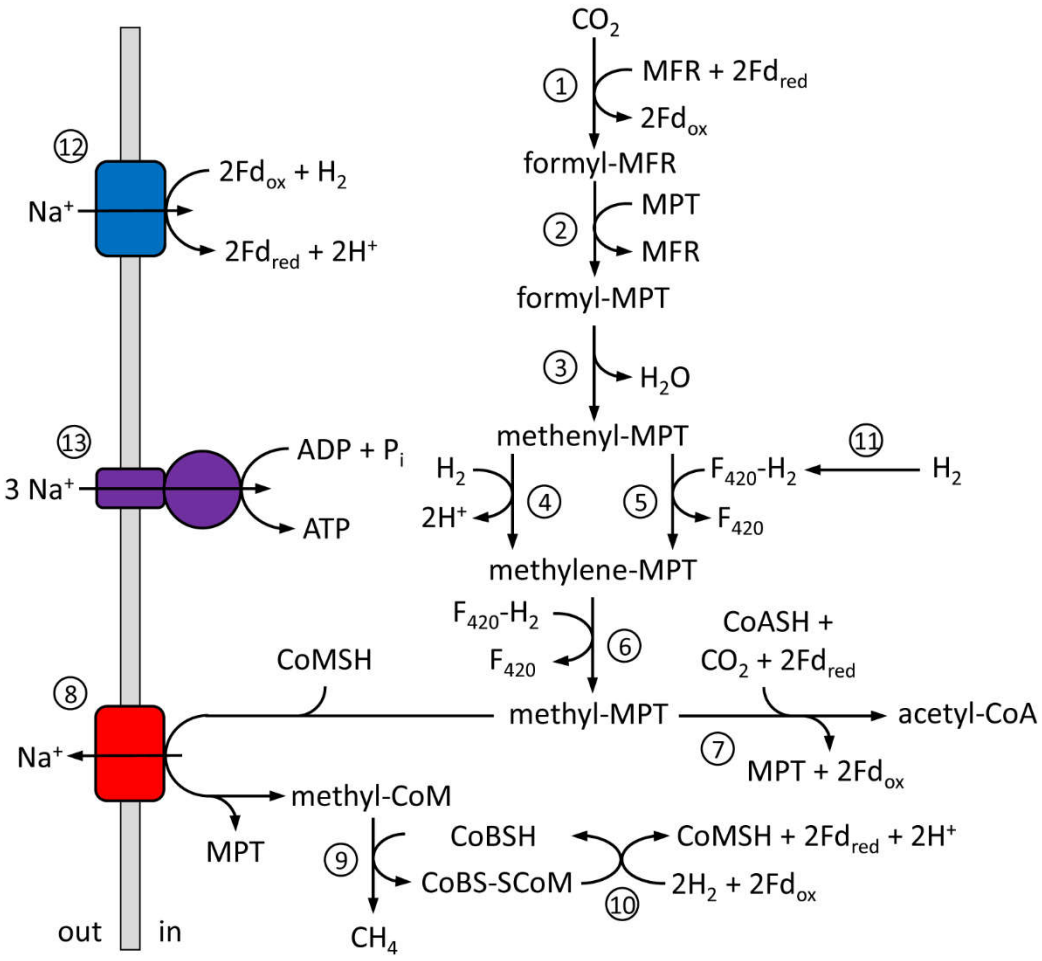

Figure 25 General metabolic pathway for *M. jannaschii*. The enzymes are (1) formylmethanofuran dehydrogenase, (2) formylmethanofuran:H_4MPT formyltransferase, (3) cyclohydrolase, (4) H_2-dependent methylene-H_4MPT dehydrogenase (Hmd), (5) F_{420}-dependent methylene-H_4MPT dehydrogenase (Mtd), (6) methylene-H_4MPT reductase (Mer), (7) CO dehydrogenase/acetyl-CoA synthase, (8) methyl-H_4MPT:CoM methyltransferase, (9) methyl-CoM reductase (Mcr), (10) hydrogenase/heterodisulfide reductase complex, (11) F_{420}-dependent hydrogenase, (12) membrane-bound ferredoxin-dependent hydrogenase, and (13) membrane-bound ATP synthase. MFR, methanofuran; H_4MPT, tetrahydromethanopterin; F_{420}, electron carrier coenzyme F_{420}; CoA, coenzyme A; CoM, coenzyme M; CoB, coenzyme B; and Fd, electron carrier ferredoxin.

In cocultures, *mtd* expression was significantly upregulated and *hmd* expression was significantly downregulated compared to monoculture cells. The distinct effect of H_2 availability on genes encoding F_{420}-dependent or H_2-dependent processes show that cells divert electron flow to different electron carriers. In coculture, there was up to 22.5-fold

increase in the expression of a putative RNA binding protein that is only found in methanogens and in the *Thermococcales* and has been proposed to regulate cellular activity at the translation level (Anantharaman et al., 2001). The decreases in the expression of genes in the putative membrane-bound, ferredoxin-dependent hydrogenase operon and in the membrane-bound, Na^+-translocating V-type ATPase operon support the kinetic observations that *M. jannaschii* is energy limited when grown syntrophically. Therefore, syntrophic growth ameliorated H_2 inhibition in *T. paralvinellae* but the growth of *M. jannaschii* is severely impaired. In environments such as low-H_2 hydrothermal vents along subduction zones and some mid-ocean ridges, hot marine sediments, oil reservoirs, and high saline shale beds where organic compounds are present, sulfur is absent, and H_2 efflux rates are low, thermophilic methanogens like *M. jannaschii* can likely grow and produce CH_4 through syntrophy but at very slow rates for this organism. H_2 inhibition of *Thermococcus* however could be prevented through syntrophic growth with thermophilic methanogens. This likely explains the presence of thermophilic H_2 producers and thermophilic, hydrogenotrophic methanogens in marine sediments and petroleum reservoirs and may be a source of CH_4 in those habitats.

This study demonstrates the utility of measuring growth kinetic parameters and differential gene expression patterns for two species grown in coculture. Dual-RNA-Seq based gene expression analysis can be used to differentiate the mRNA transcripts produced by two different species that otherwise often show high sequence similarity in their common genes. This approach can also be used to better understand what happens when two different organisms are competing for the same resource. In this manner, we will be better equipped to model cooperative, competitive, and neutral interactions

between different species in a given environment and predict the biogeochemical outcome of a mixed community living in a habitat.

CHAPTER 5

SUMMARY

Hyperthermophilic heterotrophs belonging to genus *Thermococcus* are commonly found in many subsurface environments such as coal and shale beds, marine sediments, and oil reservoirs. These environments lack sufficient environmental flux rates to remove excess metabolic products, such as H_2, that can inhibit the growth and metabolism of the *Thermococcus* present. Similarly, methanogens belonging to genus *Methanocaldococcus* are found to co-localize with *Thermococcus* in these low-H_2 environments that could be limiting to the growth and metabolism of the methanogens. It is important to study the H_2 stress survival strategies of these organisms and their cooperation with one another for survival to better understand their biogeochemical impact in hot subsurface environments. This dissertation presents three research projects to study thermophilic H_2 stress and syntrophy; (1) elucidating the potential for thermophilic and hyperthermophilic H_2 syntrophy in hydrothermal vent fluids and establishing a coculture with model organisms representative of *in situ* H_2 syntrophy (2) describing energetics of the model H_2-producing hyperthermophilic heterotroph, *Thermococcus paralvinellae*, and showing how the organism deals with H_2 stress, and (3) describing the energetics of the model H_2-consuming hyperthermophilic methanogen, *Methanocaldococcus jannaschii*, and how it deals with H_2 stress. It also examines if H_2 stress (i.e., H_2 inhibition for the heterotroph, H_2 limitation for the methanogen) is ameliorated when *T. paralvinellae* and *M. jannaschii* are grown in coculture through H_2 syntrophy.

The first project showed that thermophilic H_2 syntrophy can support methanogenesis within natural hydrothermal vent microbial assemblages. It may also be an important energy source for thermophilic autotrophs in marine geothermal environments that have low H_2 concentrations. In 2015, our laboratory tested for H_2 syntrophy in microcosms incubated at 55°C and 80°C using five 20-35°C hydrothermal fluids collected from Axial Seamount in the northeastern Pacific Ocean. The hydrothermal fluids were incubated anaerobically in duplicate with either high (>200 μM) H_2, low (~20 μM) H_2, or tryptone (protein) with no H_2 added as the energy sources for growth and CH_4 production. Total CH_4 production was ~100-fold higher in microcosms containing high H_2 relative to low H_2 at both incubation temperatures. Microcosms with tryptone (protein) but no added H_2, also showed more total CH_4 production than microcosms with low H_2 due to H_2 syntrophy. The 80°C microcosms produced more CH_4 through H_2 syntrophy than the 55°C microcosms. There was no growth or CH_4 production in separate incubations when neither H_2 nor organics were added. Furthermore, neither the addition of acetate nor formate alone to microcosms led to any CH_4 production suggesting that H_2 is the substrate that allows for methanogenesis. Following incubation, the 80°C microcosms only contained archaeal DNA, primarily from the H_2-producing heterotroph *Thermococcus* and the H_2-consuming methanogens *Methanocaldococcus* and *Methanothermococcus* (Topçuoğlu et al. 2016). These microbes were the predominant hyperthermophiles found in Axial Seamount vent fluids in other studies (Ver Eecke et al. 2012, Fortunato and Huber 2016). These results indicate that *in situ* methanogenesis at thermophilic temperatures is limited by H_2 availability, and

that heterotrophs can provide the H_2 necessary for growth and methanogenesis in the absence of added H_2 through H_2 syntrophy.

For the second project, the *T. paralvinellae* was examined for its growth and H_2 production mechanism and energetics. *T. paralvinellae* is particularly adept at H_2 production on polysaccharide and peptide substrates. However, when there is high H_2 accumulation in the environment, H_2 inhibition pushes *T. paralvinellae* to use alternate electron carriers, such as formate, with an ATP production penalty (Hensley et al., 2016; Topcuoglu et al., 2018). *T. paralvinellae* was grown in a chemostat on maltose with and without 65 μM of aqueous H_2 in the medium. The 65 μM of aqueous H_2 in the medium is to produce an inhibitory H_2 stress condition for *T. paralvinellae*. The amount of acetate and formate in the medium was measured using UPLC. The gene expression profile was analyzed by RNA-seq. To examine electron flow in *T. paralvinellae* under H_2 stress, we also created a constraint-based metabolic network model using the *T. paralvinellae* complete genome sequence. We utilized flux balance analysis (FBA) for *in silico* simulation of the entire metabolic activity of a cell with limitations based on genomic and experimental knowledge. The negative kinetic effect of H_2 inhibition on *T. paralvinellae* was evident in chemostat runs with H_2 background. There was a significant decrease in batch phase growth rates and steady state cell concentrations with high H_2 background. Produced metabolite production measurements, RNA-seq analyses of differentially expressed genes and *in silico* experiments we performed with the *T. paralvinellae* metabolic model showed that ~ 65 μM H_2 in the background led to growth inhibition, expression of formate hydrogenlyase genes, and formate secretion, with a modeled decrease in energy production due to diminished H^+ translocation on the membrane.

The third project compared the metabolic changes in hyperthermophilic heterotroph *Thermococcus paralvinellae* and the methanogen *Methanocaldococcus jannaschii,* in monocultures and cocultures to understand their H_2 stress and syntrophy strategies. *M. jannaschii* was grown in a chemostat under H_2-replete (70 μM H_2) and H_2-limited (15-30 μM H_2) conditions, and it was grown syntrophically in sealed bottles with the H_2-producing hyperthermophilic heterotroph *Thermococcus paralvinellae*. We measured specific growth rates and cell-specific CH_4 production rates for *M. jannaschii* with varying H_2 fluxes and determined *M. jannaschii* growth yields at H_2-replete, H_2-limited and H_2 syntrophy conditions. We also examined the growth rate and growth yield of *T. paralvinellae*. Furthermore, differential gene expression analysis using RNA-Seq was used to determine if changes occur in *M. jannaschii* for the expression of genes for carbon assimilation, CH_4 production, or energy generation when H_2 decreases in availability. The specific growth rate and cell-specific CH_4 production rate of *M. jannaschii* decreased when grown in monoculture under H_2-limited conditions. This showed that growth and methanogenesis rates are limited by H_2 concentration. The growth yield for *M. jannaschii* was the highest when the cells were grown under H_2-limited conditions. In cocultures, while *M. jannaschii* was capable of growth and methanogenesis solely on the H_2 produced by *T. paralvinellae*, the growth and CH_4 production rates of *M. jannaschii* decreased in coculture compared to when *M. jannaschii* was grown in monoculture. H_2 syntrophy did not stimulate the growth rate or growth yield of *T. paralvinellae.* However, H_2 stress in *T. paralvinellae* was ameliorated as seen by production of formate when the cells are grown in monoculture but not in coculture. RNA-seq analysis showed there was a distinct effect of H_2 availability on genes encoding

F_{420}-dependent or H_2-dependent processes. Cells divert electron flow to different electron carriers with changes in H_2 concentration. When *M. jannaschii* was grown under H_2-limited conditions, *mtd* expression was significantly upregulated, suggesting a preference for F_{420} as an electron carrier in the methanogenesis pathway under H_2-limited conditions. Similarly, in cocultures, where *M. jannaschii* was H_2 limited as well, *mtd* expression was significantly upregulated and *hmd* expression was significantly downregulated compared to monoculture cells.

This dissertation helps establish a pipeline to model the physiological and biogeochemical behavior and cellular interactions of high-temperature microbial communities in subseafloor environments down to the molecular level by coupling kinetic, gene expression, and modeling activities and predicting their impact on an environment. Most laboratory-based studies on the physiology and biogeochemistry of high-temperature anaerobes have focused on pure cultures. It is likely that thermophilic and hyperthermophilic archaea and bacteria are influenced by, or even dependent upon, other microbial species, and yet our understanding of interspecies cell-cell interactions among subsurface microorganisms is very limited. There is a need for proper interpretation of the large amount of metagenomics, metatranscriptomic, and RNA stable-isotope probing (RNA-SIP) data, which are becoming increasingly common from field studies. This study is a first step towards understanding several types of interspecies interactions. Other interactions to be explored in future studies include H_2 syntrophy with a non-methanogen, competition for H_2 between a methanogen and a non-methanogenic hydrogenotroph, microbe-mineral interactions, and competition for resources between closely related species.

BIBLIOGRAPHY

Adams, M.W., Holden, J.F., Menon, A.L., Schut, G.J., Grunden, A.M., Hou, C., et al. (2001) Key role for sulfur in peptide metabolism and in regulation of three hydrogenases in the hyperthermophilic archaeon *Pyrococcus furiosus*. *J. Bacteriol.* 183: 716–24.

Ahsanul Islam, M., Edwards, E.A., Mahadevan, R., Hedrick, D., and Koenigsberg, S. (2010) Characterizing the metabolism of *Dehalococcoides* with a constraint-based model. *PLoS Comput. Biol*. 6: 8.

Alain, K., Querellou, J., Lesongeur, F., Pignet, P., Crassous, P., Raguénès, G., et al. (2002) Caminibacter hydrogeniphilus gen. nov., sp. nov., a novel thermophilic, hydrogen-oxidizing bacterium isolated from an East Pacific Rise hydrothermal vent. *Int. J. Syst. Evol. Microbiol.* 52: 1317–1323.

Alain, K., Pignet, P., Zbinden, M., Quillevere, M., Duchiron, F., Donval, J.P., et al. (2002) *Caminicella sporogenes* gen. nov., sp. nov., a novel thermophilic spore-forming bacterium isolated from an East-Pacific Rise hydrothermal vent. *Int. J. Syst. Evol. Microbiol.* 52: 1621-1628.

Alain, K., Postec, A., Grinsard, E., Lesongeur, F., Prieur, D., and Godfroy, A. (2010) *Thermodesulfatator atlanticus* sp. nov., a thermophilic, chemolithoautotrophic, sulfate-reducing bacterium isolated from a Mid-Atlantic Ridge hydrothermal vent. *Int. J. Syst. Evol. Microbiol.* 60: 33–38.

Alm, E.W., Oerther, D.B., Larsen, N., Stahl, D.A., and Raskin, L. (1996) The oligonucleotide probe database. *Appl. Environ. Microbiol.* 62: 3557-3559.

Amo, T., Paje, M.L.F., Inagaki, A., Ezaki, S., Atomi, H., and Imanaka, T. (2002*)* *Pyrobaculum calidifontis* sp. nov., a novel hyperthermophilic archaeon that grows in atmospheric air. *Archaea* 1: 113–21.

Anantharaman V., Koonin E.V., Aravind L. (2001) TRAM, a predicted RNA-binding domain, common to tRNA uracil methylation and adenine thiolation enzymes. *FEMS Microbiol. Lett.* 197: 215-221.

Anders, S., Huber, W., Nagalakshmi, U., Wang, Z., Waern, K., Shou, C., et al. (2010) Differential expression analysis for sequence count data. *Genome Biol.* 11: R106.

Anderson, I., Rodriguez, J., Susanti, D., Porat, I., Reich, C., Ulrich, L.E., et al. (2008) Genome sequence of *Thermofilum pendens* reveals an exceptional loss of biosynthetic pathways without genome reduction. *J. Bacteriol.* 190: 2957–65.

Anderson, I.J., Sun, H., Lapidus, A., Copeland, A., Glavina Del Rio, T., Tice, H., et al. (2009) Complete genome sequence of *Staphylothermus marinus* Stetter and Fiala 1986 type strain F1. *Stand. Genomic Sci.* 1: 183–8.

Andrews, S.C., Berks, B.C., McClay, J., Ambler, A., Quail, M.A., Golby, P., and Guest, J.R. (1997) A 12-cistron *Escherichia coli* operon (*hyf*) encoding a putative proton-translocating formate hydrogenlyase system. *Microbiology* 143: 3633-3647.

Arai, H., Kanbe, H., Ishii, M., and Igarashi, Y. (2010) Complete genome sequence of the thermophilic, obligately chemolithoautotrophic hydrogen-oxidizing bacterium *Hydrogenobacter thermophilus* TK-6. *J. Bacteriol.* 192: 2651–2.

Auernik, K.S., Maezato, Y., Blum, P.H., and Kelly, R.M. (2008) The genome sequence of the metal-mobilizing, extremely thermoacidophilic archaeon *Metallosphaera sedula* provides insights into bioleaching-associated metabolism. *Appl. Environ. Microbiol.* 74: 682–92.

Aziz, R.K., Bartels, D., Best, A.A., DeJongh, M., Disz, T., Edwards, R.A., et al. (2008) The RAST server: rapid annotations using subsystems technology. *BMC Genomics* 9: 75.

Bae, S.S., Kim, T.W., Lee, H.S., Kwon, K.K., Kim, Y.J., Kim, M.S., et al. (2012) H_2 production from CO, formate or starch using the hyperthermophilic archaeon, *Thermococcus onnurineus*. *Biotechnol. Lett*. 34: 75-79.

Belay, N., Sparling, R., and Daniels, L. (1984) Dinitrogen fixation by a thermophilic methanogenic bacterium. *Nature* 312: 286-288.

Bertoldo, C. and Antranikian, G. (2006) The Order *Thermococcales*. *Prokaryotes* 3: 69-81.

Blöchl, E., Rachel, R., Burggraf, S., Hafenbradl, D., Jannasch, H.W., and Stetter, K.O. (1997) *Pyrolobus fumarii*, gen. and sp. nov., represents a novel group of archaea, extending the upper temperature limit for life to 113 degrees C. *Extremophiles* 1: 14–21.

Boettger, J., Lin, H.-T., Cowen, J.P., Hentscher, M., and Amend, J.P. (2013) Energy yields from chemolithotrophic metabolisms in igneous basement of the Juan de Fuca ridge flank system. *Chem. Geol.* 337–338: 11–19.

Bonch-Osmolovskaya E.A., Miroshnichenko M.L., Lebedinsky A.V., Chernyh N.A., Nazina T.N., Ivoilov V.S. *et al.* (2003) Radioisotopic, culture-based, and oligonucleotide microchip analyses of thermophilic microbial communities in a continental high-temperature petroleum reservoir. *Appl. Environ. Microbiol.* 69: 6143-6151.

Bonch-Osmolovskaya, E.A., and Stetter, K.O. (1991) Interspecies hydrogen transfer in cocultures of thermophilic Archaea. *Syst. Appl. Microbiol.* 14: 205-208.

Bonch-Osmolovskaya, E.A., Miroshnichenko, M.L., Kostrikina, N.A., Chernych, N.A., and Zavarzin, G.A. (1990) *Thermoproteus uzoniensis* sp. nov., a new extremely thermophilic archaebacterium from Kamchatka continental hot springs. *Arch. Microbiol.* 154: 556–559.

Bonch-Osmolovskaya, E.A., Miroshnichenko, M.L., Lebedinsky, A. V, Chernyh, N.A., Nazina, T.N., Ivoilov, V.S., et al. (2003) Radioisotopic, culture-based, and oligonucleotide microchip analyses of thermophilic microbial communities in a continental high-temperature petroleum reservoir. *Appl. Environ. Microbiol.* 69: 6143–51.

Bonin, A.S. and Boone, D.R. (2006) The Order *Methanobacteriales*. In, *The Prokaryotes*. Springer New York, New York, NY, pp. 231–243.

Boone, D.R., Castenholz, R.W., and Garrity, G.M. (2001) Bergey's manual of systematic bacteriology Springer.

Borrel, G., Adam, P.S., and Gribaldo, S. (2016) Methanogenesis and the Wood–Ljungdahl Pathway: An Ancient, Versatile, and Fragile Association. *Genome Biol. Evol.* 8: 1706–1711.

Bourbonnais, A., Lehmann, M. F., Butterfield, D. A., and Juniper, S. K. (2012) Subseafloor nitrogen transformations in diffuse hydrothermal vent fluids of the Juan de Fuca Ridge evidenced by the isotopic composition of nitrate and ammonium. *Geochem. Geophys. Geosyst.*, 13:Q02T01.

Boyd, E.S., Jackson, R.A., Encarnacion, G., Zahn, J.A., Beard, T., Leavitt, W.D., et al. (2007) Isolation, characterization, and ecology of sulfur-respiring crenarchaea inhabiting acid-sulfate-chloride-containing geothermal springs in Yellowstone National Park. *Appl. Environ. Microbiol.* 73: 6669–77.

Brock, T.D. (1978) Thermophilic Microorganisms and Life at High Temperatures Springer New York.

Butterfield, D.A., Roe, K.K., Lilley, M.D., Huber J.A., Baross, J.A., Embley, R.W., and Massoth, G.J. (2004) "Mixing, reaction and microbial activity in the sub-seafloor revealed by temporal and spatial variation in diffuse flow vents at Axial Volcano", in *The Subseafloor Biosphere at Mid-Ocean Ridges*, ed. W. S. D. Wilcock, E. F. DeLong, D. S. Kelley, J. A. Baross, and S. C. Cary (Washington, D. C.: American Geophysical Union Press), 269-289.

Canganella, F. and Jones, W.J. (1994) Fermentation studies with thermophilic Archaea in pure culture and in syntrophy with a thermophilic methanogen. *Curr. Microbiol.* 28: 293–298.

Caporaso, J.G., Kuczynski, J., Stombaugh, J., Bittinger, K., Bushman, F.D., Costello, E.K., et al. (2010) QIIME allows analysis of high-throughput community sequencing data. *Nat. Methods* 7: 335-336.

Caress, D.W., Clague, D.A., Paduan, J.B., Martin, J., Dreyer, B., Chadwick, Jr., W.W., et al. (2012) Repeat bathymetric surveys at 1-metre resolution of lava flows erupted at Axial Seamount in April 2011. *Nat. Geosci.* 5: 483-488.

Carothers, W.W. and Kharaka, Y.K. (1978) Aliphatic acid anions in oil-field waters: implications for origin of natural gas. *Am. Assoc. Pet. Geol. Bull.* 62: 2441-2453.

Caumette, P., Brochier-Armanet, C., and Normand, P. (2015) Taxonomy and Phylogeny of Prokaryotes. In, *Environmental Microbiology: Fundamentals and Applications*. Springer Netherlands, Dordrecht, pp. 145–190.

Chaban, B., Ng, S.Y.., and Jarrell, K.F. (2006) Archaeal habitats — from the extreme to the ordinary. *Can. J. Microbiol.* 52: 73–116.

Chadwick, Jr., W.W., Clague, D.A., Embley, R.W., Perfit, M.R., Butterfield, D.A., Caress, D.W., et al. (2013) The 1998 eruption of Axial Seamount: new insights on submarine lava flow emplacement from high-resolution mapping. *Geochem. Geophys. Geosyst.* 14: 3939-3968.

Chadwick, Jr., W.W., Nooner, S.L., Butterfield, D.A., and Lilley, M.D. (2012) Seafloor deformation and forecasts of the April 2011 eruption at Axial Seamount. *Nat. Geosci.* 5: 474-477.

Chelliah, V., Juty, N., Ajmera, I., Ali, R., Dumousseau, M., Glont, M., et al. (2015) BioModels: ten-year anniversary. *Nucleic Acids Res.* 43: D542-D548.

Ciobanu, M.C., Burgaud, G., Dufresne, A., Breuker, A., Rédou, V., Ben Maamar, S., et al. (2014) Microorganisms persist at record depths in the subseafloor of the Canterbury Basin. *ISME J.* 8: 1370-1380.

Costa K.C., Yoon S.H., Pan M., Burn J.A., Baliga N.S., Leigh J.A. (2013) Effects of H_2 and formate on growth yield and regulation of methanogenesis in *Methanococcus maripaludis*. *J. Bacteriol*. 195: 1456-1462.

Dahle H., Garshol F., Madsen M., Birkeland N.K. (2008) Microbial community structure analysis of produced water from a high-temperature North Sea oil-field. *Antonie van Leeuwenhoek* 93: 37-49.

Daly, R.A., Borton, M.A., Wilkins, M.J., Hoyt, D.W., Kountz, D.J., Wolfe, R.A., et al. (2016) Microbial metabolisms in a 2.5-km-deep ecosystem created by hydraulic fracturing in shales. *Nat. Microbiol.* 1: 16146.

Das, S., Paul, S., Bag, S.K., and Dutta, C. (2006) Analysis of *Nanoarchaeum equitans* genome and proteome composition: indications for hyperthermophilic and parasitic adaptation. *BMC Genomics* 7: 186.

Davidova I.A., Duncan K.E., Perez-Ibarra B.M., Suflita J.M. (2012) Involvement of thermophilic archaea in the biocorrosion of oil pipelines. *Environ. Microbiol.* 14: 1762-1771.

Deppenmeier, U. (2002) Redox-driven proton translocation in methanogenic Archaea. *Cell. Mol. Life Sci.* 59: 1513-1533.

Dobin A., Davis C.A., Schlesinger F., Drenkow J., Zaleski C., Jha S. *et al.* (2013) STAR: ultrafast universal RNA-seq aligner. *Bioinformatics* 29: 15-21.

Dodd, M.S., Papineau, D., Grenne, T., Slack, J.F., Rittner, M., Pirajno, F., et al. (2017) Evidence for early life in Earth's oldest hydrothermal vent precipitates. *Nature* 543: 60–64.

Doddema H.J., Vogels G.D. (1978) Improved identification of methanogenic bacteria by fluorescence microscopy. *Appl. Environ. Microbiol.* 36: 752-754.

Ebrahim, A., Lerman, J.A., Palsson, B.O., and Hyduke, D.R. (2013) COBRApy: COnstraints-Based Reconstruction and Analysis for Python. *BMC Syst. Biol.* 7: 74.

Eder, W. and Huber, R. (2002) New isolates and physiological properties of the *Aquificales* and description of *Thermocrinis albus* sp. nov. *Extremophiles*.

Ehrhardt C.J., Haymon R.M., Lamontagne M.G., Holden P.A. (2007) Evidence for hydrothermal Archaea within the basaltic flanks of the East Pacific Rise. *Environ. Microbiol.* 9: 900-912.

Embree M., Liu J.K., Al-Bassam M.M., Zengler K. (2015) Networks of energetic and metabolic interactions define dynamics in microbial communities. *Proc. Natl. Acad. Sci. USA* 112: 15,450-15,455.

Enoki M., Shinzato N., Sato H., Nakamura K., Kamagata Y. (2011) Comparative proteomic analysis of *Methanothermobacter thermoautotrophicus* ΔH in pure culture and in coculture with a butyrate-oxidizing bacterium. *PLoS One* 6: e24309.

Eren, A.M., Vineis, J.H., Morrison, H.G., and Sogin M.L. (2013) A filtering method to generate high quality short reads using Illumina paired-end technology. *PLoS ONE* 8:e66643.

Evans, P.N., Parks, D.H., Chadwick, G.L., Robbins, S.J., Orphan, V.J., Golding, S.D., and Tyson, G.W. (2015) Methane metabolism in the archaeal phylum Bathyarchaeota revealed by genome-centric metagenomics. *Science* 350: 434–438.

Feinberg, L.F., Srikanth, R., Vachet, R.W., and Holden, J.F. (2008) Constraints on anaerobic respiration in the hyperthermophilic Archaea *Pyrobaculum islandicum* and *Pyrobaculum aerophilum*. *Appl. Environ. Microbiol.* 74: 396–402.

Feist, A.M., Henry, C.S., Reed, J.L., Krummenacker, M., Joyce, A.R., Karp, P.D., et al. (2007) A genome-scale metabolic reconstruction for *Escherichia coli* K-12 MG1655 that accounts for 1260 ORFs and thermodynamic information. *Mol. Syst. Biol.* 3: 121.

Feist, A.M., Scholten, J.C.M., Palsson, B.Ø., Brockman, F.J., and Ideker, T. (2006) Modeling methanogenesis with a genome-scale metabolic reconstruction of *Methanosarcina barkeri*. *Mol. Syst. Biol.* 2: 2006.0004.

Fiala, G., Stetter, K.O., Jannasch, H.W., Langworthy, T.A., and Madon, J. (1986) *Staphylothermus marinus* sp. nov. Represents a Novel Genus of Extremely Thermophilic Submarine Heterotrophic Archaebacteria Growing up to 98 °C. *Syst. Appl. Microbiol.* 8: 106–113.

Flores G.E., Campbell J.H., Kirshtein J.D., Meneghin J., Podar M., Steinberg J.I. *et al.* (2011) Microbial community structure of hydrothermal deposits from geochemically different vent fields along the Mid-Atlantic Ridge. *Environ. Microbiol.* 13: 2158-2171.

Fortunato C.S., Larson B., Butterfield D.A., Huber J.A. (2018) Spatially distinct, temporally stable microbial populations mediate biogeochemical cycling at and below the seafloor in hydrothermal vent fluids. *Environ. Microbiol.* 20: 769–784.

Fortunato, C.S. and Huber, J.A. (2016) Coupled RNA-SIP and metatranscriptomics of active chemolithoautotrophic communities at a deep-sea hydrothermal vent. *ISME J.* 10: 1925–1938.

Fortunato, C.S., Larson, B., Butterfield, D.A., and Huber, J.A. (2018) Spatially distinct, temporally stable microbial populations mediate biogeochemical cycling at and below the seafloor in hydrothermal vent fluids. *Environ. Microbiol.* 20: 769–784.

Francisco, D.E., Mah, R.A., and Rabin, A.C. (1973) Acridine orange-epifluorescence technique for counting bacteria in natural waters. *Trans. Amer. Micros. Soc.* 92: 416-421.

Garrity, G.M., Holt, J.G., Whitman, W.B., Keswani, J., Boone, D.R., Koga, Y., et al. (2001) Phylum All. Euryarchaeota phy. nov. In, *Bergey's Manual® of Systematic Bacteriology*. Springer New York, New York, NY, pp. 211–355.

Gaw Van Praagh, C. V, Kashefi, K., Reysenbach, A.-L., Holmes, D.E., Lovley, D.R., and Tor, J.M. (2002) Geoglobus ahangari gen. nov., sp. nov., a novel hyperthermophilic archaeon capable of oxidizing organic acids and growing autotrophically on hydrogen with Fe(III) serving as the sole electron acceptor. *Int. J. Syst. Evol. Microbiol.* 52: 719–728.

Goecks, J., Nekrutenko, A., Taylor, J., Galaxy Team, T., Hirst, M., Bainbridge, M., et al. (2010) Galaxy: a comprehensive approach for supporting accessible, reproducible, and transparent computational research in the life sciences. *Genome Biol*. 11: R86.

Hamilton-Brehm, S.D., Gibson, R.A., Green, S.J., Hopmans, E.C., Schouten, S., van der Meer, M.T.J., et al. (2013) Thermodesulfobacterium geofontis sp. nov., a hyperthermophilic, sulfate-reducing bacterium isolated from Obsidian Pool, Yellowstone National Park. *Extremophiles* 17: 251–263.

Hartzell, P. and Reed, D.W. (2006) The Genus *Archaeoglobus* Archeal Sulfate Reducers. 82–100.

Hendrickson E.L., Haydock A.K., Moore B.C., Whitman W.B., Leigh J.A. (2007) Functionally distinct genes regulated by hydrogen limitation and growth rate in methanogenic Archaea. *Proc. Natl. Acad. Sci. USA* 104: 8930-8934.

Henry, C.S., DeJongh, M., Best, A.A., Frybarger, P.M., Linsay, B., and Stevens, R.L. (2010) High-throughput generation, optimization and analysis of genome-scale metabolic models. *Nat. Biotechnol.* 28: 977-982.

Hensel, R., Matussek, K., Michalke, K., Tacke, L., Tindall, B.J., Kohlhoff, M., et al. (1997) *Sulfophobococcus zilligii* gen. nov., spec, nov. a novel hyperthermophilic archaeum isolated from hot alkaline springs of Iceland. *Syst. Appl. Microbiol.* 20: 102–110.

Hensley S.A., Moreira E., Holden J.F. (2016) Hydrogen production and enzyme activities in the hyperthermophile *Thermococcus paralvinellae* grown on maltose, tryptone, and agricultural waste. *Front. Microbiol.* 7: 167.

Hensley, S.A. (2015) ScholarWorks@UMass Amherst Agricultural Waste Remediation and H2 Production by Hyperthermophilic Heterotrophs: Bioinformatics, Taxonomy, and Physiology.

Hensley, S.A., Jung, J.H., Park, C.S., and Holden, J.F. (2014) *Thermococcus paralvinellae* sp. nov. and *Thermococcus cleftensis* sp. nov. of hyperthermophilic heterotrophs from deep-sea hydrothermal vents. *Int. J. Syst. Evol. Microbiol*. 64: 3655-3659.

Hensley, S.A., Moreira, E., and Holden, J.F. (2016) Hydrogen production and enzyme activities in the hyperthermophile *Thermococcus paralvinellae* grown on maltose, tryptone, and agricultural waste. *Front. Microbiol.* 7: 167.

Hetzer, A., McDonald, I.R., and Morgan, H.W. (2008) *Venenivibrio stagnispumantis* gen. nov., sp. nov., a thermophilic hydrogen-oxidizing bacterium isolated from Champagne Pool, Waiotapu, New Zealand. *Int. J. Syst. Evol. Microbiol.* 58: 398–403.

Holden J.F., Breier J.A., Rogers K.L., Schulte M.D., Toner BM. (2012). Biogeochemical processes at hydrothermal vents: microbes and minerals, bioenergetics, and carbon fluxes. *Oceanography* 25: 196-208.

Holden, J.F. (2009) Extremophiles: hot environments. In Schaechter M (ed.), The Desk Encyclopedia of Microbiology, 2nd Edition, Elsevier Publishing. 495-514

Huber, G., Spinnler, C., Gambacorta, A., and Stetter, K.O. (1989) *Metallosphaera sedula* gen, and sp. nov. Represents a New Genus of Aerobic, Metal-Mobilizing, Thermoacidophilic Archaebacteria. *Syst. Appl. Microbiol.* 12: 38–47.

Huber, H. and Prangishvili, D. (2006) Sulfolobales. In, *The Prokaryotes*. Springer New York, New York, NY, pp. 23–51.

Huber, H. and Stetter, K.O. (2006) Desulfurococcales. In, *The Prokaryotes*. Springer New York, New York, NY, pp. 52–68.

Huber, H., Huber, R., and Stetter, K.O. (2006) Thermoproteales. *Prokaryotes Vol. 3* 1982: 10–22.

Huber, H., Thomm, M., König, K., Thies, G., and Stetter, K.O. (1982). *Methanococcus thermolithotrophicus*, a novel thermophilic lithotrophic methanogen. *Arch. Microbiol.* 132: 47-50.

Huber, J.A., Butterfield, D.A., and Baross, J.A. (2002). Temporal changes in archaeal diversity and chemistry in a mid-ocean ridge subseafloor habitat. *Appl. Environ. Microbiol.* 68: 1585-1594.

Huber, J.A., Butterfield, D.A., and Baross, J.A. (2003) Bacterial diversity in a subseafloor habitat following a deep-sea volcanic eruption. *FEMS Microbiol. Ecol.* 43: 393-409

Huber, J.A., Butterfield, D.A., and Baross, J.A. (2006) Diversity and distribution of subseafloor Thermococcales populations in diffuse hydrothermal vents at an active deep-sea volcano in the northeast Pacific Ocean. *J. Geophys. Res.* 111:G04016.

Huber, J.A., Johnson, H.P., Butterfield, D.A., and Baross, J.A. (2006) Microbial life in ridge flank crustal fluids. *Environ. Microbiol.* 8: 88-99.

Huber, J.A., Mark Welch, D.B., Morrison, H.G., Huse, S.M., Neal, P.R., Butterfield, D.A., and Sogin, M. L. (2007) Microbial population structures in the deep marine biosphere. *Science* 318: 97-100.

Huber, R., Dyba, D., Huber, H., Burggraf, S., and Rachel, R. (1998) Sulfur-inhibited *Thermosphaera aggregans* sp. nov., a new genus of hyperthermophilic archaea isolated after its prediction from environmentally derived 16s rRNA sequences. *Int. J. Syst. Bacteriol.* 48: 1–38.

Huber, R., Eder, W., Heldwein, S., Wanner, G., Huber, H., Rachel, R., and Stetter, K.O. (1998) *Thermocrinis ruber* gen. nov., sp. nov., A pink-filament-forming hyperthermophilic bacterium isolated from yellowstone national park. *Appl. Environ. Microbiol.* 64: 3576–83.

Huber, R., Sacher, M., Vollmann, A., Huber, H., and Rose, D. (2000) Respiration of Arsenate and Selenate by Hyperthermophilic Archaea. *Syst. Appl. Microbiol.* 23: 305–314.

Huber, R., Stetter, K.O., Huber, R., and Stetter, K.O. (2001) *Aquificales*. In, *Encyclopedia of Life Sciences*. John Wiley & Sons, Ltd, Chichester, UK.

Hügler, M., Huber, H., Molyneaux, S.J., Vetriani, C., and Sievert, S.M. (2007) Autotrophic CO_2 fixation via the reductive tricarboxylic acid cycle in different lineages within the phylum Aquificae: evidence for two ways of citrate cleavage. *Environ. Microbiol.* 9: 81–92.

Huse, S.M., Young, V.B., Morrison, H.G., Antonopoulos, D.A., Kwon, J., Dalal, S., et al. (2014). Comparison of brush and biopsy sampling methods of the ileal pouch for assessment of mucosa-associated microbiota of human subjects. *Microbiome* 2: 5-13.

Inagaki F., Nunoura T., Nakagawa S., Teske A., Lever M., Lauer A. *et al.* (2006) Biogeographical distribution and diversity of microbes in methane hydrate-bearing deep marine sediments on the Pacific Ocean Margin. *Proc. Natl. Acad. Sci. USA* 103: 2815-2820.

Inskeep, W.P., Jay, Z.J., Tringe, S.G., Herrgård, M.J., Rusch, D.B., and YNP Metagenome Project Steering Committee and Working Group Members (2013) The YNP Metagenome Project: Environmental Parameters Responsible for Microbial Distribution in the Yellowstone Geothermal Ecosystem. *Front. Microbiol.* 4: 67.

Ishii, S., Kosaka, T., Hori, K., Hotta, Y., and Watanabe, K. (2005) Coaggregation facilitates interspecies hydrogen transfer between *Pelotomaculum thermopropionicum* and *Methanothermobacter thermautotrophicus*. *Appl. Environ. Microbiol.* 71: 7838–45.

Ishii, S., Kosaka, T., Hotta, Y., and Watanabe, K. (2006) Simulating the contribution of coaggregation to interspecies hydrogen fluxes in syntrophic methanogenic consortia. *Appl. Environ. Microbiol.* 72: 5093–6.

Itoh, T., Suzuki, K., Sanchez, P.C., and Nakase, T. (2003) *Caldisphaera lagunensis* gen. nov., sp. nov., a novel thermoacidophilic crenarchaeote isolated from a hot spring at Mt Maquiling, Philippines. *Int. J. Syst. Evol. Microbiol.* 53: 1149–1154.

Itoh, T., Suzuki, K.I., and Nakase, T. (1998) *Thermocladium modestius* gen. nov., sp. nov., a new genus of rod-shaped, extremely thermophilic crenarchaeote. *Int. J. Syst. Bacteriol.* 48: 879–887.

Itoh, T., Suzuki, K.-I., Sanchez, P.C., and Nakasel, T. (1999) *Caldivirga maquilingensis* gen. nov., sp. nov., a new genus of rod-shaped crenarchaeote isolated from a hot spring in the Philippines. *Int. J. Syst. Bacteriol.* 49: 1157–1163.

Jan, R.L., Wu, J., Chaw, S.M., Tsai, C.W., and Tsen, S.D. (1999) A novel species of thermoacidophilic archaeon, *Sulfolobus yangmingensis* sp. nov. *Int. J. Syst. Bacteriol.* 49 Pt 4: 1809–1816.

Jay, Z.J., Beam, J.P., Kozubal, M.A., Jennings, R. deM., Rusch, D.B., and Inskeep, W.P. (2016) The distribution, diversity and function of predominant *Thermoproteales* in high-temperature environments of Yellowstone National Park. *Environ. Microbiol.* 18: 4755–4769.

Jeon, J.H., Lim, J.K., Kim, M.-S., Yang, T.-J., Lee, S.-H., Bae, S.S., et al. (2015) Characterization of the *frh*AGB-encoding hydrogenase from a non-methanogenic hyperthermophilic archaeon. *Extremophiles* 19: 109-118.

Jiang, L., Long, C., Wu, X., Xu, H., Shao, Z., and Long, M. (2014) Optimization of thermophilic fermentative hydrogen production by the newly isolated *Caloranaerobacter azorensis* H53214 from deep-sea hydrothermal vent environment. *Int. J. Hydrogen Energ.* 39: 14154-14160.

Johnson, M.R., Conners, S.B., Montero, C.I., Chou, C.J., Shockley, K R., and Kelly, R.M. (2006) The *Thermotoga maritima* phenotype is impacted by syntrophic interaction with *Methanococcus jannaschii* in hyperthermophilic coculture. *Appl. Environ. Microbiol.* 72: 811-818.

Jones, W.J., Leigh, J.A., Mayer, F., Woese, C.R., and Wolfe, R.S. (1983) *Methanococcus jannaschii* sp. nov., an extremely thermophilic methanogen from a submarine hydrothermal vent. *Arch. Microbiol.* 136: 254-261.

Jørgensen, B.B. (2017) Microbial life in deep subseafloor coal beds. *Proc. Natl. Acad. Sci. U. S. A.* 114: 11568–11570.

Jung, J.H., Kim, Y.T., Jeon, E.J., Seo, D.H., Hensley, S.A., Holden, J.F., et al. (2014) Complete genome sequence of hyperthermophilic archaeon *Thermococcus* sp. ES1. J Biotechnol 174: 14-15.

Junzhang, L., Bin, H., Gongzhe, C., Jing, W., Yun, F., Xiaoming, T., and Weidong, W. (2014) A study on the microbial community structure in oil reservoirs developed by water flooding. *J. Pet. Sci. Eng.* 122: 354-359.

Kaksonen, A.H., Spring, S., Schumann, P., Kroppenstedt, R.M., and Puhakka, J.A. (2006) *Desulfotomaculum thermosubterraneum* sp. nov., a thermophilic sulfate-reducer isolated from an underground mine located in a geothermally active area. *Int. J. Syst. Evol. Microbiol.* 56: 2603-2608.

Kanai, T., Imanaka, H., Nakajima, A., Uwamori, K., Omori, Y., Fukui, T., et al. (2005) Continuous hydrogen production by the hyperthermophilic archaeon, *Thermococcus kodakaraensis* KOD1. *J. Biotechnol.* 116: 271-282.

Karadagli, F., and Rittmann, B.E. (2005) Kinetic characterization of *Methanobacterium bryantii* M.o.H. *Environ. Sci. Technol.* 39: 4900-4905.

Kashefi, K., Holmes, D.E., Reysenbach, A.-L., and Lovley, D.R. (2002) Use of Fe(III) as an electron acceptor to recover previously uncultured hyperthermophiles: isolation and characterization of *Geothermobacterium ferrireducens* gen. nov., sp. nov. *Appl. Environ. Microbiol.* 68: 1735–42.

Kashefi, K., Tor, J.M., Holmes, D.E., Gaw Van Praagh, C. V., Reysenbach, A.L., and Lovley, D.R. (2002) Geoglobus ahangari gen. nov., sp. nov., a novel hyperthermophilic archaeon capable of oxidizing organic acids and growing autotrophically on hydrogen with Fe(III) serving as the sole electron acceptor. *Int. J. Syst. Evol. Microbiol.* 52: 719–728.

Kawasumi, T., Igarashi, Y., Kodama, T., and Minoda, Y. (1984) *Hydrogenobacter thermophilus* gen. nov., sp. nov., an Extremely Thermophilic, Aerobic, Hydrogen-Oxidizing Bacterium. *Int. J. Syst. Bacteriol.* 34: 5–10.

Kelley, D.S., Baross, J.A., and Delaney, J.R. (2002) Volcanoes, fluids, and life at mid-ocean ridge spreading centers. *Annu. Rev. Earth Planet. Sci.* 30: 385–491.

Kelley, D.S., Delaney, J.R., Chadwick, Jr., W.W., Philip, B., and Merle, S.G. (2015) Axial Seamount 2015 eruption: a 127-m thick, microbially-covered lava flow. Abstract retrieved from Annual Fall Meeting of the American Geophysical Union database. (abstract OS41B-08)

Kim, M.S., Bae, S.S., Kim, Y.J., Kim, T.W., Lim, J. K., Lee, S.H., et al. (2013) CO-dependent H_2 production by genetically engineered *Thermococcus onnurineus* NA1. *Appl. Environ. Microbiol.* 79: 2048-2053.

Kim, Y.J., Lee, H.S., Kim, E.S., Bae, S.S., Lim, J.K., Matsumi, R., et al. (2010) Formate-driven growth coupled with H_2 production. *Nature* 467: 352-355.

Kim, Y.T., Jung, J.H., Stewart, L.C., Kwon, S.W., Holden, J.F., and Park, C.-S. (2015) Complete genome sequence of the hyperthermophilic methanogen Methanocaldococcus bathoardescens JH146T isolated from the basalt subseafloor. *Mar. Genomics* 24: 229–230.

Kojima, H., Umezawa, K., and Fukui Correspondence, M. (2016) *Caldimicrobium thiodismutans* sp. nov., a sulfur-disproportionating bacterium isolated from a hot spring, and emended description of the genus *Caldimicrobium*. *Int. J. Syst. Evol. Microbiol.* 1828–1831.

Kormas, K.A., Smith, D.C., Edgcomb, V., and Teske, A. (2003). Molecular analysis of deep subsurface microbial communities in Nankai Trough sediments (ODP Leg 190, Site 1176). *FEMS Microbiol. Ecol.* 45: 115-125.

Kotlar, H.K., Lewin, A., Johansen, J., Throne-Holst, M., Haverkamp, T., Markussen, S., et al. (2011) High coverage sequencing of DNA from microorganisms living in an oil reservoir 2.5 kilometres subsurface. *Environ. Microbiol. Rep.* 3: 674–681.

Kozhevnikova, D.A., Taranov, E.A., Lebedinsky, A. V, Bonch-Osmolovskaya, E.A., and Sokolova, T.G. (2016) Hydrogenogenic and sulfidogenic growth of *Thermococcus* archaea on carbon monoxide and formate. *Microbiology* 85: 400-410.

Kristjansson, J.K., Schönheit, P., and Thauer, R.K. (1982) Different K_s values for hydrogen of methanogenic bacteria and sulfate reducing bacteria: an explanation for the apparent inhibition of methanogenesis by sulfate. *Arch. Microbiol.* 131: 278-282.

Kurosawa, N., Itoh, Y.H., Iwai, T., Sugai, A., Uda, I., Kimura, N., et al. (1998) *Sulfurisphaera ohwakuensis* gen. nov., sp. nov., a novel extremely thermophilic acidophile of the order Sulfolobales. *Int. J. Syst. Bacteriol.* 48: 451–456.

Kurr, M., Huber, R., Konig, H., Jannasch, H.W., Fricke, H., Trincone, A., et al. (1991) *Methanopyrus kandleri*, gen. and sp. nov. represents a novel group of hyperthermophilic methanogens, growing at 110ºC. *Arch. Microbiol.* 156: 239–247.

L'Haridon, S., Reysenbach, A.L., Glénat, P., Prieur, D., and Jeanthon, C. (1995) Hot subterranean biosphere in a continental oil reservoir. *Nature* 377: 223-224.

Lang, S.Q., Butterfield, D.A., Schulte, M., Kelley, D.S., and Lilley, M.D. (2010) Elevated concentrations of formate, acetate and dissolved organic carbon found at the Lost City hydrothermal field. *Geochim. Cosmochim. Acta* 74: 941-952.

LaRowe D.E., Burwicz E., Arndt S., Dale A.W., Amend J.P. (2017) Temperature and volume of global marine sediments. *Geology* 45: 275-278.

Lauerer, G., Kristjansson, J.K., Langworthy, T.A., König, H., and Stetter, K.O. (1986) Methanothermus sociabilis sp. nov., a Second Species within the Methanothermaceae Growing at 97°C. *Syst. Appl. Microbiol.* 8: 100–105.

Lee, H.S., Kang, S.G., Bae, S.S., Lim, J.K., Cho, Y., Kim, Y.J., et al. (2008) The complete genome sequence of *Thermococcus onnurineus* NA1 reveals a mixed heterotrophic and carboxydotrophic metabolism. *J. Bacteriol.* 190: 7491-7499.

Lewin, A., Johansen, J., Wentzel, A., Kotlar, H.K., Drabløs, F., and Valla, S. (2014) The microbial communities in two apparently physically separated deep subsurface oil reservoirs show extensive DNA sequence similarities. *Environ. Microbiol.* 16: 545-558.

Liao, Y., Smyth, G.K., and Shi, W. (2014) featureCounts: an efficient general purpose program for assigning sequence reads to genomic features. *Bioinformatics* 30: 923-930.

Lim, J.K., Mayer, F., Kang, S.G., and Müller, V. (2014) Energy conservation by oxidation of formate to carbon dioxide and hydrogen via a sodium ion current in a hyperthermophilic archaeon. *Proc. Natl. Acad. Sci. USA* 111: 11,497–11,502.

Lin, J., Hao, B., Cao, G., Wang, J., Feng, Y., Tan, X., and Wang, W. (2014) A study on the microbial community structure in oil reservoirs developed by water flooding. *J. Pet. Sci. Eng.* 122: 354–359.

Lin, T.J., El Sebae, G., Jung, J.-H., Jung, D.-H., Park, C.-S., and Holden, J.F. (2016) *Pyrodictium delaneyi* sp. nov., a hyperthermophilic autotrophic archaeon that reduces Fe(III) oxide and nitrate. *Int. J. Syst. Evol. Microbiol.* 66: 3372–3376.

Lin, T.J., Ver Eecke, H.C., Breves, E.A., Dyar, M.D., Jamieson, J.W., Hannington, M.D., et al. (2016) Linkages between mineralogy, fluid chemistry, and microbial communities within hydrothermal chimneys from the Endeavour Segment, Juan de Fuca Ridge. *Geochem. Geophys. Geosyst.* 17: 300-323.

Lipson D.A. (2015) The complex relationship between microbial growth rate and yield and its implications for ecosystem processes. *Front. Microbiol.* 6: 615.

Lovley, D.R., and Goodwin, S. (1988) Hydrogen concentrations as an indicator of the predominant terminal electron-accepting reactions in aquatic sediments. *Geochim. Cosmochim. Acta* 52: 2993-3003.

Lovley, D.R., Chapelle, F.H., and Woodward, J.C. (1994) Use of dissolved H_2 concentrations to determine distribution of microbially catalyzed redox reactions in anoxic groundwater. *Env. Sci Technol* 28: 1205–1210.

Lovley, D.R., Dwyer, D.F., and Klug, M.J. (1982) Kinetic analysis of competition between sulfate reducers and methanogens for hydrogen in sediments. *Appl. Environ. Microbiol.* 43: 1373-1379.

Loy, A., Horn, M., and Wagner, M. (2003) probeBase: an online resource for rRNA-targeted oligonucleotide probes. *Nucleic Acids Res.* 31: 514-516.

Ludwig, W., Strunk, O., Westram, R., Richter, L., Meier, H, Yadhukumar, et al. (2004) ARB: a software environment for sequence data. *Nucleic Acids Res.* 32: 1363-1371.

Luo H.W., Zhang H., Suzuki T., Hattori S., Kamagata Y. (2002) Differential expression of methanogenesis genes of *Methanothermobacter thermoautotrophicus* (formerly *Methanobacterium thermoautotrophicum*) in pure culture and in cocultures with fatty acid-oxidizing syntrophs. *Appl. Environ. Microbiol.* 68: 1173-1179.

Mardanov, A. V., Beletsky, A. V., Kadnikov, V. V., Slobodkin, A.I., and Ravin, N. V. (2016) Genome Analysis of *Thermosulfurimonas dismutans*, the First Thermophilic Sulfur-Disproportionating Bacterium of the Phylum Thermodesulfobacteria. *Front. Microbiol.* 7: 950.

Martin, W., Baross, J., Kelley, D., and Russell, M.J. (2008) Hydrothermal vents and the origin of life. *Nat. Rev. Microbiol.* 6: 805–814.

Mayer, F. and Müller, V. (2014) Adaptations of anaerobic archaea to life under extreme energy limitation. *FEMS Microbiol. Rev.* 38: 449-472.

Mayhew, L.E., Ellison, E.T., McCollom, T.M., Trainor, T.P., and Templeton, A.S. (2013) Hydrogen generation from low-temperature water–rock reactions. *Nat. Geosci.* 6: 478–484.

McCollom, T.M. and Seewald, J.S. (2003) Experimental constraints on the hydrothermal reactivity of organic acids and acid anions: I. Formic acid and formate. *Geochim. Cosmochim. Acta* 67: 3625-3644.

McDermott, J.M., Seewald, J.S., German, C.R., and Sylva, S.P. (2015) Pathways for abiotic organic synthesis at submarine hydrothermal fields. *Proc. Natl. Acad. Sci. USA* 112: 7668-7672.

McDowall, J.S., Murphy, B.J., Haumann, M., Palmer, T., Armstrong, F.A., and Sargent, F. (2014) Bacterial formate hydrogenlyase complex. *Proc. Natl. Acad. Sci. USA* 111:11,497-11,502.

Mehta, M.P. and Baross, J.A. (2006) Nitrogen fixation at 92 degrees C by a hydrothermal vent archaeon. *Science* 314: 1783–6.

Meyer, B., Kuehl, J. V., Deutschbauer, A.M., Arkin, A.P., and Stahl, D.A. (2013) Flexibility of Syntrophic Enzyme Systems in *Desulfovibrio* Species Ensures Their Adaptation Capability to Environmental Changes. *J. Bacteriol.* 195: 4900–4914.

Meyer, J.L., Akerman, N.H., Proskurowski, G., and Huber, J.A. (2013) Microbiological characterization of post-eruption “snowblower” vents at Axial Seamount, Juan de Fuca Ridge. *Front. Microbiol.* 4:153.

Miroshnichenko, M.L., Hippe, H., Stackebrandt, E., Kostrikina, N.A., Chernyh, N.A., Jeanthon, C., et al. (2001). Isolation and characterization of *Thermococcus sibiricus* sp. nov. from a Western Siberia high-temperature oil reservoir. *Extremophiles* 5: 85-91.

Miroshnichenko, M.L., Lebedinsky, A. V., Chernyh, N.A., Tourova, T.P., Kolganova, T. V., Spring, S., and Bonch-Osmolovskaya, E.A. (2009) *Caldimicrobium rimae* gen. nov., sp. nov., an extremely thermophilic, facultatively lithoautotrophic, anaerobic bacterium from the Uzon Caldera, Kamchatka. *Int. J. Syst. Evol. Microbiol.* 59: 1040–1044.

Morgan R.M., Pihl T.D., Nölling J., Reeve J.N. (1997) Hydrogen regulation of growth, growth yields, and methane gene transcription in *Methanobacterium thermoautotrophicum* ΔH. *J. Bacteriol.* 179: 889-898.

Morris, B.E., Henneberger, R., Huber, H., and Moissl-Eichinger, C. (2013) Microbial syntrophy: interaction for the common good. *FEMS Microbiol Rev* 37: 384–406.

Mukhopadhyay B., Johnson E.F., Wolfe R.S. (2000) A novel p_{H2} control on the expression of flagella in the hyperthermophilic strictly hydrogenotrophic methanarchaeon *Methanococcus jannaschii*. *Proc. Natl. Acad. Sci. USA* 97: 11,522-11,527.

Muralidharan, V., Rinker, K.D., Hirsh, I.S., Bouwer, E.J., and Kelly, R.M. (1997) Hydrogen transfer between methanogens and fermentative heterotrophs in hyperthermophilic cocultures. *Biotechnol Bioeng* 56: 268–278.

Nakagawa S., Takai K., Inagaki F., Chiba H., Ishibashi J., Kataoka S. *et al.* (2005) Variability in microbial community and venting chemistry in a sediment-hosted backarc hydrothermal system: impacts of subseafloor phase-separation. *FEMS Microbiol. Ecol.* 54: 141-155.

Nakagawa, S., Nakamura, S., Inagaki, F., Takai, K., Shirai, N., and Sako, Y. (2004) *Hydrogenivirga caldilitoris* gen. nov., sp. nov., a novel extremely thermophilic, hydrogen- and sulfur-oxidizing bacterium from a coastal hydrothermal field. *Int. J. Syst. Evol. Microbiol.* 54: 2079–2084.

Nakagawa, S., Shtaih, Z., Banta, A., Beveridge, T.J., Sako, Y., and Reysenbach, A.L. (2005) *Sulfurihydrogenibium yellowstonense* sp. nov., an extremely thermophilic, facultatively heterotrophic, sulfur-oxidizing bacterium from Yellowstone National Park, and emended descriptions of the genus *Sulfurihydrogenibium*, *Sulfurihydrogenibium subterraneum* and *Sulfurihydrogenibium azorense*. *Int. J. Syst. Evol. Microbiol.* 55: 2263–2268.

Nakagawa, T., Takai, K., Suzuki, Y., Hirayama, H., Konno, U., Tsunogai, U., and Horikoshi, K. (2006) Geomicrobiological exploration and characterization of a novel deep-sea hydrothermal system at the TOTO caldera in the Mariana Volcanic Arc. *Environ. Microbiol.* 8: 37-49.

Nakase, T., Suzuki, K., and Itoh, T. (2002) *Vulcanisaeta distributa* gen. nov., sp. nov., and *Vulcanisaeta souniana* sp. nov., novel hyperthermophilic, rod-shaped crenarchaeotes isolated from hot springs in Japan. *Int. J. Syst. Evol. Microbiol.* 52: 1097–1104.

Nazina, T.N., Shestakova, N.M., Grigor'yan, A.A., Mikhailova, E.M., Tourova, T.P., Poltaraus, A.B., et al. (2006) Phylogenetic diversity and activity of anaerobic microorganisms of high-temperature horizons of the Dagang oil field (P. R. China). *Microbiology* 75: 55–65.

Nilsen, R.K., Beeder, J., and Thorstenson, T. (1996) Distribution of thermophilic marine sulfate reducers in North Sea oil field waters and oil reservoirs. *Appl. Environ. Microbiol.* 62: 1793–1798.

Nisbet, E.G. and Sleep, N.H. (2001) The habitat and nature of early life. *Nature* 409: 1083–1091.

Nishizawa, M., Miyazaki, J., Makabe, A., Koba, K., and Takai, K. (2014) Physiological and isotopic characteristics of nitrogen fixation by hyperthermophilic methanogens: key insights into nitrogen anabolism of the microbial communities in Archean hydrothermal systems. *Geochim. Cosmochim. Acta* 138: 117-135.

Nohara, K., Orita, I., Nakamura, S., Imanaka, T., and Fukui, T. (2014) Genetic examination and mass balance analysis of pyruvate/amino acid oxidation pathways in the hyperthermophilic archaeon *Thermococcus kodakarensis*. *J. Bacteriol* 196: 3831-3839.

Nunoura, T., Miyazaki, M., Suzuki, Y., Takai, K., and Horikoshi, K. (2008) *Hydrogenivirga okinawensis* sp. nov., a thermophilic sulfur-oxidizing chemolithoautotroph isolated from a deep-sea hydrothermal field, Southern Okinawa Trough. *Int. J. Syst. Evol. Microbiol.* 58: 676–681.

Okpala, G.N., Chen, C., Fida, T., and Voordouw, G. (2017) Effect of Thermophilic Nitrate Reduction on Sulfide Production in High Temperature Oil Reservoir Samples. *Front. Microbiol.* 8: 1573.

Orcutt, B.N., Sylvan, J.B., Knab, N.J., and Edwards, K.J. (2011) Microbial ecology of the dark ocean above, at, and below the seafloor. *Microbiol. Mol. Biol. Rev.* 75: 361–422.

Orphan, V.J., Taylor, L.T., Hafenbradl, D., and Delong, E.F. (2000) Culture-dependent and culture-independent characterization of microbial assemblages associated with high-temperature petroleum reservoirs. *Appl. Environ. Microbiol.* 66: 700–11.

Paper, W., Jahn, U., Hohn, M.J., Kronner, M., Nather, D.J., Burghardt, T., et al. (2007) *Ignicoccus hospitalis* sp. nov., the host of "*Nanoarchaeum equitans*". *Int. J. Syst. Evol. Microbiol.* 57: 803–808.

Perevalova, A.A., Svetlichny, V.A., Kublanov, I. V, Chernyh, N.A., Kostrikina, N.A., Tourova, T.P., et al. (2005) *Desulfurococcus fermentans* sp. nov., a novel hyperthermophilic archaeon from a Kamchatka hot spring, and emended description of the genus *Desulfurococcus*. *Int. J. Syst. Evol. Microbiol.* 55: 995–999.

Perez-Rodriguez, I., Grosche, A., Massenburg, L., Starovoytov, V., Lutz, R.A., and Vetriani, C. (2012) *Phorcysia thermohydrogeniphila gen. nov., sp. nov., a thermophilic, chemolithoautotrophic, nitrate-ammonifying* bacterium from a deep-sea hydrothermal vent. *Int. J. Syst. Evol. Microbiol.* 62: 2388–2394.

Perner, M., Kuever, J., Seifert, R., Pape, T., Koschinsky, A., Schmidt, K., et al. (2007) The influence of ultramafic rocks on microbial communities at the Logatchev hydrothermal field, located 15°N on the Mid-Atlantic Ridge. *FEMS Microbiol. Ecol.* 61: 97-109.

Phipson, B., Lee, S., Majewski, I.J., Alexander, W.S., and Smyth, G.K. (2016) Robust hyperparameter estimation protects against hypervariable genes and improves power to detect differential expression. *Ann. Appl. Stat.* 10: 946-963.

Pledger, R.J. and Baross, J.A. (1989) Characterization of an extremely thermophilic *Archaebacterium* isolated from a black smoker polychaete (*Paralvinella* sp.) at the Juan de Fuca Ridge. *Syst. Appl. Microbiol.* 12: 249-256.

Price, M.T., Fullerton, H., and Moyer, C.L. (2015) Biogeography and evolution of *Thermococcus* isolates from hydrothermal vent systems of the Pacific. *Front. Microbiol* 6: 968.

Price, R.E. and Giovannelli, D. (2017) A Review of the Geochemistry and Microbiology of Marine Shallow-Water Hydrothermal Vents. In, *Reference Module in Earth Systems and Environmental Sciences*. Elsevier.

Prokofeva, M.I., Kostrikina, N.A., Kolganova, T. V., Tourova, T.P., Lysenko, A.M., Lebedinsky, A. V., and Bonch-Osmolovskaya, E.A. (2009) Isolation of the anaerobic thermoacidophilic crenarchaeote *Acidilobus saccharovorans* sp. nov. and proposal of *Acidilobales* ord. nov., including *Acidilobaceae* fam. nov. and *Caldisphaeraceae* fam. nov. *Int. J. Syst. Evol. Microbiol.* 59: 3116–3122.

Prokofeva, M.I., Miroshnichenko, M.L., Kostrikina, N.A., Chernyh, N.A., Kuznetsov, B.B., Tourova, T.P., and Bonch-Osmolovskaya, E.A. (2000) *Acidilobus aceticus* gen. nov., sp. nov., a novel anaerobic thermoacidophilic archaeon from continental hot vents in Kamchatka. *Int. J. Syst. Evol. Microbiol.* 50: 2001–2008.

Purcell, D., Sompong, U., Yim, L.C., Barraclough, T.G., Peerapornpisal, Y., and Pointing, S.B. (2007) The effects of temperature, pH and sulphide on the community structure of hyperthermophilic streamers in hot springs of northern Thailand. *FEMS Microbiol Ecol* 60: 456–466.

Reveillaud J., Reddington E., McDermott J., Algar C., Meyer J.L., Sylva S. *et al.* (2016). Subseafloor microbial communities in hydrogen-rich vent fluids from hydrothermal systems along the Mid-Cayman Rise. *Environ. Microbiol.* 18: 1970-1987.

Reysenbach, A.L., Götz, D., Beveridge, T.J., Simoneit, B.R.T., Banta, A., and Rushdi, A.I. (2002) *Persephonella marina* gen. nov., sp. nov. and *Persephonella guaymasensis* sp. nov., two novel, thermophilic, hydrogen-oxidizing microaerophiles from deep-sea hydrothermal vents. *Int. J. Syst. Evol. Microbiol.* 52: 1349–1359.

Robinson, J., and Tiedje, J. (1984). Competition between sulfate-reducing and methanogenic bacteria for H_2 under resting and growing conditions. *Arch. Microbiol.* 137: 26-32.

Roussel, E.G., Bonavita, M.A.C., Querellou, J., Cragg, B.A., Webster, G., Prieur, D., and Parkes, R.J. (2008) Extending the sub-sea-floor biosphere. *Science* 320: 1046.

Sako, Y., Nomura, N., Uchida, A., Ishida, Y., Morii, H., Koga, Y., et al. (1996) A Novel Hyperthermophilic Archaeon Growing Temperatures up to 100°C Aerobic at. *Int. J. Syst. Bacteriol. Int. Union Microbiol. Soc.* 46: 1070-1077.

Sako, Y., Nunoura, T., and Uchida, A. (2001) *Pyrobaculum oguniense* sp. nov., a novel facultatively aerobic and hyperthermophilic archaeon growing at up to 97 SC. *Int. J. Syst. Evol. Microbiol.* 51: 303–309.

Sapra, R., Bagramyan, K., and Adams, M.W.W. (2003) A simple energy-conserving system: proton reduction coupled to proton translocation. *Proc. Natl. Acad. Sci. USA* 100: 7545-7550.

Schönheit P., Moll J., Thauer R.K. (1980). Growth parameters (K_s, μ_{max}, Y_s) of *Methanobacterium thermoautotrophicum*. *Arch. Microbiol.* 127: 59-65.

Schut, G.J., Boyd, E.S., Peters, J.W., and Adams, M.W.W. (2013) The modular respiratory complexes involved in hydrogen and sulfur metabolism by heterotrophic hyperthermophilic archaea and their evolutionary implications. *FEMS Microbiol. Rev.* 37: 182–203.

Segerer, A., Neuner, A., Kristjansson, J.K., and Stetter1, K. 0 (1986) Thermophilic Sulfur-Metabolizing Archaebacteria. *Int. J. Syst. Bacteriol.* 86.

Segerer, A.H., Trincone, A., Gahrtz, M., and Stetter, K.O. (1991) *Stygiolobus azoricus* gen. nov., sp. nov. Represents a Novel Genus of Anaerobic, Extremely Thermoacidophilic Archaebacteria of the Order *Sulfolobales*. *Int. J. Syst. Bacteriol.* 41: 495–501.

Shima, S. and Suzuki, K.I. (1993) Hydrogenobacter acidophilus sp. nov., a Thermoacidophilic, Aerobic, Hydrogen-Oxidizing Bacterium Requiring Elemental Sulfur for Growth. *Int. J. Syst. Bacteriol.* 43: 703–708.

Siebers, B., Zaparty, M., Raddatz, G., Tjaden, B., Albers, S.-V., Bell, S.D., et al. (2011) The complete genome sequence of *Thermoproteus tenax*: a physiologically versatile member of the Crenarchaeota. *PLoS One* 6: e24222.

Sleep, N.H., Meibom, A., Fridriksson, T., Coleman, R.G., and Bird, D.K. (2004) H_2-rich fluids from serpentinization: geochemical and biotic implications. *Proc. Natl. Acad. Sci. U. S. A.* 101: 12818–23.

Slobodkin, A.I., Reysenbach, A.-L., Slobodkina, G.B., Baslerov, R. V., Kostrikina, N.A., Wagner, I.D., and Bonch-Osmolovskaya, E.A. (2012) *Thermosulfurimonas dismutans* gen. nov., sp. nov., an extremely thermophilic sulfur-disproportionating bacterium from a deep-sea hydrothermal vent. *Int. J. Syst. Evol. Microbiol.* 62: 2565–2571.

Slobodkin, A.I., Tourova, T.P., Kostrikina, N.A., Chernyh, N.A., Bonch-Osmolovskaya, E.A., Jeanthon, C., and Jones, B.E. (2003) *Tepidibacter thalassicus* gen. nov., sp. nov., a novel moderately thermophilic, anaerobic, fermentative bacterium from a deep-sea hydrothermal vent. *Int. J. Syst. Evol. Microbiol.* 53: 1131-1134.

Slobodkina, G.B., Kolganova, T. V., Querellou, J., Bonch-Osmolovskaya, E.A., and Slobodkin, A.I. (2009) *Geoglobus acetivorans* sp. nov., an iron(III)-reducing archaeon from a deep-sea hydrothermal vent. *Int. J. Syst. Evol. Microbiol.* 59: 2880–2883.

Sokolova, T.G., Jeanthon, C., Kostrikina, N.A., Chernyh, N.A., Lebedinsky, A.V., Stackebrandt, E., and Bonch-Osmolovskaya, E.A. (2004) The first evidence of anaerobic CO oxidation coupled with H_2 production by a hyperthermophilic archaeon isolated from a deep-sea hydrothermal vent. *Extremophiles* 8: 317-323.

Steinsbu, B.O., Thorseth, I.H., Nakagawa, S., Inagaki, F., Lever, M.A., Engelen, B., et al. (2010) *Archaeoglobus sulfaticallidus* sp. nov., a thermophilic and facultatively lithoautotrophic sulfate-reducer isolated from black rust exposed to hot ridge flank crustal fluids. *Int. J. Syst. Evol. Microbiol.* 60: 2745–2752.

Stetter, K.O. (2006) Hyperthermophiles in the history of life. *Philos. Trans. R. Soc. Lond. B. Biol. Sci.* 361: 1837-42–3.

Stetter, K.O. (1999) Extremophiles and their adaptation to hot environments. *FEBS. Lett.* 452: 22–5.

Stetter, K.O., Huber, R., Blöchl, E., Kurr, M., Eden, R.D., Fielder, M., et al. (1993) Hyperthermophilic archaea are thriving in deep North Sea and Alaskan oil reservoirs. *Nature* 365: 743-745.

Stetter, K.O., König, H., and Stackebrandt, E. (1983) *Pyrodictium* gen. nov., a New Genus of Submarine Disc-Shaped Sulphur Reducing Archaebacteria Growing Optimally at 105°C. *Syst. Appl. Microbiol.* 4: 535–551.

Stetter, K.O., Thomm, M., Winter, J., Wildgruber, G., Huber, H., Zillig, W., et al. (1981) *Methanothermus fervidus*, sp. nov., a novel extremely thermophilic methanogen isolated from an Icelandic hot spring. *Zentralblatt für Bakteriol. Mikrobiol. und Hyg. I. Abt. Orig. C Allg. Angew. und ökologische Mikrobiol.* 2: 166–178.

Stewart, L.C., Jung, J.H., Kim, Y.T., Kwon, S.W., Park, C.S., and Holden, J.F. (2015). *Methanocaldococcus bathoardescens* sp. nov., a hyperthermophilic methanogen isolated from a volcanically active deep-sea hydrothermal vent. *Int. J. Syst. Evol. Microbiol.* 65: 1280-1283.

Stewart, L.C., Llewellyn, J.G., Butterfield, D.A., Lilley, M.D., and Holden, J.F. (2016). Hydrogen and thiosulfate limits for growth of a thermophilic, autotrophic *Desulfurobacterium* species from a deep-sea hydrothermal vent. *Environ. Microbiol. Rep.* 8: 196-200.

Swingley, W.D., Meyer-Dombard, D.R., Shock, E.L., Alsop, E.B., Falenski, H.D., Havig, J.R., and Raymond, J. (2012) Coordinating Environmental Genomics and Geochemistry Reveals Metabolic Transitions in a Hot Spring Ecosystem. *PLoS One* 7: e38108.

Takács, M., Tóth, A., Bogos, B., Varga, A., Rákhely, G., and Kovács, K.L. (2008) Formate hydrogenlyase in the hyperthermophilic archaeon, *Thermococcus litoralis*. *BMC Microbiol*. 8: 88.

Takai K., Gamo T., Tsunogai U., Nakayama N., Hirayama H., Nealson K.H., Horikoshi K. (2004) Geochemical and microbiological evidence for a hydrogen-based, hyperthermophilic subsurface lithoautotrophic microbial ecosystem (HyperSLiME) beneath an active deep-sea hydrothermal field. *Extremophiles* 8: 269-282.

Takai, K., Nakagawa, S., Sako, Y., and Horikoshi, K. (2003) *Balnearium lithotrophicum* gen. nov., sp. nov., a novel thermophilic, strictly anaerobic, hydrogen-oxidizing chemolithoautotroph isolated from a black smoker chimney in the Suiyo Seamount hydrothermal system. *Int. J. Syst. Evol. Microbiol*. 53: 1947–1954.

Takai, K., Nunoura, T., Horikoshi, K., Shibuya, T., Nakamura, K., Suzuki, Y., et al. (2009) Variability in microbial communities in black smoker chimneys at the NW Caldera vent field, Brothers Volcano, Kermadec Arc. *Geomicrobiol. J.* 26: 552-569.

Takai, K., Nunoura, T., Ishibashi, J., Lupton, J., Suzuki, R. Hamasaki, H., et al. (2008) Variability in the microbial communities and hydrothermal fluid chemistry at the newly discovered Mariner hydrothermal field, southern Lau Basin. *J. Geophys. Res.* 113:G02031.

Takai, K., Nakamura, K., Toki, T., Tsunogai, U., Miyazaki, M., Miyazaki, J., et al. (2008) Cell proliferation at 122ºC and isotopically heavy CH_4 production by a hyperthermophilic methanogen under high-pressure cultivation. *Proc. Natl. Acad. Sci.* 105: 10949–10954.

Thauer, R.K., Kaster, A.K., Seedorf, H., Buckel, W., and Hedderich, R. (2008) Methanogenic archaea: ecologically relevant differences in energy conservation. *Nat. Rev. Microbiol.* 6: 579–591.

Topçuoğlu, B.D., Meydan, C., Orellana, R., and Holden, J.F. (2018) Formate hydrogenlyase and formate secretion ameliorate H_2 inhibition in the hyperthermophilic archaeon *Thermococcus paralvinellae*. *Environ. Microbiol.*

Topçuoğlu, B.D., Stewart, L.C., Morrison, H.G., Butterfield, D.A., Huber, J.A., and Holden, J.F. (2016) Hydrogen Limitation and Syntrophic Growth among Natural Assemblages of Thermophilic Methanogens at Deep-sea Hydrothermal Vents. *Front. Microbiol.* 7: 1240.

Ünal, B., Perry, V. R., Sheth, M., Gomez-Alvarez, V., Chin, K.J., and Nüsslein, K. (2012) Trace elements affect methanogenic activity and diversity in enrichments from subsurface coal bed produced water. *Front. Microbiol.* 3:175.

van Der Maaten L., Hinton G. (2008) Visualizing data using t-SNE. *J. Mach. Learn. Res.* 9: 2579-2605.

van Haaster, D.J., Silva, P.J., Hagedoorn, P.L., Jongejan, J.A., and Hagen, W.R. (2008) Reinvestigation of the steady-state kinetics and physiological function of the soluble NiFe-hydrogenase I of *Pyrococcus furiosus*. *J. Bacteriol.* 190: 1584-1587.

Vanwonterghem, I., Evans, P.N., Parks, D.H., Jensen, P.D., Woodcroft, B.J., Hugenholtz, P., and Tyson, G.W. (2016) Methylotrophic methanogenesis discovered in the archaeal phylum Verstraetearchaeota. *Nat. Microbiol.* 1: 16170.

Ver Eecke, H.C., Akerman, N.H., Huber, J.A., Butterfield, D.A., and Holden, J.F. (2013) Growth kinetics and energetics of a deep-sea hyperthermophilic methanogen under varying environmental conditions. *Environ. Microbiol. Rep.* 5: 665-671.

Ver Eecke, H.C., Butterfield, D.A., Huber, J.A., Lilley, M.D., Olson, E.J., Roe, K.K., et al. (2012) Hydrogen-limited growth of hyperthermophilic methanogens at deep-sea hydrothermal vents. *Proc. Natl. Acad. Sci.* 109: 13674–13679.

Ver Eecke, H.C., Kelley, D.S., and Holden, J.F. (2009) Abundances of hyperthermophilic autotrophic Fe(III) oxide reducers and heterotrophs in hydrothermal sulfide chimneys of the northeastern Pacific Ocean. *Appl. Environ. Microbiol.* 75: 242-245.

Verhaart, M.R.A., Bielen, A.A.M., Oost, J. van der, Stams, A.J.M., and Kengen, S.W.M. (2010) Hydrogen production by hyperthermophilic and extremely thermophilic bacteria and archaea: mechanisms for reductant disposal. *Environ. Technol.* 31: 993-1003.

Verhees, C.H., Kengen, S.W.M., Tuininga, J.E., Schut, G.J., Adams, M.W.W., De Vos, W.M., and Van Der Oost, J. (2003) The unique features of glycolytic pathways in Archaea. *Biochem. J.* 375: 231–246.

Vetriani, C., Speck, M.D., Ellor, S. V, Lutz, R.A., and Starovoytov, V. (2004*) Thermovibrio ammonificans* sp. nov., a thermophilic, chemolithotrophic, nitrate-ammonifying bacterium from deep-sea hydrothermal vents. *Int. J. Syst. Evol. Microbiol.* 54: 175–81.

Völkl, P., Huber, R., Drobner, E., Rachel, R., Burggraf, S., Trincone, A., and Stetter, K.O. (1993) *Pyrobaculum aerophilum* sp. nov., a novel nitrate-reducing hyperthermophilic archaeum. *Appl. Environ. Microbiol.* 59: 2918–26.

Waldron, P.J., Petsch, S.T., Martini, A.M., Nüsslein, K., and Nüslein, K. (2007) Salinity constraints on subsurface archaeal diversity and methanogenesis in sedimentary rock rich in organic matter. *Appl. Environ. Microbiol.* 73: 4171–9.

Walker, C.B., Redding-Johanson, A.M., Baidoo, E.E., Rajeev, L., He, Z., Hendrickson, E.L., et al. (2012) Functional responses of methanogenic archaea to syntrophic growth. *Int. Sociey Microb. Ecol.* 6: 2045–2055.

Wang, Q., Garrity, G.M., Tiedje, J.M., and Cole, J.R. (2007) Naïve Bayesian classifier for rapid assignment of rRNA sequences into the new bacterial taxonomy. *Appl. Environ. Microbiol.* 73: 5261-5267.

Waters, E., Hohn, M.J., Ahel, I., Graham, D.E., Adams, M.D., Barnstead, M., et al. (2003) The genome of *Nanoarchaeum equitans*: insights into early archaeal evolution and derived parasitism. *Proc. Natl. Acad. Sci. U. S. A.* 100: 12984–8.

Wery, N., Moricet, J.M., Cueff, V., Jean, J., Pignet, P. Lesongeur, F., et al. (2001) *Caloranaerobacter azorensis* gen. nov., sp. nov., an anaerobic thermophilic bacterium isolated from a deep-sea hydrothermal vent. *Int. J. Syst. Evol. Microbiol.* 51: 1789-1796.

Wolf T., Kämmer P., Brunke S., Linde J. (2018) Two's company: studying interspecies relationships with dual RNA-seq. *Curr. Opin. Microbiol.* 42: 7-12.

Xavier, K.B., da Costa, M.S., and Santos, H. (2000) Demonstration of a novel glycolytic pathway in the hyperthermophilic archaeon *Thermococcus zilligii* by ^{13}C-labeling experiments and nuclear magnetic resonance analysis. *J. Bacteriol.* 182: 4632-4636.

Yim, K.J., Song, H.S., Choi, J.S., and Roh, S.W. (2015) Thermoproteus thermophilus sp. nov., a hyperthermophilic crenarchaeon isolated from solfataric soil. *Int. J. Syst. Evol. Microbiol.* 65: 2507–2510.

Yoshida, N., Nakasato, M., Ohmura, N., Ando, A., Saiki, H., Ishii, M., and Igarashi, Y. (2006) *Acidianus manzaensis* sp. nov., a Novel Thermoacidophilic Archaeon Growing Autotrophically by the Oxidation of H_2 with the Reduction of Fe3+. *Curr. Microbiol.* 53: 406–411.

Zar, J.H. (1996). Biostatistical Analysis, 3rd Edition. Prentice Hall Press, Upper Saddle River, New Jersey.

Zeikus, J.G. and Wolfe, R.S. (1972) *Methanobacterium thermoautotrophicus* sp. n., an anaerobic, autotrophic, extreme thermophile. *J. Bacteriol.* 109: 707–15.

Zillig, W., Gierl, A., Schreiber, G., Wunderl, S., Janekovic, D., Stetter, K.O., and Klenk, H.P. (1983) The Archaebacterium *Thermofilum pendens* Represents, a Novel Genus of the Thermophilic, Anaerobic Sulfur Respiring Thermoproteales. *Syst. Appl. Microbiol.* 4: 79–87.

Zillig, W., Holz, I., Janekovic, D., Klenk, H.P., Imsel, E., Trent, J., et al. (1990) *Hyperthermus butylicus*, a hyperthermophilic sulfur-reducing archaebacterium that ferments peptides. *J. Bacteriol.* 172: 3959–65.